GEOLOGICA ULTRAIECTINA

Mededelingen van de
Faculteit Aardwetenschappen
Universiteit Utrecht

No. 140

MIXING PROPERTIES OF THERMAL CONVECTION IN THE EARTH'S MANTLE

Jörg Schmalzl

GEOLOGICA ULTRAIECTINA

Mededelingen van de
Faculteit Aardwetenschappen
Universiteit Utrecht

No. 140

MIXING PROPERTIES OF THERMAL CONVECTION IN THE EARTH'S MANTLE

Jörg Schmalzl

CIP-GEGEVENS KONINKLIJKE BIBLIOTHEEK, DEN HAAG

Schmalzl, Jörg Thomas

Mixing properties of thermal convection in the Earth's mantle / Jörg Thomas Schmalzl. - Utrecht : Faculteit Aardwetenschappen, Universiteit Utrecht. - (Geologica Ultraiectina, ISSN 0072-1026; no. 140)
Proefschrift Universiteit Utrecht. - Met lit. opg. -Met samenvatting in Nederlands.
ISBN 90-71577-94-5
Trefw.: geodynamica / aardmantel.

MIXING PROPERTIES OF THERMAL CONVECTION IN THE EARTH'S MANTLE

MENGING IN DE MANTEL VAN DE AARDE
DOOR THERMISCHE CONVECTIE

(met een samenvatting in het Nederlands)

PROEFSCHRIFT

TER VERKRIJGING VAN DE GRAAD VAN DOCTOR
AAN DE UNIVERSITEIT UTRECHT OP GEZAG VAN DE
RECTOR MAGNIFICUS, PROF. DR J.A. VAN GINKEL
INGEVOLGE HET BESLUIT VAN HET COLLEGE VAN DEKANEN
IN HET OPENBAAR TE VERDEDIGEN
OP DINSDAG 2 APRIL 1996 DES NAMIDDAGS TE 2:30 UUR

DOOR

JÖRG THOMAS SCHMALZL

GEBOREN OP 15 APRIL 1964, TE WESSELING, DUITSLAND

PROMOTER: PROF. DR. N. J. VLAAR

CO-PROMOTER: DR. U. HANSEN

The research reported in this thesis has been carried out at the Department of Geophysics, Institute of Earth Sciences, Utrecht University, Budapestlaan 4, 3584 CD Utrecht, The Netherlands. This work was supported by the Netherlands Science Foundation (NWO; project number NLS 61-278) This is Geodynamics Research Institute (Utrecht University) contribution 96.009.

The following publications have resulted from this study:

Schmalzl, J. and U. Hansen, Mixing the Earth's Mantle by thermal convection - a scale dependent phenomenon, Geophys. Res. Lett., 21,11, 1994.

Schmalzl, J. Houseman, G. and U. Hansen, Mixing properties of 3D Stationary Convection, Physics of Fluids, 21, 1027-1033, 1995.

Schmalzl, J. Houseman, G. and U. Hansen, Mixing in 3D time-dependent Convection, accepted for publication in Journal of Geophysical Research, 1996.

Contents

1 Introduction 1
1.1 Summary 3

2 Mixing in the Earth's mantle 5
2.1 The structure of the mantle 5
2.2 Reservoirs within the Earth's mantle 7
2.3 Possible source mechanism for the observed mantle reservoirs 11
2.4 Time scale for the mantle heterogeneities 12
2.5 Length scale of the mantle heterogeneities 13
2.6 References 14

3 The kinematics of mixing 18
3.1 2D stationary flows 19
3.2 2D time dependent flows 20
3.3 3D flows 22
3.4 Statistical description of mixing processes 24
3.5 References 26

4 Basic equations 27
4.1 References 29

5 The numerical methods 30
5.1 The solution of the Equation for the 2D case 30
5.1.1 The equation of motion 30
5.1.2 The equation of heat transport 32
5.2 The numerical solution of the Equation for the 3D case 34
5.3 Passive Tracers 35
5.4 References 37

6 Mixing in the Earth's mantle by thermal convection - a scale dependent phenomenon 39
6.1 Abstract 40
6.2 Introduction 40
6.3 Model and methods 41
6.4 Results 43
6.5 Conclusion 51

6.6 References 52

7 Mixing properties of 3D stationary convection 54

7.1 Abstract 55

7.2 Introduction 56

7.3 Model and Methods 57

7.4 Results 59

7.4.1 Convection with a square pattern 59

7.4.2 Convection with a hexagonal pattern 66

7.5 Conclusions 67

7.6 References 70

8 Mixing in vigorous, time-dependent 3D convection and application to the Earth's mantle 72

8.1 Abstract 73

8.2 Introduction 73

8.3 Model and Methods 76

8.4 Results 78

8.4.1 Mixing within a cell 80

8.4.2 Mixing between cells 86

8.4.3 Dependence of the mixing process on the initial position of the tracer cloud 89

8.4.4 The influence of the vigor of convection on the mixing process ... 90

8.5 Discussion and Conclusion 93

8.6 References 97

9 Samenvatting (summary in Dutch) 100

10 Acknowledgements 103

11 Curriculum Vitae 104

1 Introduction

Over the last two decades it has become widely accepted that convective flows within the Earth's mantle form the mechanism which turns the heat from the Earth's interior into mechanical work, thus providing the mechanism behind tectonic activities on Earth. Moreover, the thermal structure of the Earth's interior and it's chemical composition will be widely determined by the process of mantle convection. Due to the inaccessibility of the Earth's interior to direct measurements, the knowledge about the nature of the convective flow is still incomplete. Most of the information about the Earth's structure and evolution has been obtained by remote sensing techniques, with seismology being the most important one. Nowadays, tomographic image reconstruction is used to reveal not only the radial structure of the Earth's interior but also lateral inhomogeneities. Despite the increasing power in seismology and other remote sensing techniques , there remains the problem that they all provide a single snapshot of the Earth's interior in time. While these snapshots certainly have the role of important boundary conditions for the study of the dynamic evolution, they do not allow to reconstruct (or to predict) the temporal evolution of the Earth's interior.

Geochemical observations, in contrast, provide time-averaged observations, thus being able to reveal information about the temporal evolution of the Earth. Isotope ratios of basaltic rocks, sampled at mid-ocean ridges and at oceanic islands, indicate that the Earth' mantle is heterogeneous on scales ranging from less than a meter up to several thousand kilometers. Occasionally it has been concluded that these observations can only be explained by several reservoirs in the Earth's mantle which have not been mixed by convection through Earth's history. The weak point of the geochemical observations is the fact that they only provide information at discrete points thus giving only little information about the spatial distribution of the possible source reservoirs for the basaltic rocks.

The structure of mantle convection will greatly influence the generation and the survival of compositional heterogeneities. Conversely, geochemical observations can be used to obtain information about heterogeneities in the mantle and then, with certain model assumptions, information about the pattern of the mantle flow. In order to link the geochemical observations to the temporal and spatial pattern of convection it is necessary to develop an understanding of the mixing properties of convective flows. It is, for example, necessary to understand wether composi-

tional heterogeneities can survive over significant times within a flow, or wether the presence of such heterogeneities requires a strict separation of convection cells. In the latter case the geochemical observation would indicate separate convecting layers within the Earth, while in the first case the presence of heterogeneities could be explained by a dynamic Earth model in which convection extends from the lithosphere to the boundary between mantle and core at a depth of about 3000km. It is the aim of this work to investigate the mixing properties of convective flows in order to bridge the gap between geochemical observations and the resulting implications for a dynamical model of the Earth's interior.

Mixing processes play an important role in various natural phenomena and also in technical applications. Consequently, the study of mixing has received an increasing attention within the last years. These studies reveal that mixing is in general a complex phenomenon and it has thus far not been possible to develop a unifying theory of mixing. Under most circumstances, the mixing process defies an analytical description, so that either laboratory experiments or computational experiments need to be employed. Laboratory experiments have been used extensively to investigate mixing properties for particular applications, on a case-by-case level, rather than to study general properties. In the context of mantle convection laboratory experiments seem less appropriate, mainly due to the fact that the relevant material properties and the relevant scales can not be reached.

In this work computational fluid dynamic has been chosen as the research method. Although being limited by the available power of present day computers, numerical experiments offer the possibility to simulate the circumstances within the Earth interior, at least up to a reasonable approximation. Moreover, computational fluid dynamic allows to take into account the tremendous spatial and temporal scales which are involved in the phenomenon of mantle convection easily .

While most of the numerical mixing studies focus on the mixing properties of kinematically prescribed flow fields, this effort concentrates on the evolution of thermally driven convective flows, as numerically calculated from first principles. The model scenario resembles the Earth's mantle in a sense that we consider vigorous thermal convection in a highly viscous fluid. It must be emphasized at this point that the model is still oversimplified, as compared to the Earth's mantle.

The dependence of the viscosity on both, temperature and pressure, the presence of internal radiogenic heat and the use of a Cartesian, rather than a spherical geometry will probably influence the mixing behavior. This and other further complications,

like the strain rate dependence of the rheology, have been neglected in this study, partially because of limitations of the computers, and partially in order to be able to delineate the different causes and consequences. For that reason convection patterns with an increasing degree of complexity, ranging from two-dimensional, over stationary three-dimensional to time dependent three-dimensional flows have been investigated.

1.1 Summary

In chapter 2 some of the geochemical evidence which has been derived from isotope ratios of mid ocean ridge basalts and ocean island basalts is discussed. These measurements clearly indicate that the Earth's mantle is chemically heterogeneous and has at least four distinct chemical reservoirs. The observed length-scale of these heterogeneities varies between less than a meter and up to several thousand kilometers. Some of the components seem to have existed since 150 Myr. after the Earth's formation. The existence of these reservoirs imposes certain constraints on the possible nature of mantle convection as well as on the subduction process of lithospheric plates which act as a source for geochemically distinct material in the Earth's mantle.

In chapter 3 we discuss some general aspects of the kinematics involved in the mixing process of two fluids. Due to the broadness of this subject I focus on the recently discovered phenomenon of Lagrangian chaos. In regions within the flow which exhibit this chaotic Lagrangian structure the mixing is strongly enhanced. They have been observed both in two-dimensional, time-periodic as well as in three dimensional flows.

The mathematical equations that describe our physical model can be found in chapter 4. In this chapter we also described approximations made and the appropriate scaling which has been applied.

The numerical methods are described in chapter 5. For the two dimensional experiments described within this thesis we used a finite element model. The three-dimensional experiments have been carried out using a mixed spectral finite-difference approach. The passive tracer algorithm used to monitor the mass transport in both the two-dimensional and the three dimensional simulations is described at the end of this chapter.

In chapter 6 we introduce a particle correlation function and the corresponding

correlation dimension to characterize the mixing efficiency of a 2D convective flow as a function of it's vigor and structure. This method is shown to characterize the mixing process in a detailed manner. This study suggests that the mixing properties of the flow depend on the spatial scale. At a moderate vigor of convection, heterogeneities within a circulation cell are destroyed rapidly while two adjoined cells can remain unmixed substantially longer.

The mixing properties of three dimensional stationary convection are the topic of the following chapter 7. Individual flow-lines as shown by Poincaré sections of the tracer paths lie on two-dimensional surfaces with distorted toroidal topology. The space occupied by the convective fluid is filled by sets of these toroidal surfaces nested on within another. Unlike experiments in less viscous fluids we did not observe any regions where the Lagrangian tracer motion was chaotic.

In the final chapter 8 we present numerical investigations on mixing in vigorous three dimensional convection. In comparison to the two dimensional experiments these flows proved to be very efficient in homogenizing the heterogeneities within each convective cell. This is primarily due to the toroidal motion of the tracers. This toroidal movement is analogous to the motion observed in the stationary three-dimensional flows. Opposingly the mixing across the boundaries of convection cells was found to be much slower than expected from the two dimensional simulations, thus giving a possible explanation for the observed heterogeneities in the Earth's mantle.

2 Mixing in the Earth's mantle

2.1 The structure of the mantle

With the general acceptance of the plate tectonic theory it was also recognized that the heat engine which drives the plates by transforming thermal energy into mechanical work must be the process of thermal convection in the Earths mantle.

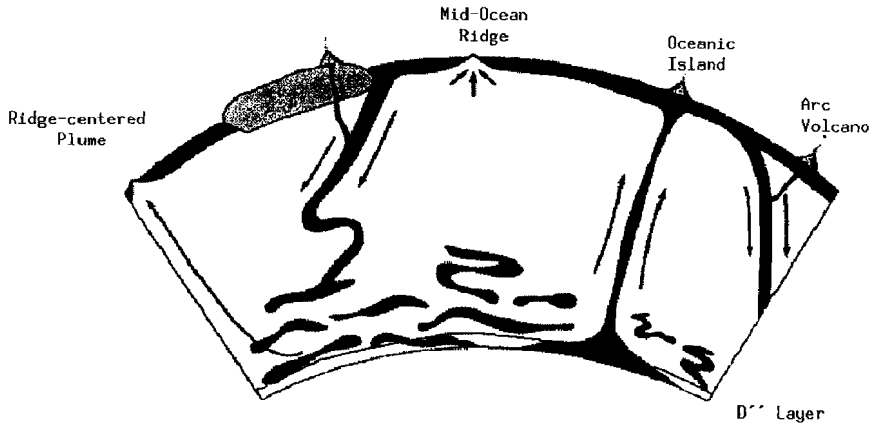

Figure 2.1:
Model of whole mantle convection as proposed by Davies (1984) and others where mixing is sluggish in the lower mantle due to increased viscosity. Therefore large heterogeneities made up of subducted material and some primordial material persist over long time scales (sketched after Kellogg, 1992).

The information available to constrain the possible patterns of convection comes both from geochemical and geophysical investigations. Geochemical studies indicate that the Earth's mantle is chemically heterogeneous. The different chemical signatures correspond to different chemical reservoirs within the Earth's mantle. With respect to the existence of different possible reservoirs within the Earth's mantle the nature of the $\approx 670km$ seismic discontinuity is of key importance because this discontinuity may cause the mantle to convect separately in the upper

and the lower layer. It is not clear whether this discontinuity is due to a phase change in a chemically homogeneous mantle (e.g. Anderson, 1976; Ringwood, 1975), whether it represents a compositional boundary (e.g. Richter and McKenzie, 1981), or whether it is a combination of both.
The two extreme scenarios in this debate are whole mantle-convection with no influence of the $\approx 670km$ discontinuity on the structure of the mantle flow (Fig. 2.1) and, on the other hand, layered mantle convection where the upper and lower mantle convect separately with no interchange of material (Fig. 2.2)

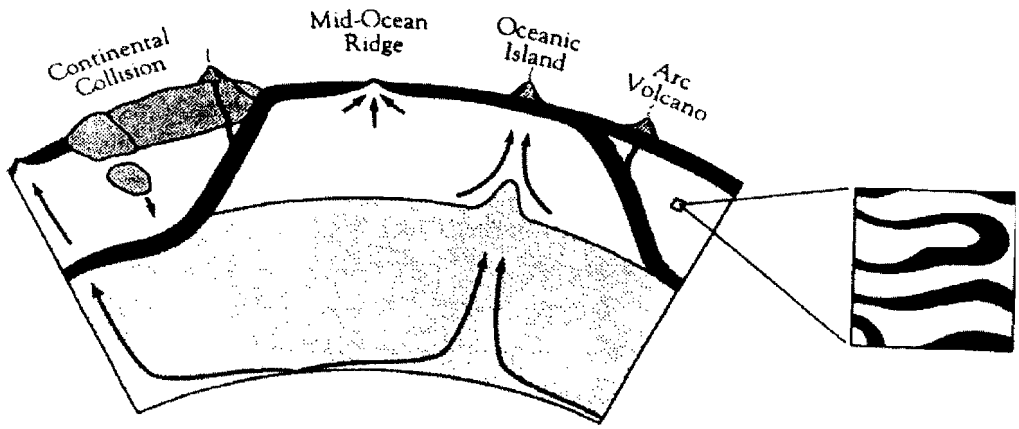

Figure 2.2:
Model of layered mantle convection as described by Allégre and Turcotte (1986). The mantle consists of two reservoirs which remain largely isolated through time. The upper mantle provides source material for the basalts found at the mid-ocean ridges (MORB) whereas the lower mantle is the source for the Oceanic Island basalts (OIB). Subducted lithosphere does not penetrate into the lower mantle but is stirred into the upper mantle thus giving it a *marble-cake* structure (sketched after Kellogg, 1992).

In between these two points of view a variety of models are possible. As suggested by Silver (1988) the mantle may be partially layered and slabs may penetrate into the lower mantle. Numerical investigations by Machetel and Weber (1991) show

that phase changes can cause convection to vary intermittently between whole mantle convection and layered mantle convection.
In recent publications Steinbach and Yuen (1994) and Tackley et al. (1994) have investigated the possibility of layered mantle convection where mass-transport between upper and lower mantle happens episodically. In this models relatively heavy material is accumulated over the boundary between upper and lower mantle. When the amount of accumulated material has reached a critical size it is able to penetrate into the lower mantle in an avalanche-like-fashion.
The fate of subducted oceanic lithosphere is also related to the structure of mantle convection. For whole mantle convection a subducted slab may sink to the core-mantle boundary where it may form a layer associated with the D'' region of the mantle (Fig. 2.1).
In the layered mantle convection models slabs can not penetrate into the lower mantle but are stirred and homogenized within the upper mantle, forming the source reservoir for the basalts which are found at the mid-ocean ridges (MORB) (Fig. 2.2).
Seismic tomography confirms this observation. v. d. Hilst et al. (1991) and v. d. Hilst and Seno (1993) observed both subducted slabs which where able to penetrate into the lower mantle as well as slabs which where deflected by the phase change at the $\approx 670km$ discontinuity and thus stayed in the upper mantle.
From the discussion it seems clear that the nature of the $\approx 670km$ discontinuity is of crucial importance to the mass exchange between the upper- and lower mantle. However, in order to put geochemical observations into the right perspective with respect to the structure of mantle convection a more general understanding of mixing properties of mantle convection must be developed.
Questions that arise and have been addressed to some extent in the literature (Hoffman and McKenzie, 1984; Davies, 1984, Christensen, 1988) are: 'Can heterogeneities survive long enough in whole mantle convection to explain the observed chemical heterogeneities ?' Or, conversely, can subducted oceanic plates be stirred efficiently enough in order to explain the relatively homogeneous MORB reservoir ?'

2.2 Reservoirs within the Earth's mantle

Over the last decades a growing data base of isotope ratios of basalts found at

the mid-ocean ridges (MORB's) and basalts from ocean islands (OIB's) has been collected. These relatively young basalts originate from the the underlying mantle thus containing information about the chemical composition of the mantle. Significant conclusions can be drawn from the isotope ratios of the rare Earth elements Neodymium (Nb), Strontium (Sr) and Lead (Pb). They all have a sufficiently long half-live period with stable daughter elements and are therefore well suited for geochronologic dating. Investigations on the isotope ratio of rare earth elements have shown that the normal mid-ocean ridge basalts have an almost uniform composition (Gast, 1968; Bougault et al., 1980; Allègre, 1980). In contrast OIB's display a variety of different compositions. Fig 2.3 shows the isotope data from various islands.
The linear correlation between the Nd and Sr data in Fig 2.3 indicates the existence of at least two reservoirs in the mantle, one reservoir from which MORB's originate, depleted in incompatible trace elements and a complementary enriched reservoir containing some original material undepleted by melt extraction or material enriched by additional crustal material (DePaolo and Wasserburg, 1976).
Recent studies which include also isotope data from Pb indicated that the simple idea of a two-component linear mixing system does not hold (Fig 2.4, 2.5).

Based on the Nd-Sr-Pb data, White (1985) categorized the basalts into 5 groups: The MORB group which shows a strong correlation between Nd, Sr and Pb isotopes and has a high $^{143}Nd/^{144}Nd$ and a low $^{87}Sr/^{86}Sr$ ratio. The other groups have been named after the islands where the basalts with the specific isotope ratios have been found like Samoa or Kerguelen group. The Kerguelen group, for example, shows a low $^{143}Nd/^{144}Nd$, $^{297}Pb/^{204}Pb$ ratio and a high $^{87}Sr/^{86}Sr$ ratio.
White (1985) pointed out that MORB seemed to have mixed with all of the OIB's to some extent whereas there is little evidence of mixing within the OIB's group itself. Fig. 2.4 shows that the different OIB's are distinct in their isotope composition. As a possible explanation he suggested the entrainment of plumes, coming from the lower mantle and being the source for the OIB's, into the upper mantle which is the source region for MORB.
Zindler and Hart (1986) proposed a different model for the explanation of the observed heterogeneities. They postulated the existence of four mantle components: The depleted mantle source N-MORB, two enriched sources EM1 and EM2 and a source region of radiogenic Pb, called HIMU. They also proposed the existence

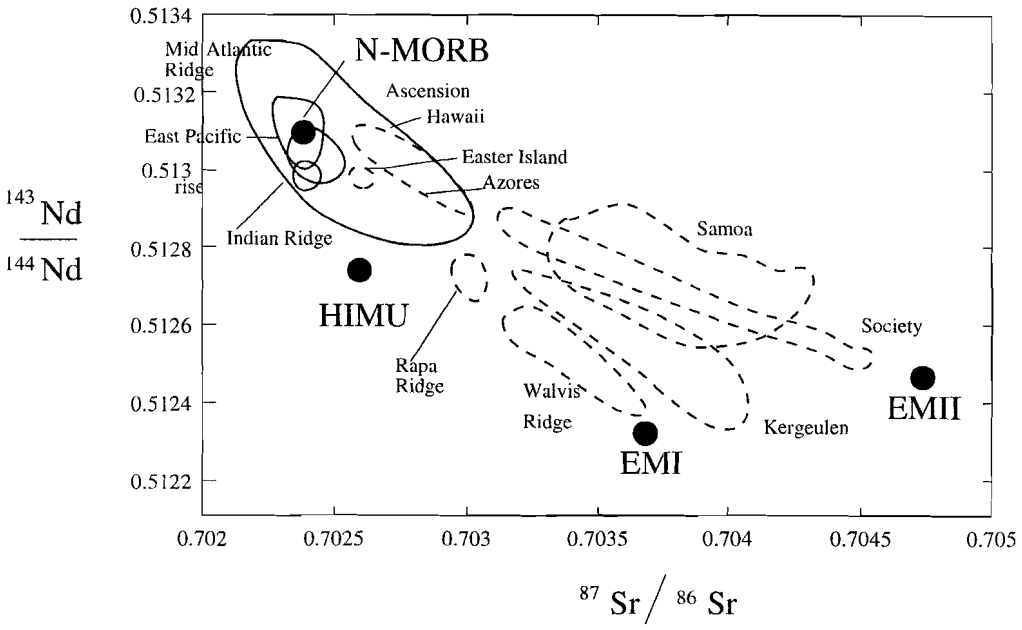

Figure 2.3:
Correlation between the isotope signature of $^{87}Sr/^{86}Sr$ versus $^{143}Nd/^{144}Nd$. The solid lines denote the values found for MORB's whereas the dashed lines indicate the isotope ratios from OIB's. The solid circles represent the mantle components as suggested by Zindler and Hart (1986) which are discussed in the text. The values for the isotope ratios of the different OIB's lie in a trend indicating the mixing between two reservoirs, one reservoir with a high $^{143}Nd/^{144}Nd$ ratio and a low $^{87}Sr/^{86}Sr$ ratio and one reservoir with a low $^{143}Nd/^{144}Nd$ ratio and a high $^{87}Sr/^{86}Sr$ ratio. (sketched after Zindler and Hart, 1986).

of a large region of mantle material, called PREMA which is composed of these four components. Isotope ratios of these possible sources have been added to Fig. 2.3. It is possible to match the observed isotopic heterogeneous samples by mixing those five components.

The data do not allow a determination of the location of the chemical reservoirs. For Hawaii and Iceland there must be a primitive or undepleted reservoir which is believed to be below the 670 km seismic discontinuity in the lower mantle. For the ocean islands such as Tristan, Gough, Kerguelen, St. Helena, the Azores and the Society islands the presence of a depleted mantle reservoir which contains incompletely homogenized crust and entrained sediments is assumed (Hoffman and

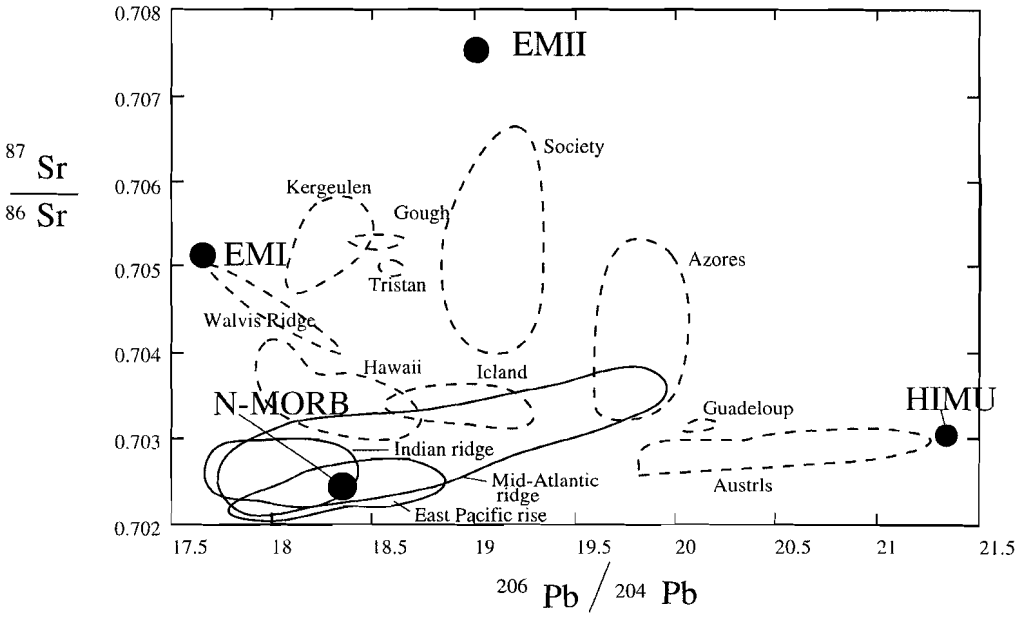

Figure 2.4:
Correlation between the isotope signature of $^{206}Pb/^{204}Pb$ versus $^{87}Sr/^{86}Sr$. As in Fig. 2.3 the solid lines denote the values found for MORB's whereas the dashed lines indicate the isotope ratios from OIB's. The solid circles represent the mantle components as suggested by Zindler and Hart (1986). From the different isotope ratios of the different OIB's one can conclude that the theory which explains the different isotope ratios by the mixing of two reservoirs is over-simplified. (sketched after Zindler and Hart, 1986).

White, 1982; Zindler et al., 1982). Some authors (Allégre and Turcotte, 1983) argue that the isotope signatures must have developed in the continental crust and lithosphere since chemical heterogeneities would not persist long enough in the convecting mantle to develop the observed isotopic variations.
Concluding this chapter one can state that the isotope ratios of $^{143}Nd/^{144}Nd$ and $^{87}Sr/^{86}Sr$ indicate that mantle derived rocks could be generated by mixing of two source reservoirs with different isotopic composition. However taking into account the isotope signature from $^{297}Pb/^{204}Pb$ it becomes clear that there must be at least four source reservoirs available if the observed isotope composition must be explained by mantle mixing.

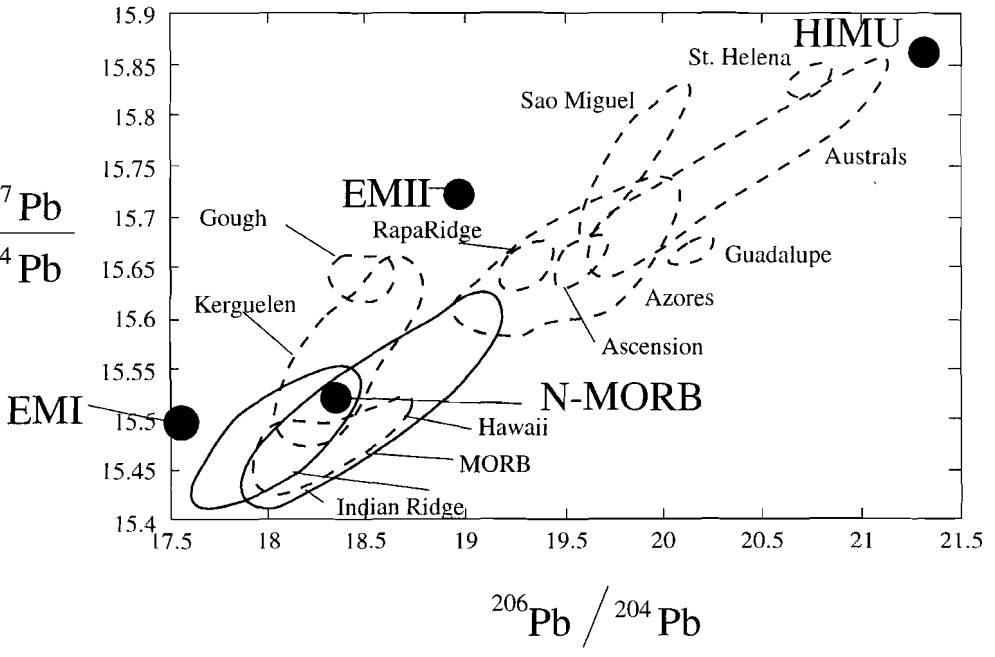

Figure 2.5:
Correlation between the isotope signature of two different Pb ratios. Like in Fig. 2.3 these data seemed to emphasize mixing between two reservoirs (sketched after Zindler and Hart, 1986).

2.3 Possible source mechanism for the observed mantle reservoirs

One potential source mechanism which creates the mantle reservoirs is the ongoing tectonic cycle. The generation and subduction of both oceanic and continental crust are contributing to the differentiation of the Earth's mantle.
The creation of oceanic crust leads to strong concentrations of incompatible elements in the basaltic crust through the process of partial melting. During the lifetime of oceanic plate there is chemical exchange between the plate and the ocean. The plate is furthermore covered with sediments which originate primarily from the continental crust. This leads to a change in the chemical composition of the plate.
As the oceanic lithosphere becomes cooler and thicker it becomes gravitationally unstable and sinks back into the mantle. During this subduction process parts of

the sediments are entrained by the mantle flow.
At a depth of 100 km, the overlaying wedge of the oceanic crust is partially melted due to dehydration (Tatsumi et al., 1983). The rising melted material is forming arc volcanos thus adding material to the continental crust. Magmas from arc volcanos contain both subducted sediments and subducted oceanic crust.
This complex formation of continental crust has led to a concentration of incompatible elements within the continental crust reservoir. As a result of this enrichment of continental plates, the bulk mantle is depleted in exactly these elements.
One conclusion that can be drawn from the complementary nature of the continental crust and the MORB source reservoir is that the material from which the crust has been extracted must be mixed back into the source reservoir.
The question of what happens to the subducted lithosphere is still under discussion. Early publication (Dickinson and Luth, 1971) suggested that the subducted lithosphere lies at the base of the mantle or is underplating continental lithosphere (Oxburg and Pamentier, 1977). Meanwhile it has become clear that a large part of the subducted oceanic lithosphere must have been mixed back into the Earth's mantle (Silver et al., 1988). This conclusion has been drawn from the depleted nature of the MORB reservoir.

2.4 Time scale for the mantle heterogeneities

The most important argument from which it is concluded that heterogeneities within the mantle may be as old as the Earth mantle itself comes from the isotope ratio of Helium (^3He to ^4He).
Observation of ^3He in ocean water in the vicinity of the mid-ocean ridges (Clark et al, 1969; Mamyrinetal et al., 1969)has been interpreted as an indication that the Earth's mantle has not been completely outgased. Contrary to ^4He which is produced by decay of Uranium and Thorium, ^3He is only produced within the Earth in very small quantities and thus nearly all of the ^3He must originate from the formation of the Earth (Kellogg, 1993). Since Helium is a very volatile gas it is assumed to be lost by melting processes which are associated with the formation of lithosphere. Hence, it is not reintroduced into the mantle during the subduction of lithospheric. Mass balance calculations by Allégre (1983) showed that a larger volumetric fraction of the mantle has been outgased than the fraction of the mantle that has been depleted by extraction of continental crust. Concerning the

time-scale for the lifespan of mantle heterogeneities Allégre (1983) concluded that this data require separate components to have existed in the mantle since 150 Myr after the Earths formation, i.e. 4.4 Gyr.
Isotope ratios of magmas found on Iceland and Hawaii speak against the interpretation that the mantle has been degased. These magmas are depleted in Nd, Sr and Pb (like MORB) however they still do have a high $^3He/^4He$ ratio as indicated in Fig. 2.6 (Zindler and Hart, 1986). The origin of these basalts is not clear yet.

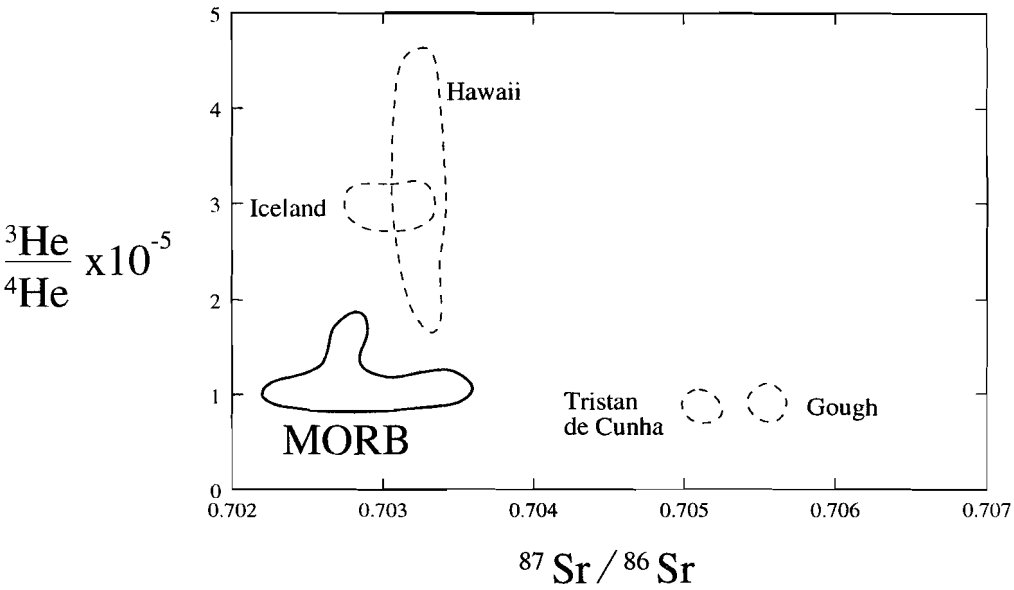

Figure 2.6:
Correlation between the isotope signature $^{87}Sr/^{86}Sr$ and $^3He/^4He$. Unlike MORB the magmas found in Iceland and Hawaii have a high concentration of ^3He.

2.5 Length scale of the mantle heterogeneities

As indicated in Fig. 2.2, 2.3 the Sr , and Pb isotope signatures for MORB's collected in the Southern Hemisphere at the Indian Ridge and those MORB's collected in the Northern Hemisphere (e.g. Mid Atlantic Ridge) are significantly different (Dupret and Allégre, 1983; Hart, 1984). This anomaly, which is referred to in the literature as the *Dupal anomaly*, has persisted for at least 115 Myr. and is the largest scale of heterogeneity observed in the mantle (Weis et al., 1989) .

The smallest scale on which heterogeneities are observed ultimately depends on the efficiency of the solid state diffusion. The length-scale of a heterogeneity that can be destroyed over a geological time scale by solid state diffusion is is estimated to be less than 1m (Sneeringer et al., 1984). An example of such a small scale mantle heterogeneity are the high-temperature peridotites found in Beni-Bousera, Rhonda an Lherz (Allégre and Turcotte, 1986). In the peridotitic matrix of this massive Boudier and Nicolas (1972) found embedded bands of pyroxenite with a basaltic composition which had a width between a few centimeters and a few meters. These heterogeneities may be caused by the *marble-cake* structure of the mantle as sketched in Fig. 2.2. The variation in isotope composition of these bands was found to be comparable to those of the ocean island basalts (Pové and Allégre, 1980; Reisberg and Zindler, 1986). Pearson et al. (1991) interpreted these bands as being formed from melting of subducted oceanic lithosphere.

2.6 References

Allegre, C. J., O. Brevart, B. Dupre and J. F. Minister, Isotopic and chemical effects produced in a continously differentiating convecting earth mantle, Phlios. Trans. R. Soc. London, Ser. A, 297, 447-477, 1980.

Allegre, C.J., T. Staudacher, P. Sarda, and M. Kurz, Constraintns on evolution of Earth's mantle from rare gas systematics, Nature, 303, 762-766, 1983.

Allegre, C. J., and D. L. Turcotte, Implications of a two-compoment marble cake mantle, Nature, 323, 123-127, 1986.

Anderson, D. L., The 650-km mantle discontinuity, Geophys. Res. Lett., 5, 347-349, 1976.

Boudier, F. and A. Nicolas, Fusion partielle gabbroique dans la lherzolite de Lanzo, Bull. Suisse Mineral. Petrol., 52, 39-56, 1972.

Bougault, H., J. L. Joron and M. Treuil, The primordial chondritic nature and large-scale heterogeneities in the mantle: Evidence from high and low partition coefficient elements in oceanic basalts, Phil. Trans. R. Soc. London, Ser. A, 297, 203-213, 1980.

Christensen, U., Mixing by time-dependent convection, Earth and Planetary Scie. Let., 95, 382-394, 1989

Clark, W. B., M. A. Beg, and H. Craig, Exess ^3He in the sea: Evidence for terrestrial primordial helium, Earth Planet Sci. Lett., 6, 213-220, 1969.

Davies, G. F., Geophysical and isotopic constraints on mantle convection : an interim synthesis, J. Geophys. Res., 89, 6017-6040, 1984.

DePaolo, D. J. and G. J. Wasserburg, Nd isotopic variations and petrogenetic models, Geophys. Res. Lett., 3, 249-252, 1976.

Dickinson, W. R. and W. C. Luth, A model of plate tectonic evolution of mantle layers, Science, 174, 400-404, 1971.

Dupret, B. and C. J. Allégre, Pb-Sr isotopic variation in Indian Ocean Basalts and mixing phenomena, Nature, 303, 142-146, 1983.

Gast, P. W., Trace element fractionation and the origin of tholeiitic and alkaline magma types, Geochim. Cosmochim. Acta, 32, 1057-1086, 1968.

Hart, S.R., A large-scale isotope anomaly in the Southern Hemisphere mantle, Nature, 309, 753-757, 1984.

Hilst van der, R., R. Engdahl, W. Spakman und G. Nolet, Tomographic imaging of subducted lithosphere below northwest Pacific island arcs, Nature, 353, 37-43, 1991.

Hilst, van der, R., Seno, S., Effects of relative plate motion on the deep structure and penetration depth of slabs below the Izu-Bonin and Mariana island arcs, Earth. Planet. Sci. Lett., 120, 395-407, 1993.

Hoffman, N. R. A. and D. P. McKenzie, The destruction of geochemical heterogeneities by differential fluid motion during mantle convection, Geophys. J. R. Astron. Soc., 82, 163-206, 1985

Hofmann, A.W und W. M. White, Mantle plumes from ancient oceanic crust, Earth Planet. Sci. Lett., 57, 421-436, 1982.

Kellogg, L. H., Mixing in the mantle, Annu. Rev. Earth PlanetSci., 365-388,

1992.

Kellogg, L. H., Chaotic mixing in the Earth's mantle, Advances in Geophysics, 34, 1-33, 1993.

Machetel, P. and P. Weber, Intermittent layered convection in a model mantle with an endothermic phase-change at 670km, Nature, 350, 55-57, 1991.

Mamyrintal, B. A., I. N. Tolstikhin, G. S. Anufriev and I. L. Kamanskiy, Anomalous isotopic composition of helium in volcainc gases, Dokl. Akad. Nauk SSSR, 184, 1197-1199, 1969.

Oxburg, E. R., E. M. Parmentier, Compositional and density stratification in oceanic lithosphere - causes and concequences, J. Geol. Soc. London, 133, 343-355, 1977.

Pearson, D. G. G. R. Davis, P. H. Nixon, P. B. Greenwood and D. P. Mattey, Oxygen isotope evidence for the origin of pyroxenities in the Beni Bousera peridotite massife, North Morocco: Derivation fom subducted oceanic lithosphere, Earth Planet. Sci. Lett., 102, 289-301, 1991.

Pove, M. and C. J. Allégre, Orogenic lherzolite complexes studied by $^{87}Rb-^{87}Sr$: A clue to understand the mantle convection processes, Earth Planet. Sci. Lett., 51, 71-93, 1980.

Reisberg, L. and A. Zindler, Extreme isotopic variation in the upper mantle: Evidence from Ronda, Earth Planet. Sci. Lett., 81, 29-45, 1986.

Richter, F. M. und D. P. McKenzie, On some consequences and possible causes of layered mantle convection, J. Geophys. Res., 86, 6133-6142, 1981.

Ringwood, A. E., Composition and Petrology of the Earth's Mantle, NewYork, 618pp, McGraw-Hill, 1975.

Silver, P. G., Carlson, R. W. und P. Olson, Deep slabs, geochemical heterogeneity, and the large-scale structure of mantle convection : Investigation of an enduring paradox, Ann. Rev. Earth Planet. Sci., **16**, 477-541, 1988

Sneeringer, M., S. R. Hart and N. Shimizu, Strontium and Samarium diffusion in diopside, Geochim. Cosmochim. Acta, 48, 1589-1608, 1984

Steinbach, V. and D. A. Yuen, Effects of depth-dependent properties on thermal anomalies produced in flush instabilities from phase transitions, Phys. Earth. Pla. Inter., 86, 165-183, 1994.

Tatsumi, Y., M. Sakyama, H. Fukyama, and I. Kushiro, Generation of arc basalt magmas and thermal structure of the mantle wedge in subduction zones, J. Geophys. Res., 88, 5815-5825, 1983.

Tackley, P. J., D. J. Stevenson, G. A. Glatzmeier and G. Schubert, Effects of multiple phase transitions in a 3-D spherical model of convection in the Earth's mantle, J. Geophys. Res., 99, 15877-15901, 1994.

Weis, D. Y. Bassias, I. Gautier and J.-P. Mennessier, Dupal anomaly existence 115 ma ago: Evidence from isotopic study of the Kerguelen plateau (South Indian Ocean), Geochim. Cosmochim. Acta, 53, 2126-2131, 1989.

White, W. M., Sources of oceanic basalts: Radiogenic isotopic evidence, Geology, 13, 115-118, 1985

Zindler, A., Jagoutz, E. and S. Goldstein, Nd, Sr, and Pb isotopic systematics in a three-component mantle: a new perspective, Nature, 298, 519-523, 1982.

Zindler, A. and S. Hart, Chemical geodynamics, Ann. Rev. Earth Sci., 14, 493-571, 1986.

3 The kinematics of mixing

Mechanical mixing of two fluids can be described by a series of stretching and folding processes.

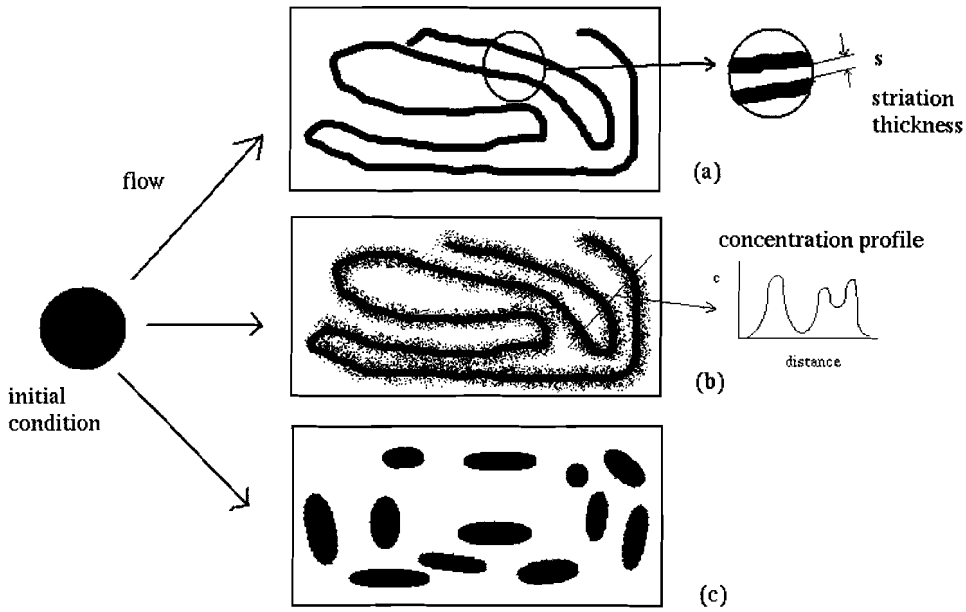

Figure 3.1
Basic processes during mixing of two fluids. The black fluid blob on the left hand side schematically represents the initial condition. In (a) two fluids with similar properties, neglible interfacial tension and no interdiffusion are considered. The initial blob is stretched and folded by the the action of the flow. In (b) the same process is considered but with interdiffusion working on a time-scale comparable to the stretching and folding process. In (c) the blob breaks into smaller fragments due to interfacial tension. (sketched after Ottino, 1989)

The sketch in Fig. 3.1 illustrates this process. The most simple case of two liquids

having similar properties, no interfacial tension and neglible inter-diffusion is shown in Fig. 3.1(a). The initial material region, as sketched on the left hand side of Fig. 3.1, is stretched and folded by the action of the flow. One possible method to quantify the extent to which such a mixing process has proceeded is by measuring the striation thickness s. As sketched on the right hand side of Fig. 3.1(a) the striation thickness s is the typical thickness of one component of fluid being involved in the mixing process.
When interdiffusion operates on a time-scale comparable to those of the mechanical mixing process the boundaries of the fluids become diffuse and the extent of the mixing process is given by level curves of the concentration (Fig. 3.1(b)). These level curves of the concentration, are sketched on the right hand side of Fig. 3.1(b). The distance between local minima and maxima is the equivalent to the striation thickness s, while the interfaces between the two fluids are not sharp anymore but are smoothed by interdiffusion.
In (c) the blob breaks into smaller pieces due to interfacial tension forces. The smaller fragments may again undergo a stretching process and subsequently break up into yet smaller fragments.

In principale an exact description of this mixing process can be given by the location of the interfaces in space and time. Such an exact description is difficult since the velocity fields involved in mixing processes are usually complex. Even relatively simple velocity fields can lead to an exponential growth of the interfacial area (Ottino, 1989). Such an exponential growth is the typical signature of a chaotic flow. It is important to study the conditions under which such chaotic flows are produced since they greatly influence the mixing behavior (Ottino, 1989).

In what follows we will discuss some general properties of 2D and 3D flows which influence the mixing process. This discussion will especially focus on the phenomena of chaotic advection which has first been reported by Aref (1984). Since this description is necessarily incomplete we refer to the comprehensive book by Ottino (1989) for a more complete discussion.

3.1 2D stationary flows

The equations describing the trajectory of a fluid particle in an incompressible,

two dimensional flow can be written as:

$$\frac{dx}{dt} = \frac{\partial \psi}{\partial y}, \frac{dy}{dt} = \frac{-\partial \psi}{\partial x}$$

where ψ is the streamfunction. Regardless of the form of ψ such a system is always can be described as Hamiltonian system (e. g. Aref, 1984). A Hamiltonian system is characterized by the first order differential equation

$$\frac{dq_k}{dt} = \frac{\partial H}{\partial p_k}, \frac{dp_k}{dt} = \frac{-\partial H}{\partial q_k}$$

where p_k and q_k are the components of generalized coordinates p, q and H is the Hamiltonian which is a scalar function of p, q.
In mechanical systems q represents the position and p the momentum. If p, q have N components each, the Hamiltonian system is said to have N-degrees of freedom. It can be shown analytically that the motion of a fluid particle in an incompressible, stationary, two-dimensional flow is a Hamiltonian system with one degree of freedom. Such a system is always integrable and cannot be chaotic (Ottino, 1989) .
From an intuitive point of view all the particles in such a flow will follow closed curves - identical to the streamlines. The particles may move at different velocities at different positions of the streamline. Two particles, moving on one streamline, will never meet nor pass each other, although their separation may vary with position. Conversely, the overturn time, i. e. the time which a particle needs to complete a circuit on its streamline, will depend on the particular streamline.
Because of this regular structure such two-dimensional stationary flows are only poorly mixing.

3.2 2D time dependent flows

If the flow is time dependent it can generally not be shown analytically that the corresponding Hamiltonian system is integrable (Ottino, 1989). This holds even for a simple type of time-dependence like periodic flows. Since there are no analytic tools available, the investigation of such systems has only recently become possible by means of numerical techniques. Depending on the particular structure of the flow and the nature of the time-dependence, regions within the flow which exhibit chaotic particle motion are observed. By chaotic motion we mean that fluid particles having initially an infinitesimal small distance do separate exponentially

in time. The individual streamlines appear to fill entire regions of space. Thus the position of fluid particles may become effectively unpredictable over long time scales (Dombre et al., 1986). Since this chaotic structure strongly enhances the mixing it is of fundamental importance for mixing processes. This phenomenon has been termed *Lagrangian chaos* and was first reported by Aref (1984). He introduced the kinematically prescribed, *blinking vortex* flow which consists of two co-rotating point vortices separated by a fixed distance $2a$, that blink on and off periodically with a constant period T.

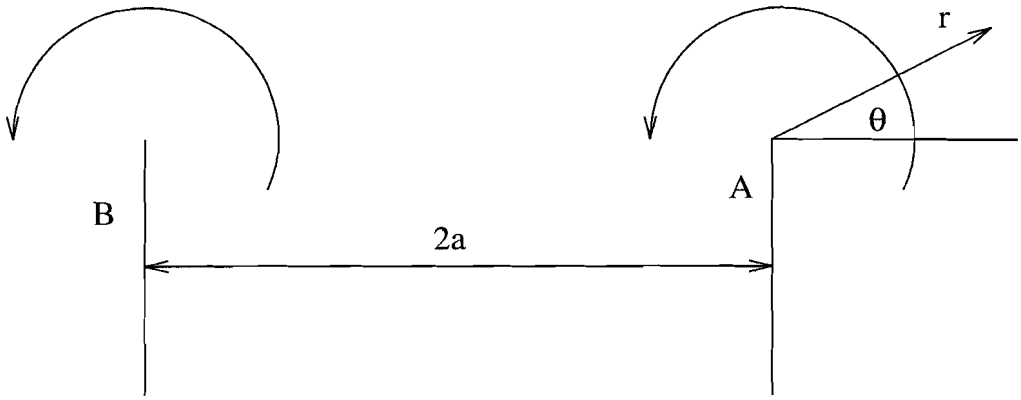

Figure 3.2
Sketch of the blinking vortex system. The two co-rotating vortices in A and B are separated by a distance 2a.

The velocity field due to a single point vortex at the origin is given by: $v_r = 0, v_\theta = \Gamma/2\pi r$, where Γ is the strength of the vortex. Placing two vortices at distances $(-a, 0)$ and $(a, 0)$ in a Cartesian co-ordinate system (Fig. 3.2), the complete mapping, in dimensionless form, is given by:

$$f_i(x,y) = (\xi_i + (x-\xi_i)cos\Delta\theta - ysin\Delta\theta, (x-\xi_i)sin\Delta\theta + ycos\Delta\theta)$$

where ξ_i denotes the position of the vortex i ($i = A, B$), $\Delta\theta = \mu/r^2$, with $\mu = \Gamma T/2\pi a^2$, and $r = ((x-\xi_i)^2 + y^2)^{1/2}$. The parameter μ is the control parameter determining how long each vortex is switched on. This system was investigated by varying the period of the flow, i.e. by starting from the integrable case, $\mu = 0$, and increasing the value of μ. Fig. 3.3. shows Poincaré sections, $t = nT$ with $n =$

$1, 2, 3, ...$, for different values of the perturbation μ . As μ increases chaotic regions form first near the vortices, then in the center region, until for $\mu = 1.5$ they occupy the entire region. This experiment shows that two-dimensional, time dependent flows can exhibit both regions of regular and chaotic Lagrangian structure. Thus parts of the flow may be very efficient in the destruction of chemical heterogeneities while in other spatial regions of the domain mixing proceeds only poorly.

3.3 3D flows

Different from two-dimensional flows three-dimensional steady flows can have a chaotic Lagrangian structure (e.g. Ottino, 1989) and thus can exhibit irregular tracer motion although being stationary in time .
Dombre et al. (1986) investigated one example of such a flow: the kinematically prescribed ABC-flow. This flow is defined in Cartesian coordinates by the velocity field $\vec{v} = (u, v, w)$:

$$u = Asin(z) + Ccos(y)$$

$$v = Bsin(x) + Acos(z)$$

$$w = Csin(y) + Bcos(x)$$

This velocity field is 2π periodic in x, y and z, and is a solution of the Euler equation. Furthermore the ABC flow is a steady solution of the Navier Stokes equation:

$$\vec{v} \cdot \nabla \vec{v} = -\nabla p + \nu \nabla^2 \vec{v} + f$$

where ν the viscosity, p is the pressure and f is some external forcing.

Depending on the values for the three parameters A, B, C, Dombre et al. (1986) investigated the Lagrangian structure of the flow. They found that for C=0 the particle motion was non chaotic, whereas for a wide range of parameter combinations the flow exhibited regions of chaotic Lagrangian structure coexisting with regions of regular particle motion.

This investigation showed that 3D flows, although stationary in time, can exhibit spatial Lagrangian chaos. For the mixing process this coexistence of regular and chaotic regions corresponds to regions which are only poorly mixing and regions

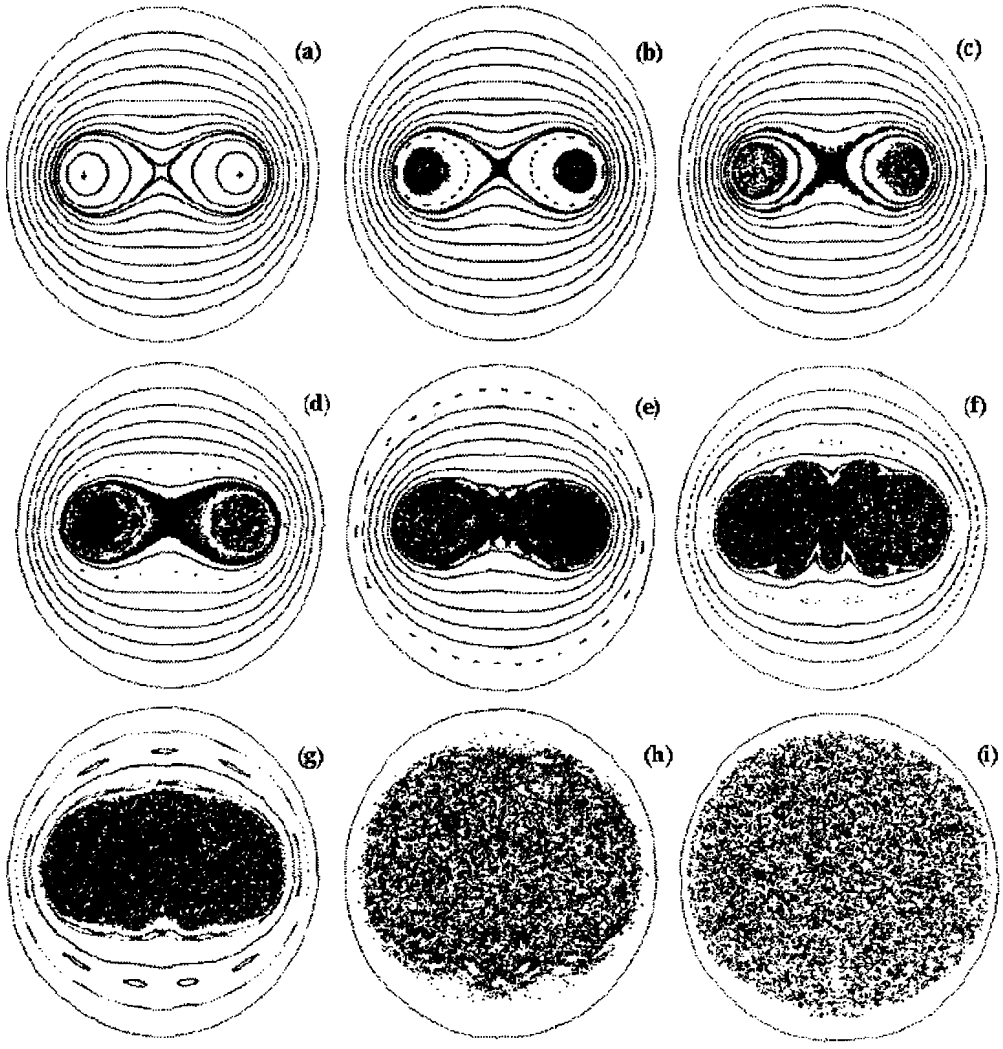

Figure 3.3
Poncaré sections corresponding to 9 different time-dependencies μ: (a) 0.05, (b) 0.1, (c) 0.125, (d) 0.15, (e) 0.20, (f) 0.35, (g) 0.50, (h) 1.0 and (i) 1.5. In (a) the tracer exhibit a regular pattern whereas with increasing value of μ one first observes chaotic islands within the flow near to the center of the vortices. For high values of μ all tracers exhibit Lagrangian chaos. (reproduced from Aref, 1984)

which are very efficient mixing.

For 3D flows, stationary or time-dependent, there does not exist a general applicable theory which constrains the mixing properties. Some flow-fields like those observed in *homogeneous turbulence* or like in special configurations like the *partioned pipe mixer*(Ottino, 1989) have been extensively investigated. But the knowledge gathered from these investigations can not be generalized.

3.4 Statistical description of mixing processes

In order to understand the mixing properties of convective flow fields some method to quantify the mixing rates and the thoroughness of mixing must be found.
Such an analysis also can lead to an distinction between regions where regular mixing occurs and those where chaotic mixing takes place.
As will be discussed further in this chapter there seems to be no general method available which can be used to quantify the mixing behavior of different kinds of flows but there are different methods available which each being well suited to quantify the mixing characteristics of a special class of flows.
One method frequently applied especially in atmospheric sciences is to compute an eddy diffusivity tensor. In this approach a localized ensemble of initial conditions is taken, the growth of the variance of the particles positions about their center of mass is subsequently computed and fitted to a power law of the form $\delta = at^{\nu}$.
This certainly provides a useful description of the divergence of tracers in a flow field that, for example, represent homogeneous turbulence. Nevertheless it fails to adequately characterize the efficiency of mixing in other cases like for convective flow fields .
The variance of the spatial coordinates of a particle cloud is too crude a measure of the clouds geometry. A cloud that is distributed along the circumferences of a disk has a higher variance than a cloud that uniformly fills the disk, even though by any reasonable criterion the latter one is better 'mixed' (Pierrehumbert, 1991) .
This can be overcome by the use of a two-partical correlation function. To compute the correlation function of a cloud of N points, one computes the $N(N-1)/2$ distances between all pairs of points, and then computes the cumulative histogram $H(r)$ giving the number of pairs with distance less than r. Grassberger and Procaccia (1983) have shown that if $log[H(r)]$ versus $log[r]$ has a subrange characterized by a constant slope, then the slope can be interpreted as a lower estimate of the spatial dimension of the set of points. For mixing of a cloud of tracer particles

in a two-dimensional flow, a reasonable criterion for well mixed-ness is that the geometry of the mixed cloud have a dimension approaching 2. Further the slope of H as a function of r provides information on the scales on which mixing has occurred.

We have applied this method successfully in order to characterize mixing in 2D convective flow as presented in chapter 6. Because the computational effort for this method increases with the square of the number of used tracers it proved impractical for quantifying mixing in 3D convective flows where the amount of tracers needed for statistical description of the mixing process is much higher.

A method whose computational effort increases only linear with the number of used tracers and proved useful when quantifying mixing in a spatially bounded domain is the *Box-counting* method. In this method the spatial domain is sub-divided into a finite number of sub-domains (boxes). To quantify the mixing process one keeps track of how many of this sub-domains contain a certain amount of tracer particles. Analytically one can determine the long time limit of a perfectly mixed tracer cloud. By varying the size of the sub-domains one can obtain information about the geometry of the mixing process. We have applied this method to quantify the mixing in 3D time-dependent convective flows as presented in chapter 9.

Another method to quantify the mixing behavior of a flow is the use of strain markers. Such a strain marker usually consists of a small ensemble of tracer which are initially very close together. This strain marker gets deformed when being advected by the flow. By keeping track of the size and orientation of the deformation information about how efficient the flow can destroy heterogeneities can be gathered (e.g. Christensen, 1989). A similar approach can also be used to determine the *finite-time Lyapunov Exponent* as described in Lichtenberg and Liberman (1983). In this method two points initially separated by a small distance δ are considered. Subsequently the trajectories emanating from each point are computed. The distance between the two points is monitored as a function of time. When the distance becomes too large (more than 10δ, say), the trajectories are reinitialized by deflating the two points towards their midpoint, in order to keep the trajectories close to each other. This is required by the definition of the Lyapunov exponent. The total number of deflation applied is kept track of, and multiplied back in at the end of the calculation. One obtains the finite-time Lyapunov estimate of the (largest) Lyapunov exponent by using this data to determine the mean exponential growth rate of the separation between the trajectories. This method has been successfully

applied to mixing in planetary atmospheres by Pierrehumbert (1991).
Although this method proved useful in characterizing Large-scale horizontal mixing in planetary atmospheres (Pierrehumbert, 1991) it seems to be primarily useful to characterize quasi stationary structures and therefore is not well suited to characterize convective mixing in three dimensions.

3.5 References

Aref, H., Stirring by chaotic advection, J. Fluid Mech., 143, 1-21, 1984

Christensen, U., Mixing by time-dependent convection, Earth and Planetary Scie. Let., 95, 382-394, 1989

Dombre, T., U. Frisch, J. M. Greene, M. Hénon, A. Mehr and A. M. Soward, Chaotic streamlines in ABC flows, J. Fluid Mech., 167, 353-391, 1986

Lichtenberg, A. and M. Liberman, Regular and Stochastic Motion, (Springer Verlag, New York), , p.499, 1983.

Ottino, J. M., The kinematics of mixing: Streching, chaos and transport, Cambridge Univ. Press, Chapter 5, 1989

Pierrehumbert, R. T., Large-scale horzontal mixing in planetary atmospheres, Phys. Fluids A, Vol. 3, No. 5, 1250-1260, 1991

4 Basic equations

Convective flow is described by the conservation equations for mass, momentum and thermal energy and an equation of state for the density.
The conservation of mass is expressed through the continuity equation,

$$\frac{\partial \rho}{\partial t} + div \rho \vec{v} = 0, \tag{4.1}$$

the conservation of momentum through the equation of motion,

$$\frac{D(\rho \vec{v})}{Dt} = \rho \vec{F} - \nabla p + \nabla^T \underline{\underline{\sigma}}, \tag{4.2}$$

and the conservation of energy through the heat-transport equation,

$$\rho c_p \frac{DT}{Dt} - T\alpha \frac{Dp}{Dt} = \nabla^T (k \nabla T) + \frac{1}{2}(\underline{\underline{\sigma}} \cdot\cdot \dot{\underline{\underline{\epsilon}}}) + H \tag{4.3}$$

The symbols are:

$\frac{D}{Dt}$: $\frac{\partial}{\partial t} + (\vec{v}\nabla)$
∇ : $(\frac{\partial}{\partial x}, \frac{\partial}{\partial y}, \frac{\partial}{\partial z})$
$\cdot\cdot$: double-scalar product , $\underline{\underline{\sigma}} \cdot\cdot \dot{\underline{\underline{\epsilon}}} = \sum_{i,k} \sigma_{ik} \cdot \dot{\epsilon_{ik}}$
$\dot{\epsilon}$: strain rate tensor, $\dot{\epsilon}_{ij} = \frac{\partial v_i}{\partial x_j} + \frac{\partial v_j}{\partial x_i}$
$\underline{\underline{\sigma}}$: deviatoric stress tensor, $\underline{\underline{\sigma}} = \eta \cdot \dot{\underline{\underline{\epsilon}}}$
η : dynamical viscosity
c_p : specific heat at constant pressure
α : thermal expansion coefficient
ρ : mass density
t : time
$\vec{v}$: velocity vector, $\vec{v} = (u, v, w)^T$
$\vec{g}$: acceleration of gravity, $\vec{g} = (0, 0, g)^T$
p : pressure
H : Internal heating per unit volume
k : thermal conductivity
T : temperature

We assume incompressibility of the fluid in order to simplify the equations. Moreover we apply the Boussinesq approximation assuming that the density is independent of the pressure and that there is only a weak variation of the density with varying temperature ($\alpha \Delta T << 1$). In the Boussinesq approximation it is assumed

that the thermodynamic parameters α, c_p, and η are independent of temperature and pressure.
We use a linear equation of state which has the form:

$$\rho = \rho_o(1 - \alpha_o(T - T_o))$$

where T_o is a reference temperature and ρ_o is a reference density. Applying these approximations to the equation of motion (4.1) we obtain:

$$\rho_o \frac{D\vec{v}}{Dt} = -\rho_o(\alpha(T - T_o))\vec{g} - \nabla p_h + \nabla^T \underline{\underline{\sigma}} \tag{4.4}$$

The equations are non-dimensionalized by using a scaling as introduced by Turcotte et al. (1973). The primed quantities are dimensionless:

$$\begin{aligned}
\vec{x}' &= \frac{\vec{x}}{d} \\
t' &= t\frac{\kappa_o}{d^2} \\
\vec{v}' &= \vec{v}\frac{d}{\kappa_o} \\
\eta' &= \frac{\eta}{\eta_o} \\
T' &= \frac{(T - T_o)}{\Delta T} \\
p' &= p_h \frac{d^2}{\kappa_o \eta_o}, \quad \textit{the hydrodynamic pressure} \\
Pr &= \frac{\nu_o}{\kappa_o}, \quad \textit{the Prandtlnumber} \\
Ra &= \frac{g\alpha\Delta T d^3}{\nu_o \kappa_o}, \quad \textit{the Rayleighnumber}
\end{aligned}$$

where

κ_o $= \frac{k}{c_p \cdot \rho_o}$ the thermal diffusivity,
ν_o $= \frac{\eta_o}{\rho_o}$ the kinematic viscosity,
d : the depth of the system and
ΔT : the temperature contrast in the system is.

Using these dimensionless quantities the equation of motion is:

$$\frac{1}{Pr}\frac{D\vec{v}'}{Dt'} = Ra_T T'\vec{e}_z - \nabla' p' + \nabla'^T \underline{\underline{\sigma}}'. \tag{4.5}$$

Since the Earth's mantle has a very high viscosity the Prandtl number is on the order of 10^{23}. Therefore we can set the left hand side of this equation to zero, thus neglecting inertia in the equation of motion.
Applying the Boussinesq equation to the heat-transport equation (4.3) we neglect the term for adiabatic heating ($T\alpha Dp/Dt$) and the term for viscous dissipation ($\frac{1}{2}(\underline{\underline{\sigma}} \cdot\cdot \dot{\underline{\underline{\epsilon}}})$) .
Thus the three equations (4.1), (4.2), (4.3), which determine our system are:

$$div(\vec{v}') = 0 \tag{4.6}$$

$$0 = RaT'\vec{e}_z - \nabla p' + \nabla^T \underline{\underline{\sigma}}' \tag{4.7}$$

$$\frac{\partial T'}{\partial t'} = -\vec{v}' \cdot \nabla T' + \nabla(\kappa \cdot \nabla T') \tag{4.8}$$

4.1 References

Turcotte, D. L., K. E. Torrance and A. T. Hsui, Convection in the Earth's mantle, Methods in computational physics, 12, 431-454, 1973

5 The numerical methods

5.1 The solution of the Equation for the 2D case

A finite element method as described in Hansen (1984, 1988) has been employed to solve the hydrodynamic equations in two spatial dimensions. The code has been tested carefully and performed well in the Benchmark comparison of Blankenbach et al. (1989).

5.1.1 The equation of motion

Introducing a scalar stream-function,

$$\vec{v} = (u, w) = (\frac{\partial \psi}{\partial z}, -\frac{\partial \psi}{\partial x}) \tag{5.1}$$

implicitly fulfills the continuity equation for incompressible fluids ($div\vec{v} = 0$). Therefore the equation of motion can be written (omitting the primes) as,

$$\nabla^4 \psi = Ra \frac{\partial T}{\partial x} \tag{5.2}$$

Since this equation is symmetric and positive definite there exists a variational principal whose minimizing is equivalent to the solving of the partial differential equation (Zienkiewicz, 1977). Therefore they can be solved by a Rayleigh-Ritz procedure. The equation of motion has the form

$$\underline{\underline{L}}\vec{u} = \vec{f} \tag{5.3}$$

with

$$\underline{\underline{L}} = (\frac{\partial^2}{\partial x^2} + \frac{\partial^2}{\partial z^2})^2$$

$$\vec{f} = Ra \frac{\partial T}{\partial x}$$

Solving the partial differential equation (PDE) (5.16) is equivalent to minimizing Π with:

$$\Pi(\vec{u}) = \int_B [\frac{1}{2}\vec{u}^T \underline{\underline{L}}\vec{u} - \vec{u}\vec{f}]\, dB + (boundary - integral) \tag{5.4}$$

where B is the area on which the PDE should be solved.

The boundary-integral is zero in our case since we used free slip boundary conditions ($\nabla^2\psi = 0$). The replacements: $\Pi(\vec{u}) \rightarrow \Pi(\psi), \underline{\underline{L}} \rightarrow \nabla^4, \vec{f} \rightarrow Ra\frac{\partial T}{\partial x}$ and applying Greens formula twice leads to:

$$\Pi(\psi) = \frac{1}{2} \cdot \int_B [(\frac{\partial^2\psi}{\partial x^2} + \frac{\partial^2\psi}{\partial z^2})^2 + 4 \cdot \frac{\partial^2\psi}{\partial x \partial z}\frac{\partial^2\psi}{\partial x \partial z} - Ra\frac{\partial T}{\partial x}]\, dB \tag{5.5}$$

In order to minimize $\Pi(\psi)$ its variation has to be zero:

$$\delta(\Pi(\psi)) = 0$$

The two-dimensional area on which the solution has to be computed is now subdivided into rectangular elements and the solution of the global system will be composed of the solution of the local elements (marked by ^{e}). In every rectangular element the streamfunction ψ is approximated by ($*$ marks approximated quantities):

$$\psi^{*e} = \sum_{i=1}^{n} \vec{N_i}^e a_i{}^e \tag{5.6}$$

where $N_i{}^e$ is a set of shape-functions, $a_i{}^e$ is the value of ψ at the nodal point i and n is the number of nodes per element. Within the elements we choose an incomplete polynomial of fourth order with 12 free parameters:

$$\begin{aligned}\psi^* = {} & \alpha_1 + \alpha_2 x + \alpha_3 z + \alpha_4 x^2 + \alpha_5 xz + \alpha_6 z^2 + \alpha_7 x^3 \\ & + \alpha_8 x^2 z + \alpha_9 x z^2 + \alpha_{10} z^3 + \alpha_{11} x^3 z + \alpha_{12} x z^3\end{aligned} \tag{5.7}$$

Therefore 12 nodal variables per element are needed. Additional to the streamfunction ψ_k itself we also used the first derivative in x and z direction (the velocities) $\frac{\partial\psi_k}{\partial x}$ and $\frac{\partial\psi_k}{\partial z}$ as variables. The nodal variable therefore forms the vector:

$$\vec{a}_k = \left(\psi_k^*, \frac{\partial\psi_k^*}{\partial z}, -\frac{\partial\psi_k^*}{\partial x}\right)^T.$$

and the shape-functions are:

$$\vec{N}_k = \left(N_k, N_{zk}, N_{xk}\right)^T$$

Using this approximation our local PDE becomes a linear system of the form :

$$\underline{\underline{S}}^e \vec{a}^e = \vec{f}^e \tag{5.8}$$

with

$$S_{ij}{}^e = \int_B \left[\left(\frac{\partial^2 N_i{}^e}{\partial x^2} - \frac{\partial^2 N_i{}^e}{\partial z^2} \right) \left(\frac{\partial^2 N_j{}^e}{\partial x^2} - \frac{\partial^2 N_j{}^e}{\partial z^2} \right) + 4 \frac{\partial^2 N_i{}^e}{\partial x \partial z} \frac{\partial^2 N_j{}^e}{\partial x \partial z} \right] dB$$

$$f_j{}^e = \int_B \left(N_j{}^e Ra \frac{\partial T}{\partial x} \right) dB$$

from which we can determine the values of the nodal variables a_i. The global solution is then composed from the local solution for each element.

5.1.2 The equation of heat transport

Introducing the scalar stream-function (ψ) in the equation of heat transport we obtain the non-dimensional form:

$$\frac{\partial T}{\partial t} - \frac{\partial \psi}{\partial x} \frac{\partial T}{\partial z} + \frac{\partial \psi}{\partial z} \frac{\partial T}{\partial x} = \nabla^2 T. \tag{5.9}$$

In order to solve this equation we apply a Galerin scheme by approximating the temperatures T on a discrete grid with ($*$ marks approximated quantities):

$$T^* = \sum_{i=1}^{n} N_i T_i. \tag{5.10}$$

Here n is the number of nodal points, T_i is the value of the temperature at a nodal point i and N_i is a set of shape functions. Multiplying the partial differential equation with a set of weight functions G_i one obtains:

$$\underline{\underline{B}} \cdot \dot{T}^* + \underline{\underline{A}} \cdot T^* + f = 0 \tag{5.11}$$

with

$$\underline{\underline{B}}_{ij} = \int_B G_j N_i dB \tag{5.12}$$

$$\underline{\underline{A}}_{ij} = \int_B [(\frac{\partial G_j}{\partial x} \frac{\partial N_i}{\partial x} + \frac{\partial G_j}{\partial z} \frac{\partial N_i}{\partial z}) + G_j (\frac{\partial \psi}{\partial z} \frac{\partial N_i}{\partial x} + \frac{\partial \psi}{\partial x} \frac{\partial N_i}{\partial z})] dB \tag{5.13}$$

$$\underline{f}_j = \oint_{R(B)} G_i \frac{\partial T}{\partial n} dR \tag{5.14}$$

We used a rectangular, bilinear type of element to solve this equation as described in Hansen (1988). In order to suppress spurious oscillations we applied an adaptive upwind technique as described in Heinrich et al. (1977).

5.2 The numerical solution of the Equation for the 3D case

To solve the equation for the 3D case a numerical model as described in Houseman (1990) has been used. This model has been extensively benchmarked as described in Busse et al. (1994).
Helmholtz's theorem says that any vector field such as $\vec{v}$ may be expressed as the sum of a component which has zero divergence ($\nabla \times \vec{A}$) and another component which has zero curl ($\nabla\phi$). Because the flow is incompressible we may write:

$$\vec{v} = \nabla \times \vec{A} \tag{5.15}$$

where $\vec{A} = (A_x, A_y, A_z)$ is the solenoidal (zero divergence) vector potential, sometimes referred to as the vector streamfunction. The use of this streamfunction, like in the 2D case, thus automatically satisfies the continuity equation.
Analogously to the 2D case we used the Boussinesq approximation and an infinite Prandtl number has been assumend. Therefore, by using a scaling as described in Houseman (1990) the equation of motion becomes:

$$\nabla^4 \vec{A} = (\alpha \rho_o g/\eta)[\vec{e}_x \frac{\partial T}{\partial y} - \vec{e}_y \frac{\partial T}{\partial x}] \tag{5.16}$$

given a temperature distribution T, the vector streamfunction $\vec{A}$ can thus be obtained by inverting the biharmonic operator ∇^4. Temperature gradients in the y-direction (x-direction) generate the streamfunction component $A_x(A_y)$. As there is no z-component on the right hand side of (5.16) the toroidal streamfunction component A_z is generally zero. A_z may however be non-zero if the viscosity distribution is horizontally varying, or if vorticity is imposed by surface boundary conditions. The vorticity is simply related to the potential function by:

$$\omega = \nabla \times \vec{v} = -\nabla^2 A \tag{5.17}$$

Because the three components of the potential function decouple in this formulation each component of equation (5.16) can be solved independently, using the appropriate boundary conditions on each of the six bounding planes. For example the x-component equation with all six bounding planes being stress-free becomes:

$$\nabla^4 A_x = f_x \tag{5.18}$$

Thus the problem becomes a more generalized 3D biharmonic problem. Houseman (1987) described a fast numerical method for its solutions using vectorized Fast Fourier transforms (FFTs) which is an extension of the long-established methods for the solution of the 2D Poisson equation (e.g. Hockney, 1965; Christiansen and Hockney, 1971). Because of the stress free boundary conditions the Fourier series representation of f_x and A_x at any vertical level contain only cosine terms for the x-dependent part and sine terms for the y-dependent part. If the appropriate 2D horizontal Fourier transform of equation (5.18) is taken the problem becomes:

$$(d^2/dz^2 - k^2)^2 \Theta_x = F_x \tag{5.19}$$

where $\Theta_x(k_x, k_y, z)$ and $F_x(k_x, k_y, z)$ are the transforms of A_x and f_x respectively, and

$$k^2 = k_x^2 + k_y^2$$

where k_x and k_y are the x- and y-direction Fourier component wavenumbers. Equation (5.19) is most easily solved in two stages. First solving:

$$(d^2/dz^2 - k^2)\Omega_x = -F_x \tag{5.20}$$

where Ω_x is the transform of ω_x and then solving

$$(d^2/dz^2 - k^2)\Theta_x = -\Omega_x. \tag{5.21}$$

The finite difference approximation for equation (5.20) and (5.21) may be written as a tridiagonal matrix equation and then solved by the cyclic reduction method. The solution of A_x is then obtained from Θ_x by Fourier synthesis in the two horizontal directions. A_y is obtained in an analogous way.

An explicit time- and space-centered finite difference method is used for the temperature equation.

5.3 Passive Tracers

In order to study the mixing properties of the flow there are two different approaches.
The first approach is to solve a transport equation, analogous to the heat-transport

equation, in a Eulerian form i.e. in a reference frame fixed to the boundaries of the fluid. Although such an approach is ideal for finding the instantaneous rate of deformation at all points within the fluid it is not well suited for determining the accumulated deformation experienced by a material particle or body co-moving with the fluid. This is primarily due to the numerical diffusion caused by the approximation of properties such as velocity, temperature, and concentration between the grid points. This unwanted diffusivity is several orders of magnitude higher than the solid state diffusion as observed for mantle rocks.
Therefore the second approach was chosen to solve the Lagrangian form of the mass-transport equations, integrating the velocity flow field calculated by solving the Eulerian form of the fluid dynamic equations. This leads to a set of first order equations:

$$\partial_t x = u(x,y,z,t), \partial_t y = v(x,y,z,t), \partial_t z = w(x,y,z,t) \tag{5.22}$$

These equations are solved by using a 4th order correct Runge-Kutta method.
For the 2D simulations this was done by post-processing the velocity data from the finite element calculations. Saving every 10th time step we applied a linear interpolation to the velocity data in time in order to calculate the tracer motion. Since the finite element solutions are given as a continuous polynomial function within each element rather than as discrete nodal values, we used the shape functions to determine the velocities in space. This was found to be very accurate and is discussed in Chapter 6.2.
Because of the large amount of data in the 3D time-dependent calculations the tracer motion had to be calculated while iterating the fluid dynamic equations. This has the disadvantage of being forced to repeat the complete set of calculations if the geometry of the tracer cloud should be changed. Apart from that one gains the advantage of having the velocity field or the time integration of the tracer motion available at very fine time intervals. Thus the time step for integrating the tracer motion was chosen to be identical to the time step used for the time-integration of the fluid dynamic equation. In space the velocity values where determined by a tri-linear interpolation. The accuracy has been checked carefully and is discussed in Chapter 7.2.

5.4 References

Blankenbach, B., F. Busse, U. Christensen, L. Cserepes, D. Gunkel, U. Hansen, H. Harder, G. Jarvis, M. Koch, G. Marquart, D. Moore, P. Olson, H. Schmeling and T. Schnaubelt, A benchmark comparison for mantle convection codes, Geophys. J. Int, 98, 23-38, 1989.

Busse, F. H., U. Chrstensen, R. Clever, L. Cserepes, C. Gable, E. Ginnandrea, L. Guillou, G. Houseman, H.-C. Nataf, M. Ogawa, M. Parmentier, C. Sotin and B. Travis, 3D convection at infinite Prandtl number in Cartesian geometry- A benchmark comparison, Geophys. Astrophys. Fluid Dyn., 75, 39-59, 1994

Christiansen, J. P. and R. W. Hockney, *DELSQPHI* a two-dimensional Possion-solver program, Comp. Phys. Comm., 2, 139-155, 1971.

Hansen U. und A. Ebel, Numerical and dynamical stability of Convection Rolls in the Rayleigh number range $10^3 - 8 \cdot 10^5$, Annales Geophysicae, 2, 3, 291-302, 1984a.

Hansen, U. und A. Ebel, Time dependent thermal convection - a possible explanation for a multi-scale flow in the Earth's mantle, Geophys. J., 94, 1988.

Heinrich, J. C., Huyacorn, P. S. und O. C. Zienkiewicz, An upwind finite element scheme for the two-dimensional convective equation, Int. J. Num. Meth. Eng., **11**, 131-143, 1977

Hockney, R. W., A fast direct solution of Poisson's equation unsing Fourier analysis, J. Assoc. Comp. Mach, 12, 95-113, 1965.

Houseman, G. A., TDPOIS, a vector-processor routine for the solution of the three-dimensional Poisson and biharmonic equation in a rectangular prism, Comp. Phys. Comm, 43, 257-267, 1987

Houseman, G. A., Boundary conditions and efficient solution algorithms for the potential function formulation of the 3-D viscous flow equations, Geophys. J. Int.,

100, 33-38, 1990

Zienkiewicz, O. C., The finite element method, McGraw-Hill, London, 3rd edition, 1977.

6 Mixing in the Earth's mantle by thermal convection - a scale dependent phenomenon

J. Schmalzl

and

U. Hansen,

(Department of Theoretical Geophysics, Utrecht University,
Budapestlaan 4, 3508 TA Utrecht, The Netherlands)

This chapter has been published in : *GEOPHYSICAL RESEARCH LETTERS*
VOL. 21, NO. 11, PAGES 987-990, JUNE 1, 1994.

6.1 Abstract

We have investigated the mixing properties of 2D Rayleigh Bénard convection in infinite Prandtl number flows. The mixing properties were monitored by injecting tracer particles into previously calculated flow fields. A particle correlation function H(r) and the corresponding correlation dimension have been used to characterize the mixing efficiency of the flow as function of its vigor and it's structure. We demonstrate that the chosen method captures the mixing process in a detailed manner. Our study suggests that mixing properties of the flow depend on the spatial scale. At Rayleighnumbers $10^6 < Ra < 10^8$ heterogeneities within one circulation cell are destroyed rapidly while two adjacent cells can remain unmixed substantially longer.

6.2 Introduction

The differentiation process within the Earth is likely to be governed by dynamical fractionation mechanisms, i.e. by stretching and folding of the mantle material by a convective flow. An understanding of the mixing properties of convection under mantle condition is necessary in order to properly recognize the implications from isotope geochemistry for the mantle flow. Do isotopic differences, as reported by Zindler and Hart (1986) and others necessarily mean that there exist different reservoirs in the Earth's mantle ? Or can, alternatively, chemical heterogeneities of significant size survive in a vigorously convecting mantle? In spite of the fact that this problem has been addressed in several investigations, including experimental studies (e.g. Solomon and Gollub, 1988),studies on kinematic flow fields (Kellog and Stewart, 1991, Christensen, 1989) and investigations using numerically obtained, dynamical flow fields (Hoffman and McKenzie, 1985, Gurnis and Davies, 1986, Christensen, 1989, Hansen et al. 1992), there is no unique view on the question how a chemical heterogeneity will be dispersed by complex convective flows. Christensen (1989) pointed out that different mixing regimes seem to exist, dependent of the type of the flow. Recent research on thermal convection at high Rayleighnumber has shown that in general a complex time dependent flow prevails, even if the viscosity of the fluid is so high that inertia forces can be neglected (e.g Hansen and Ebel, 1988). The transition to the regime of hard turbulence, as recently discovered in low Prandtl number flows (Castaing et al., 1989, Sano, 1989)

does also appear if the Prandtl number is infinite (Hansen et al., 1990, Yuen et al., 1993). This regime is characterized by a replacement of the mushroom-like plumes by droplet-like instabilities. Any investigation of the mixing properties of such flows faces at least two fundamental difficulties. First, mixing in time dependent convection is theoretically not yet understood. Aref (1984) points out that the paths of tracer particles can not be predicted (i.e. calculated) in time dependent flows even if the actual time dependence of the flow is known. The phenomenon that chaotic tracer trajectories appear in regular flows has been termed 'Lagrangian chaos' and receives currently much attention (Pierrhumbert, 1991). Second, it seems not obvious to find an appropriate way to describe and quantify the mixing process. The approaches which have been used so far by different authors (s. discussion below) do generally not allow to distinguish between mixing properties on different scales. A given flow, however, can operate differently on different scales. For example a flow can homogenize large-scale heterogeneities while small scale anomalies can persists. Oppositely we can envisage a situation in which heterogeneities are only maintained on large scales. In this paper we will explore the mixing efficiency of two dimensional Rayleigh Bénard convection as function of the vigor and of the structure of the flow. As a novelty in the field of creeping convection, we have applied the concept of the correlation-dimension in order to quantify the results. This method was originally introduced by Grassberger and Procaccia (1983) to determine the dimension of a strange attractor and has been used successfully to study the distribution of tracer in Rossby waves by Pierrhumbert (1990).

6.3 Model and methods

We have studied the heat and and mass transport by thermal convection in a two dimensional rectangular domain with a aspect-ratio (λ) of five. As pointed out by several authors (e.g. Bergé, 1989), convection in large aspect ratio domains shows a dramatic increase in complexity when compared to flows in small aspect ratio domains. Taking a box of $\lambda = 5$ seems a reasonable compromise to us, which allows the flow to develop in a fairly unrestricted way, and which keeps computational efforts still manageable. We have studied an incompressible Boussinesq fluid with infinite Prandtl number and stress-free boundary conditions. We assumed fixed temperatures at the bottom and top and adiabatic conditions at the side walls.

By using a streamfunction approach (ψ) we implicitly satisfy the incompressibility condition. In two dimensions, convection in this scenario is described by the following partial differential equations:

$$\frac{\partial^4\psi}{\partial x^4} + 2\frac{\partial^4\psi}{\partial x^2\partial z^2} + \frac{\partial^4\psi}{\partial z^4} = Ra\frac{\partial T}{\partial x} \tag{6.1}$$

(the equation of momentum transport)

$$\frac{\partial T}{\partial t} - \frac{\partial\psi}{\partial x}\frac{\partial T}{\partial z} + \frac{\partial\psi}{\partial z}\frac{\partial T}{\partial x} = \nabla^2 T \tag{6.2}$$

(the equation of heat transport)

The equations have been scaled according to Turcotte et al. (1973). Ra is the thermal Rayleighnumber, T is the dimensionless temperature, t is the non-dimensional time and x, z are the horizontal and vertical non-dimensional coordinates.

This set of equations has been solved with a finite-element method. Details of the solution procedure are given in Hansen and Ebel (1988). The code has been benchmarked extensively and compares well in the study of Blankenbach et al. (1989). For Rayleigh-numbers $Ra < 10^7$ a grid consisting of 30 elements in vertical and 154 in horizontal direction has been chosen. For higher Ra's the resolution has been increased to 50 times 254 elements. In order to resolve the thin boundary layers we have applied local grid refinements at the top and bottom boundaries.

To investigate the mixing properties of the flow we have used up to 16900 (Lagrangian) passive tracer. By post-processing the velocity data from model runs we simultaneous solved the set of first-order equations for the tracer particles:

$$\partial_t x = u(x,z,t), \partial_t z = w(x,z,t) \tag{6.3}$$

which are advanced in time using a 4th order correct Runge-Kutta method. In order to determine the accuracy of the procedure we monitored the deviation of the tracer from a closed streamline in a stationary flow after the completion of a full overturn. The deviation was found to be $O(10^{-4}D)$ where D is the layer-depth. We note that a finite element solution is given as a continuous polynomial function within each element rather than as discrete nodal values as in finite-difference methods.

The characterization of mixing properties has been approached in several different ways. For example the statistical variance of the cloud of tracer about a mean position has been calculated. Envisaging a situation where a cloud of tracers is

streaked out to a line-like feature, demonstrates the incapabilities of this method. In this case the variance is near its maximum soon although the cloud is only poorly mixed. Other authors (e.g. Christensen, 1989) have employed the method of 'box-counting'. Mixing is here characterized by counting the number of boxes which contain a given number of tracer. While this method seems attractive from the computational point of view it does not yield information about the geometry of the tracer cloud. A third approach is to employ strain-markers (groups of tracer being initially close together) and to count the amount of strain-markers which have been strained over a given limit after a given time (Christensen 1989, Kellog and Stewart, 1991). This procedure allows to delineate domains of laminar and turbulent mixing. However this method does also not allow to distinguish between mixing on different scales.

In this paper we have chosen a geometric approach to the mixing problem. We will show that the correlation-dimension as introduced in dynamical system theory by Grassberger and Procaccia (1983) is an appropriate measure to quantify mixing properties of high Rayleigh number convection. Pierrhumbert (1991) has employed this concept to study mixing in travelling Rossby waves. Following him, the correlation dimension is calculated by the following steps: Given a cloud of N particles, we first compute $N(N-1)/2$ distances between all pairs of particles. Then the two-particle correlation-function $H(r)$ is defined as number of pairs with distant less than r. If H(r) is approximated as $H(r) \sim r^{\alpha}$, the exponent α is defined as the correlation-dimension. In Fig 1. the correlation function H(r) is plotted for a tracer configuration as displayed in the top panel.

This figure demonstrates that the correlation function contains important information about the geometry of the tracer cloud. The region over which the tracer cloud is spread out is captured by the x -value of the kink in H(r) (here x= 0.18). The subrange $0 < r < 0.1$ exhibits a slope of 2, thus indicating that the tracer cloud is area-filling (i.e. well mixed) on this scale. The zero slope of the H(r) curve for large values of r reflects that the tracer cloud appears as a point like object from large distances. A subrange of slope 1 corresponds to a tracer configuration which is stretched out to a line.

6.4 Results

In order to demonstrate the capabilities of the method described above, we first

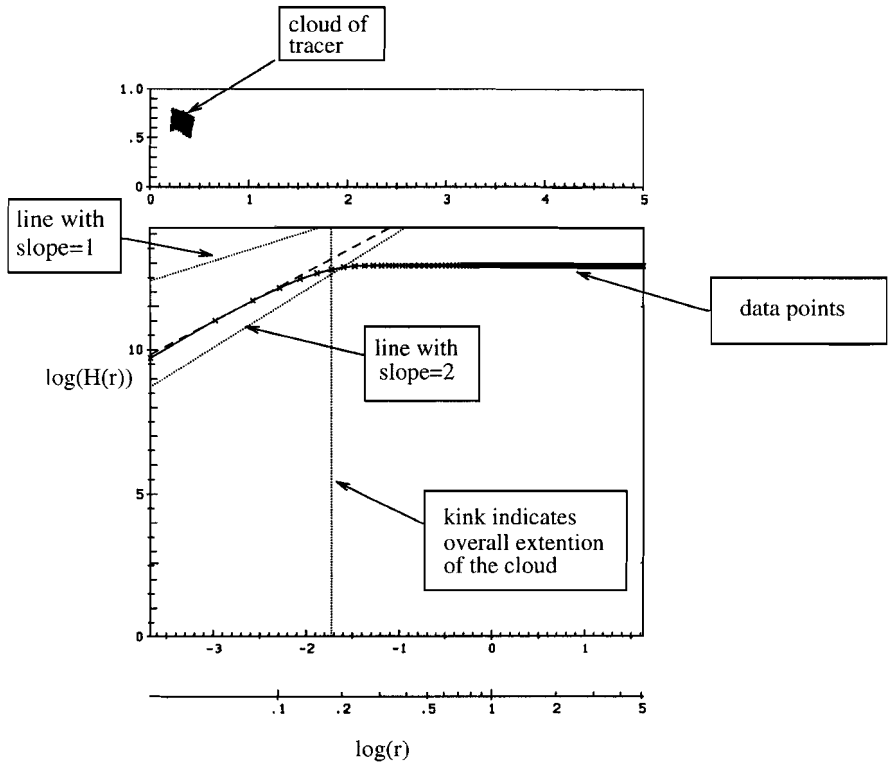

Figure 1:
Initial configuration of 16900 tracer particles (top panel) and corresponding two particle correlation function H(r). For definiton of H(r) see text. Lines with slope 1 and two are shown for reference (dotted). For r ¿ 0.1 the slope of H(r) approaches 2, for larger r the slope of H(r) is 0.

apply it to the problem of mixing in a stationary flow. In stationary flows the streamlines resemble the tracer trajectories. Thus any tracer cloud will remain within a region which is bounded by the two streamlines which are bordering the initial tracer configuration.

Within this region the tracer-cloud will be stretched an folded as demonstrated in Fig. 2. The top panel (a) of Fig. 2 shows the streamlines of a steady-state flow as obtained for Ra = 5000. The dispersion of the tracer particles from the same initial distribution as shown in Fig. 1 is displayed in Fig. 2 (b). Three different situations, after 50, 150 and 900 time steps are shown. Approximately

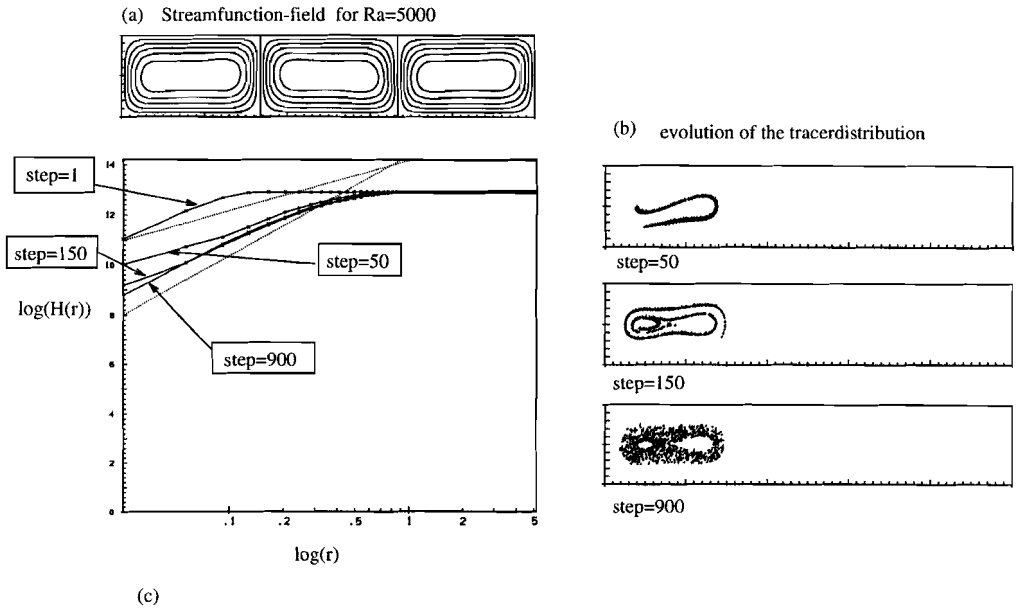

Figure 2: Streamlines (a), snapshots of the tracer distribution (b) and corresponding particle correlation function (c) for a stationary convection at Ra=5000. Initial tracer configuration as given in Fig 1. In Fig (c) the reference values of slope 1 and 2 are denoted by the dotted lines.

70 time steps correspond to one overturn. Initially the rectangular tracer cloud gets streaked out and folded (Fig. 2(b) top panel). The change of the correlation dimension (Fig. 2c) sensitively captures the stretching and folding of the cloud. The situation at step 50 is characterized by a subrange of slope 1 of H(r) for values of r in the range $r < 0.15$, thus demonstrating the stretching of the tracer cloud to a line like structure on this scale. For r in the range of $0.2 < r < 0.5$ the value of the correlation dimension slightly increases, indicating the folding of the stretched tracer cloud to a higher dimensional structure on this larger scale.

Subsequently that part of the subrange which is characterized by a slope of 2, increases on the expense of the slope 1 subrange (step=150), thus indicating the proceeding stretching and folding process. In other words, the scale of those regions in which the tracer form line-like structures is further decreasing. The asymptotic state is reached after about 900 time steps (Fig. 2b, bottom panel). The slope 1

subrange for small r, as has being identified for the previous steps has finally disappeared. The state is asymptotic in a sense, that the spatial density of tracer is time invariant. A further markable feature of this stationary flow is, that the maximum extension as indicated by the kink in H(r) (see above) reaches its maximum already shortly after the start (step = 50). This demonstrates that the advective stirring process first leads to mixing on the largest scale and subsequently on smaller scales. As mentioned by Pierrhumbert (1990) this is fundamentally different from the frequently employed eddy-diffusivity concept since diffusive mixing works on small scales first before the large scale are homogenized.

While investigating the mixing properties of stationary convection is useful to understand basic mixing properties and also in order to demonstrate the capabilities of the method, it probably tells us only little about mixing processes within the Earth's mantle. As today generally agreed on, convection in the Earth's mantle is likely to be time dependent (e.g. Hansen and Ebel 1988). Numerical and laboratory experiments have revealed that even a mild time dependence of the flow results in an enhanced mixing efficiency (Solomon and Gollub, 1988, Christensen 1989). In what follows we will apply the described technique to a series of convecting flows with increasing complexity.

The type of time dependence ranges from simple periodic fluctuations for moderate values of Ra to complex behavior for high Ra as relevant for the Earth's mantle. In the first case we consider time dependent convection at Ra $= 3 \cdot 10^6$ (Fig. 3). The flow exhibits irregular temporal fluctuations while a coherent spatial structure, consisting of three quasistationary circulation centers with superimposed boundary layer instabilities is almost preserved. This type of flow is found to be the typical flow pattern in this Ra-range (e.g. Hansen et al., 1990). In Fig. 4 the evolution of the tracer cloud (same initial condition as in the previous case) is displayed.

Fig. 5 shows the particle correlation function corresponding to the snap-shots as displayed in Fig. 4.

In order to describe the mixing-behavior appropriately, it seems necessary to distinguish between mixing within each individual cell from mixing across the cell boundaries (Hansen et al.,1992). While the boundary layer instabilities greatly facilitate the mixing within each cell, cross cell mixing operates on a much longer time scale. Fig. 4c clearly shows such a situation. Stretching and folding through BLI's has let to a significant deformation of the initial tracer cloud. Only a few tracer are advected across the rising current which separates the convection cells.

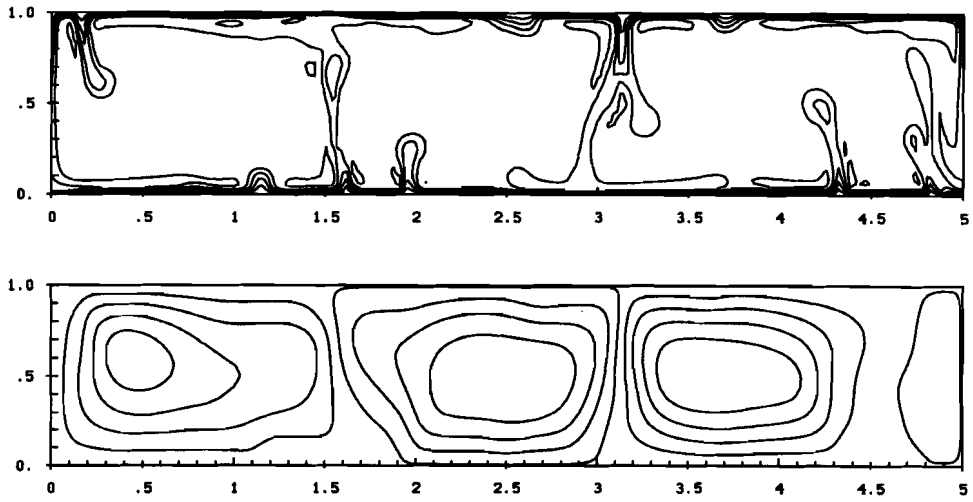

Figure 3:
Snap-shot of the temperature-field (top panel) and the streamfunction (lower panel) at a Rayleighnumber of $3 \cdot 10^6$.

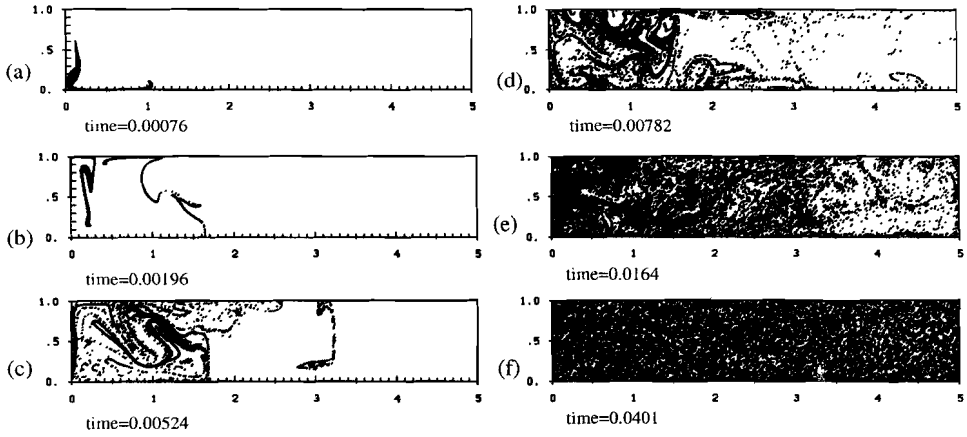

Figure 4:
The distribution of a tracer-cloud of 16900 tracer in a time-dependent flow of $Ra = 3 \cdot 10^6$. Initial tracer configuration as in Fig. 1.

Obviously the major up and down wellings which are bordering the circulation centers hinder the horizontal motion of the tracer, however without acting strictly

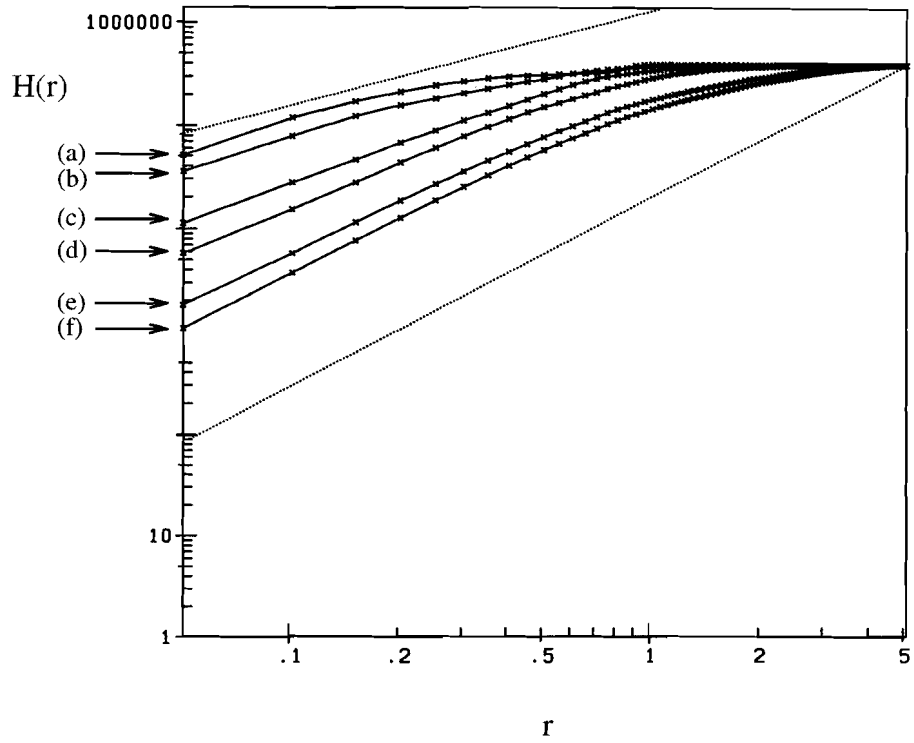

Figure 5:
H(r) for the tracer-distributions shown in Fig. 4. To limit computational effort only every 10th tracer has been used to determine H(r). The dotted lines have a slope of one and two.

as separatrices (Hoffman and McKenzie, 1985). Instead, a diffusional type of transport occurs across the cell boundaries (Fig. 4). Similar behavior has been reported by Solomon and Gollub (1988) from experimental work and numerical studies on kinematic flow fields and has been termed *advection assisted diffusion* (AAD). The motion of the tracer front, slowly progressing by AAD, is clearly reflected by the kink of the H(r) curve moving from small to larger scales (Fig. 5). Already after a short period the correlation dimension approaches a value of 2 for small distances r, thus indicating an effective mixing within each cell. We note here, that for time dependent cases H(r) displays a behavior oppositely to the one observed for stationary flows. In the stationary case the kink in H(r) reaches it's final position

already after half an overturn and the slope reaches its asymptotic value of two only after several overturns. In the time dependent flow field, H(r) almost immediately develops a slope two subrange while the kink slowly moves on towards larger scales. Fig. 6 shows the correlation dimension ($\alpha = \frac{\partial H(r)}{\partial r}$) as a function of time for this experiment for the range r < 0.3.

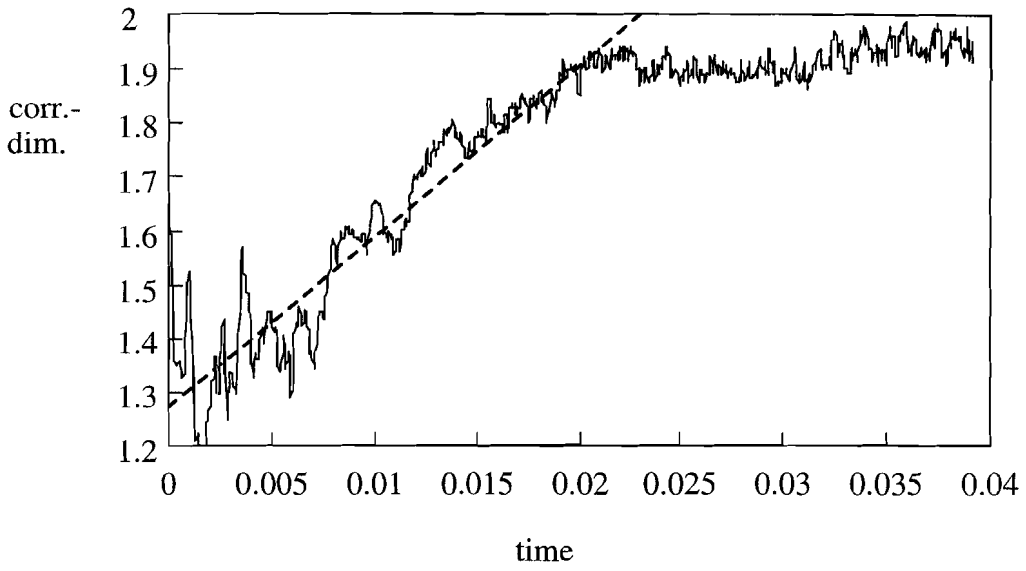

Figure 6:
The time-evolution of the correlation-dimension for a tracer-distribution as shown in Fig. 4. The slope of H(r) was determined for $r < 0.3$.

Two regions can be distinguished: The initial period displaying an increase of the correlation dimension due to the proceeding mixing process, and the final stage characterized by an almost constant slope of H(r). In the following we will use the rate of increase of the correlation dimension ($\frac{\partial \alpha}{\partial t}$) in order to quantify the mixing rate.

To determine the mixing efficiency as function of the Rayleigh number we have conducted experiments at four values of Ra, i.e. $Ra = 3 \cdot 10^6, 10^7, 10^8, 10^9$. Undoubtly the mixing efficiency will be increased with Ra due to the increasing flow velocity. Since the flow velocity depends exponentially on Ra ($v_{rms} \sim Ra^{\beta}$, with β around 2/3), an increase of Ra will lead to an increase of mixing efficiency $\frac{\partial \alpha}{\partial t}$. Moreover the mixing rate will be influenced by structural changes of the flow pattern with increasing Ra. A prominent structural change takes place at the transition to the

regime of hard turbulence at values of Ra around 10^8. Mushroom like plumes, connected from on horizontal boundary to the other disappear at this values of Ra. They are replaced by droplet like instabilities (Sano et al. 1989, Hansen et al. 1990, Yuen et al. 1993). In order to isolate the influences of the structural changes on $\frac{\partial \alpha}{\partial t}$ we used the rms velocity as scaling factor. In Fig. 7 the scaled mixing efficiency increases gradually with Ra but shows a significant step at $Ra = 10^9$.

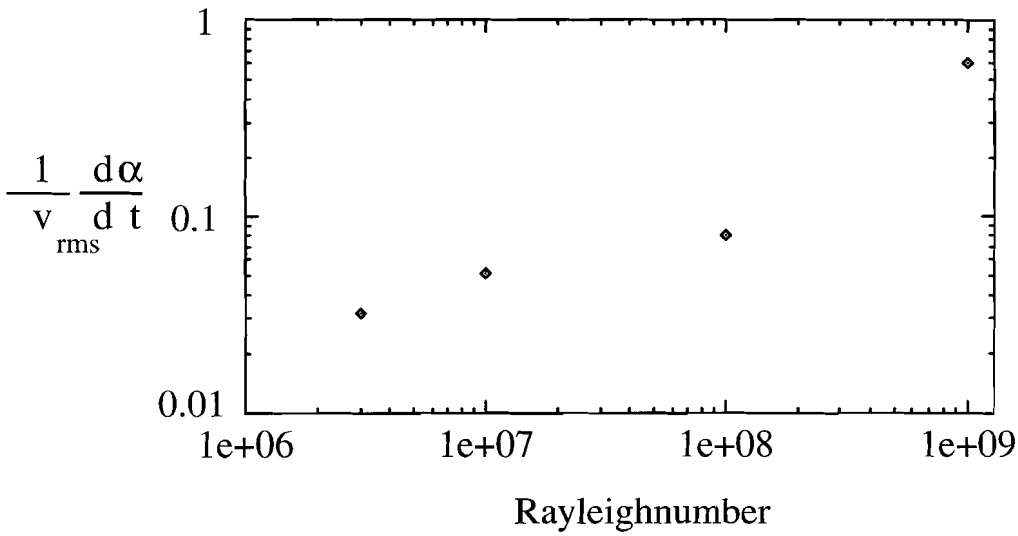

Figure 7:
The increase of the correlation-dimension (α) scaled with the root mean square velocity (v_{rms}) versus the Rayleighnumber.

We address the mild increase at lower Ra to increasing blob activity. The sharp increase is most likely connected with a transition to a new convective regime characterized by the lack of spatial coherent structure i.e. by the lack of connected up- and down-wellings which hinder the tracer motion. Besides the reported kink in the Nusselt-Rayleigh number relation (e.g. Castaing et al., 1989) and a change in the shape of the probability function from gaussian to exponential (Ching, 1991) the abrupt change in the mixing behavior may be considered as a further indication for a transition to a new convective regime.

6.5 Conclusion

We have investigated the dispersion of passive tracer particles by different convective flows. The concept of the correlation dimension has been applied to describe and to quantify the mixing process. Stationary flows have been considered in order to demonstrate the capabilities of the method. This experiments reveal, that mixing by advective stirring tends to homogenize first large scale heterogeneities before small scale mixing occurs. This in contrast to diffusion processes working upwords from small to large scales. Our results confirm the doubts of Pierumbert (1991), namely that eddie diffusivity can be used to parameterize advective mixing appropriately. With regard to the Earth's mantle mixing by advective stirring can thus principally explain a mantle which is mixed on large scales but which is compositionally heterogeneous on small scales. The mixing behavior of highly time depended convection is determined by two distinct processes. Within each quasi stationary convection cell mixing is facilitated by stretching and folding by boundary layer instabilities. The correlation dimension reflects this enhancement of the mixing by developing a subrange two on the scale of the individual cell widths. The transport of the tracer across the sinking and rising cell boundaries operates on longer time scales. The comparatively slow dispersal of the tracer across the cells is reflected by the kink approaching finally a length scale equal to the width of the box. We define mixing as the change of the correlation dimension with time. Besides the increase of the mixing efficiency with increasing Ra due to the higher velocities a further enhancement of the mixing is due to structural effects. Especially at values of $Ra > 10^8$ we have observed a significant enhancement mixing efficiency. This is correlated with a structural change of the flow field of this values of Ra as reported in recent papers on the phenomenon of hard turbulence (Castaing et al., 1989, Hansen et al., 1990, Yuen et al., 1993). This results suggest that in the range of $10^6 < Ra < 10^8$ as appropriate for the Earth's mantle distinct chemical heterogeneities cannot survive more than a few overturns on a scale comparable to a cell width. On the other hand the chemical composition of adjacent convection cells can differ considerably over long time spans. This result is in favor of horizontal compositional heterogeneities rather than vertical ones. We want to emphasize here that either an abrupt change in the style of convection (by phase or compositional boundary) or a gradual change of the mantle flow with depth (increasing viscosity, decreasing coefficient of thermal expansion) can lead to a change of the

mixing behavior and that an inclusion of these effects should be a matter of future research.

6.6 References

Aref, H., Stirring by chaotic advection, J. Fluid Mech., 143, 1-21, 1984

Bérge, P., Chaos and turbulence in Rayleigh Bénard convection, Physica Scripta, 40, 381-385, 1989.

Blankenbach, B., F. Busse, U. Christensen, L. Cserepes, D. Gunkel, U. Hansen, H. Harder, G. Jarvis, M. Koch, G. Marquart, D. Moore, P. Olson, H. Schmeling and T. Schnaubelt, A benchmark comparison for mantle convection codes, Geophys. J. Int, 98, 23-38, 1989.

Castaing, B., G. Gunaratne, F. Heslot, L. Kadanoff, A. Liebchaber, S. Thomae, X. Wu, S. Zaleski und G. Zanetti, Scaling of hard thermal turbulence in Rayleigh-Bénard convection, J. Fluid Mech., 204, 1989.

Ching, E. S. C., Probabilities for temperature differences in Rayleigh-Bernard convection, Phys. Rev. A, 44, 3622-3629, 1991

Christensen, U. R., Models of mantle convection: one or several layers, Phil. Trans. R. Soc., 328, 417-424, 1989.

Grassberger, P. and I. Procaccia, Measuring the strangeness of strange attractors, Physica, 9D, 189-208, 1983

Hansen, U. und A. Ebel, Time dependent thermal convection - a possible explanation for a multi-scale flow in the Earth's mantle, Geophys. J., 94, 1988.

Hansen, U., D.A. Yuen and S. Kroening, Transition to Hard Turbulence in Thermal Convection at Infinite Prandtl Number, Physics of Fluids, a2(12), 2157-2163, 1990.

Hansen, U., D. A. Yuen and S. E. Kroening, Heat and Mass Transport in

strongly time dependent convection at infinite Prandtl number, Geophys. Astrophys. Fluid Dynamics, 63, 67-89, 1992

Hoffman, N. R. A. and D. P. McKenzie, The destruction of geochemical heterogeneities by differential fluid motion during mantle convection, Geophys. J. R. Astron. Soc., 82, 163-206, 1985

Kellog, L. H. and C. A. Stewart, Mixing by chaotic convection in an infinite Prandtl number fluid and inplications for mantle convection, Phys. of Fluids A, 3, 1374-1378, 1991

Pierrehumbert, R. T., Chaotic Mixing of tracers and vorticity by modulated travelling Rossby waves, Geophys. Astrophys. Fluid Dynamics, 58, 285-319, 1990

Pierrehumbert, R. T., Large-scale horzontal mixing in planetary atmospheres, Phys. Fluids A, Vol. 3, No. 5, 1250-1260, 1991

Sano, M. , X. Z. Wu and A. Libchaber, Turbulence in helium-gas free convection, Phys. Rev. A, 40, 6421-6430, 1989.

Solomon, T. H. and J. P. Gollub, Chaotic particle transport in time-dependent Rayleigh-Bénard convection, Phys. Rev A, 38, 6280-6286, 1988.

Turcotte, D. L., K. E. Torrance and A. T. Hsui, Convection in the Earth's mantle, Methods in computational physics, 12, 431-454, 1973

Yuen, D. A., U. Hansen, W. Zhao, A. P. Vincent A. V. and Malevsky, Hard Turbulent Thermal Convection and Thermal Evolution of the Mantle, J. Geophys. Res., in press, 1993

Zindler, A. and S. Hart, Chemical geodynamics, Ann. Rev. Earth Sci., 14, 493-571, 1986.

7 Mixing properties of 3D stationary convection

J. Schmalzl †,

G. A. Houseman ‡

and

U. Hansen †

†(Department of Theoretical Geophysics, Utrecht University,
Budapestlaan 4, 3508 TA Utrecht, The Netherlands),

‡ (Deptartment of Mathematics and Australian Geodynamics Cooperative
Research Centre, Clayton, VIC 3168, Australia)

This chapter has been published in : *PHYSICS OF FLUIDS*
VOL. 7, NO. 5, PAGES 1027-1033, May, 1995.

7.1 Abstract

Passive tracers in steady-state 3-D convective flows with infinite Prandtl number, which is relevant for the Earth's mantle, show a remarkable flow structure. Individual flowlines as shown by Poincare sections of the tracer paths lie on a 2-D surface with distorted toroidal topology. Furthermore, the space occupied by the convecting fluid is filled by a set of these toroidal surfaces nested one within another. The small radius of the innermost toroidal surface approaches zero, defining a closed streamline whose location we have determined in specific cases using numerical solutions. The outermost of the toroidal surfaces coincides with the upper and lower surfaces of the layer and with vertical symmetry planes which separate the flow between neighbouring cells. Both square and hexagonal convection planforms show a triangular cellular structure with triangles defined by ($\pi/2$, $\pi/4$, $\pi/4$) and ($\pi/2$, $\pi/6$, $\pi/3$) respectively. The outer toroidal surface is closed by a horizontal flow line through the middle of the cell. The numerical experiments suggest that streamlines are not generally closed in any small number of orbits. Instead the toroidal surface appears to be progressively filled in by the trace of a single streamline which, in successive orbits, is displaced across the surface without returning to the same path. This flow structure ensures that, while extreme shear strains can occur, particularly in the vicinity of the cell separatrices, mixing of the material only occurs in two dimensions. Tracers initially on one toroidal surface remain on that surface indefinitely. Like for 2-D convective flow, time dependence of the solution appears to be a necessary pre-requisite for thorough spatial mixing to occur.

7.2 Introduction

Creeping convection within the Earth's interior is the mechanism which ultimately governs all geodynamical phenomena, especially the motion of the lithospheric plates.

The mixing properties of this type of convection need to be understood in order to link geochemical observations on isotope ratios of different mantle rocks to mantle dynamics. A better understanding of the chemical evolution of the Earth depends crucially on this link. That has been our motivation to study mixing properties of convection in highly viscous fluids.

Transport properties of passive contaminants in convective flows are also of interest for various other fields of engineering and science. The Lagrangian motion of fluid particles in 2D steady state flow can be treated as an Hamiltonian system with one degree of freedom thus being an integrable system (Ottino, 1989). For Lagrangian motion in 3D flow fields the Hamiltonian formalism does not apply. Arter (1983, 1985) has numerically investigated stationary convective flows with a Prandtl number between 0.1 and 5. and at Rayleigh numbers up to 60000. His results indicate the existence of chaotic motion for low Prandtl number.

A systematic approach to the problem of Lagrangian motion in 3D steady state flows has been taken by Dombre et al. (1986). They investigated numerically and analytically particle paths in a kinematically prescribed flow, the so called Arnold-Beltrami-Childress (ABC) flow. They found the existence of two different regions; one where helical streamlines were closed on a torus and another in which particle paths were found to be chaotic. The extent of the regular and the chaotic regions is strongly dependent on the values of the parameters of the flow field (Ottino, 1989). Since mixing is drastically enhanced within these chaotic regions, their existence is of primary importance. The existence of 'Lagrangian Chaos' in deterministic flow fields has first been reported by Aref (1984) who investigated the motion of tracers in a kinematic 2D time-periodic flow. He also identified regions of regular and chaotic tracer motion.

In experimental work Solomon and Gollub (1988) monitored the dispersion of impurities with a finite diffusivity in 3D convection with a roll pattern. Other authors treated numerically the problem of mixing in 2D time-dependent convective flows which is quite well understood (Christensen, 1989, Hoffman and McKenzie, 1985, Schmalzl and Hansen, 1994).

In this paper we investigate mixing in 3D stationary convection of a Boussinesq fluid at infinite Prandtl number. Using these numerically obtained flow fields, we investigate the dispersion of passive point tracers for a range of Rayleigh numbers, in both square-cell convection and artificially stabilized hexagonal-cell convection. Relevant questions which arise are: Do seperatrix-like structures exist which hinder or block the mass transport ? Does the third dimension in space have a similar effect on the mixing behavior as the time dependence has for 2D flows (i. e. leading possibly to chaotic mixing) ? Are the streaklines of advected tracers closed, and therefore 1- D, are they surface filling (2-D), or even volume filling (3-D) structures ?

The technical details of the numerical model and the tracer algorithm used are described in section 2. Section 3 describes the tracer dispersion in convective flow fields with square or hexagonal pattern and in section 4 the results are discussed.

7.3 Model and Methods

Convection in very viscous incompressible flow is defined by three conservation equations for mass, energy and heat (Richter, 1973; McKenzie et al., 1974):

$$\nabla \cdot \underline{u} = 0, \tag{7.1}$$

$$\eta \nabla^2 \underline{u} + \rho \underline{g} = \nabla p \tag{7.2}$$

$$\frac{\partial T}{\partial t} + \underline{u} \cdot \nabla T = \kappa \nabla^2 T. \tag{7.3}$$

Where $\underline{u}$ is the velocity field, ρ is density, p is pressure, $\underline{g}$ is acceleration due to gravity in $-z$ direction, η is dynamic viscosity, T is temperature and κ is thermal diffusivity. We assumed a Boussinesq fluid with constant physical properties. We have used a linearized equation of state for the density:

$$\rho = \rho_0(1 - \alpha(T - T_0)) \tag{7.4}$$

ρ_o is the density at $T = T_0 = 0$ and α is the coefficient of thermal expansion. The equations are non-dimensionalised by the depth scale d, temperature scale ΔT and timescale d^2/κ. The dimensionless equation are then completely specified by the Rayleigh number

$$R = \frac{\rho g \alpha \Delta T d^3}{\kappa \eta} \tag{7.5}$$

with ΔT being the temperature difference over the box depth d.
The momentum equation (2.2) may be formulated as a biharmonic equation and efficiently solved (Houseman, 1990a; Houseman, 1990b) if the velocity field is expressed in terms of a solenoidal vector potential function $\underline{A}$,

$$\underline{u} = \nabla \times \underline{A} \tag{7.6}$$

where the vertical component of $\underline{A}$ is zero in this problem. The solutions are obtained by using mixed spectral and finite difference techniques with an anisotropic mesh of gridpoints. The code has been benchmarked and compares well in a benchmark study (Busse et al., 1994) Stress-free conditions have been chosen for the velocity along all sides. The side walls are insulating, the top and bottom are set to the constant nondimensional temperatures 0 and 1, respectively.
The motion of the tracers is calculated by post-processing the velocity data from the stationary velocity solution. We solved the set of first order equations for the tracer particles:

$$\partial_t x = u(x,y,z), \partial_t y = v(x,y,z), \partial_t z = w(x,y,z) \tag{7.7}$$

by using a 4th order correct Runge-Kutta method. The accuracy in calculating the tracer paths is determined by two effects: First the interpolation of the velocity components within the elements, which is done by a tri-linear interpolation scheme. The second source of errors is the time integration of the tracer along the path line. In order to separate those two effects we considered a 2D kinematic flow field as described in Christensen (1989) where the velocities are known at every point in space. By comparing the numerical method with the exact analytic value of the velocities we found, with a reasonable small time step dt, the accuracy of the integration to be $O(10^{-4}d)$ after the tracer has completed one full overturn with a diameter comparable to the box depth d. The error in the particle path, which is due to the interpolation of the velocity, has been checked by giving the nodal points of an equidistant grid the appropriate value using the analytic expression for the velocity. A comparison between the motion of a tracer, for which the velocity values for its position had to be interpolated by using the surrounding 8 nodal values, with a tracer where the exact velocities were used has shown that the error in the velocity is about 0.1% for a mesh spacing of $dr = 1/32$. These errors scale as dr^2. This is the same accuracy as obtained with the 2nd order finite difference scheme, so that a higher order interpolation scheme of the data, as obtained from

the finite difference discretisation of the equation, would not add any accuracy.
A detailed study reveals that the integration errors account in a first order for along-path errors whereas the interpolation errors account, again in first order, for deviations that are perpendicular to the path.
From this observation we concluded that using a resolution of $dr = 1/32$ gives sufficient accuracy for approximately 50 overturns whereas a resolution of $dr = 1/64$ leads to accurate results for about 200 overturns.

7.4 Results

7.4.1 Convection with a square pattern

In order to investigate the mixing properties of 3D stationary convection we first considered convection with a square pattern at a Rayleigh number of Ra=30000. The square pattern is a stable solution of the equations (2.1), (2.2) and (2.3) but depending on the initial and boundary conditions, other stable solutions are possible. The topic of pattern selection in 3D Rayleigh-Bénard convection has been intensively treated by several authors (Golubitsky, 1984; McKenzie, 1988). As displayed in Fig. 1 the unit cell reflected ad infinitum in the side boundaries for our calculation is a cubic box with two plume-like upstreams in two diagonally opposite corners and two plume-like downstreams in the two other corners.
Unlike hexagonal convection patterns the up- and down-streams are symmetric in this case (by pointwise reflection in the center of the cell).
Apart from convection with a roll-pattern, which can be treated as a 2D problem and therefore is an integrable Hamiltonian system (Ottino, 1989), the square pattern is the simplest steady state convective pattern which exhibits a 3D structure.
To investigate the mixing behavior of the flow we injected a cloud of passive tracers into the convection cell. For the experiment described below a tracer cloud was placed close to the middle of the cell. Initially the block was centered at (x,y,z) = (0.3,0.4,0.4) and the size of the cubic cloud, which consists of 20^3 tracers, was taken to be 1/10th the box depth. The choice of this position is arbitrary and the effect of the initial position will be discussed below. As displayed in Fig. 2 the tracer cloud gets stretched and performs a spiraling motion towards the vertical side wall to which it was initially closest. The radius of the spiraling motion reaches

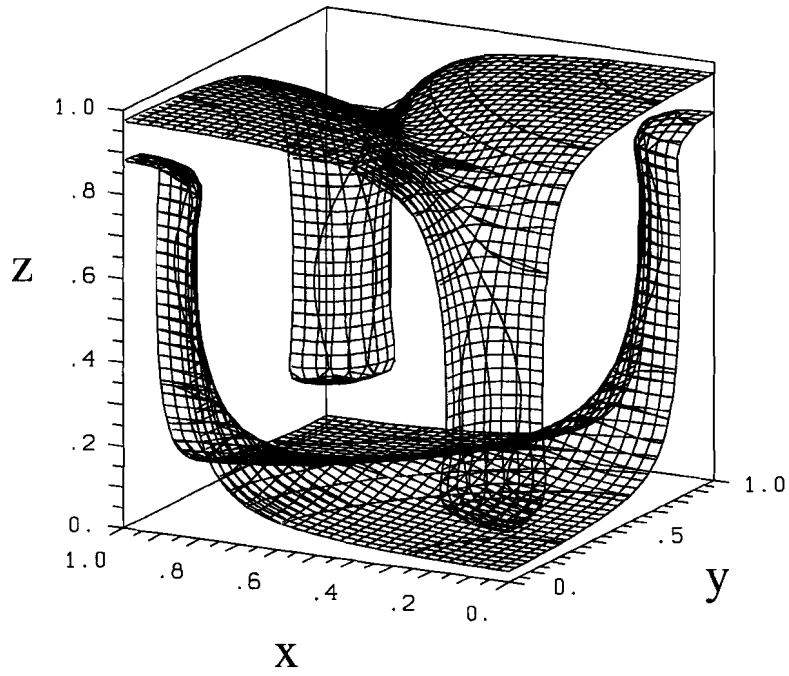

Figure 1:
The temperature field for convection with a square pattern in a cubic box at a Rayleigh number of 1000. The isosurfaces are plotted for T = 0.25 and T = 0.75.

it's maximum when the tracers are close to the sidewall. Depending on the initial position of the tracers (s. below) they almost reach the top and bottom boundary along that circular path before they are transported back to the middle of the cell. An important feature is that the dispersion of the tracers is limited to one quarter of the cell. In the particular the structure of the square pattern symmetry planes exist on which the x- and the y-component of the velocity vanish. Since there is no advective flux across these planes they act as separatrices which separate the square region into four distinct reservoirs. These quarters are defined by two vertical, diagonal surfaces which are also symmetry planes for the temperature field. In Fig. 3, the last plot from Fig. 2 is projected onto the x-y plane in order to clarify the symmetry.

As shown in Fig.4 the tracer follows a pathline which describes as torus embedded

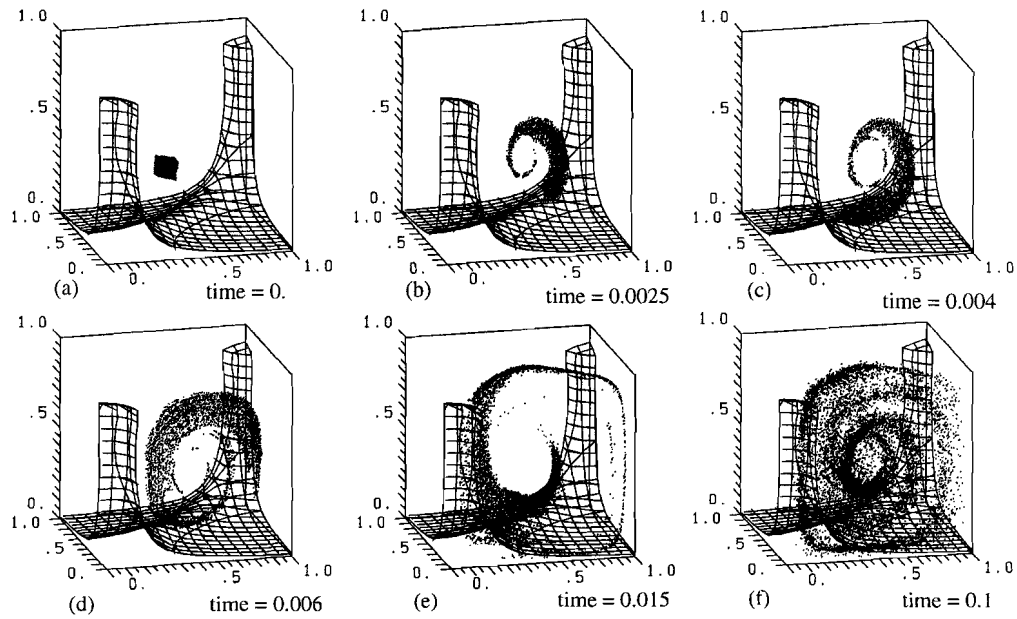

Figure 2:
Dispersion of a cloud of 20^3 tracer in a convective flow-field for $Ra = 3 \cdot 10^4$. The temperature isosurface is for T = 0.75.

in R^3. The time needed for an overturn about the small diameter is by about an order of magnitude longer than the overturn time about the large diameter. In order to clarify if the the tracer motion is restricted to the surface of the torus or is, conversely, volume filling on the torus, we have used the method of Poincare sections. In our case this method monitors the intersections of a streakline in R^3 with one, or more, planes. Poincaré sections can bring out clearly some relevant geometric structures and allow us to display some 3D structures on a 2D plot in a unique way. Fig. 5 shows the Poincaré section for the streakline displayed in Fig.4. The position of the intersecting plane is $y = 0.5$.

The first plot of Fig. 5 displays the intersection points after approximately 4 overturns. The tracer is progressing from larger values of x towards smaller values of x while the radius of spiraling motion is increasing. On the second plot, Fig. 5(b), the tracer has completed one overturn around the small diameter of the torus which corresponds between 9 and 10 overturns around the large diameter of the torus. After the completion of one orbit around the small diameter of the torus the tracer did not rejoin the initial streakline but is shifted to smaller x. Fig. 5(c)

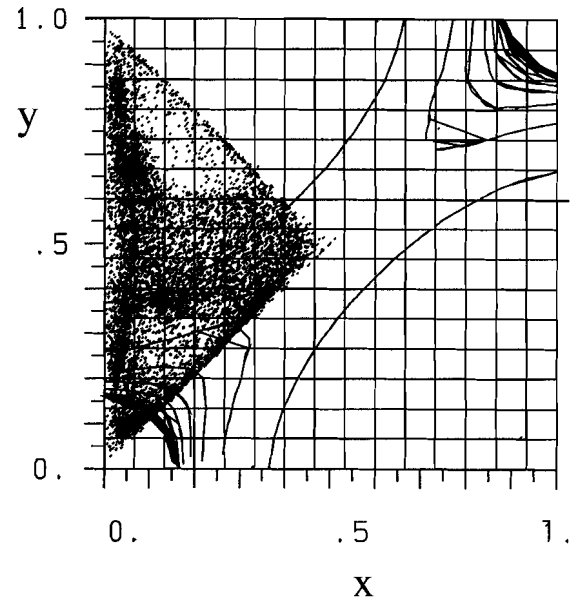

Figure 3:
The tracer configuration as in Fig. 2(f) projected onto the x-y plane.

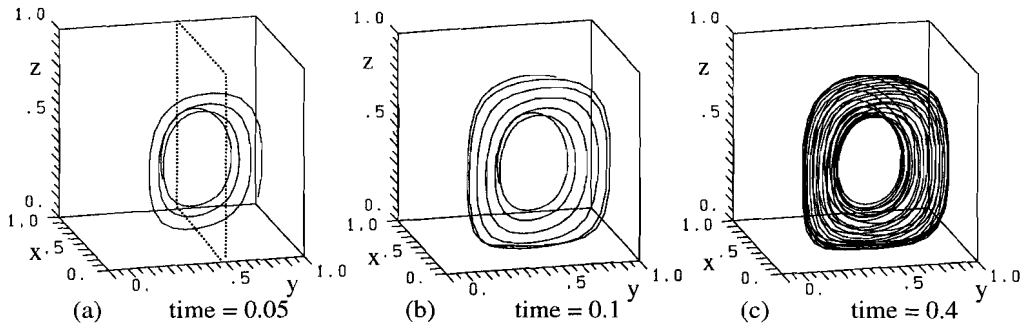

Figure 4:
Streakline of one tracer started at time = 0. at position (0.25,0.35,0.35). The temperature isosurface is for T = 0.75 and the dotted lines in (a) indicating the position of the Poincaré section as plotted in Fig. 5.

finally displays the situation after four orbits around the small diameter.

In order to demonstrate the dependence of the geometric structure of the pathline on the initial position we next describe the motion of 5 particles with different initial positions (p1=(0.5,0.236,0.129), p2=(0.5,0.236,0.1), p3 = (0.5,0.25,0.35), p4=(0.5,0.1,0.05), p5=(0.5,0.2,0.45) and p6=(0.5,0.2,0.5)) their Poincaré sections

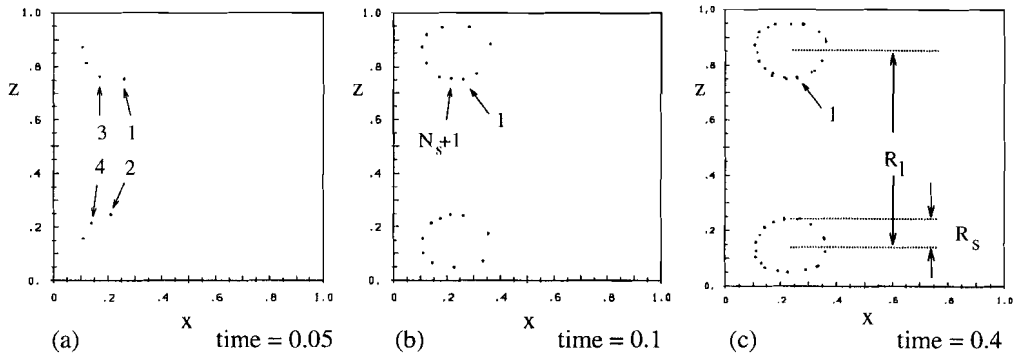

Figure 5:

Poincaré section at y = 0.5 for particle path shown in Fig.4. The '1' denotes the first intersection of the tracer. The successive numbers in (a) denotes the next intersection points. In (b) the tracer has completed one overturn around the small diameter of the torus. In (b) the intersection point $N_s + 1$ is the first intersection after the completion of on overturn around the small diameter of the torus (R_s). In (c) the tracer has completed 4 overturn around the sma ll diameter of the torus. R_l indicates the large diameter of the torus whereas R_s mark s the small diameter of the torus.

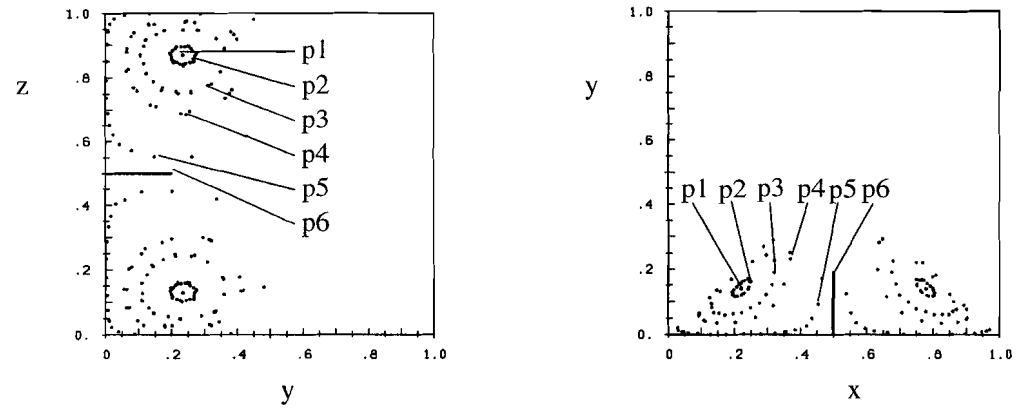

Figure 6:

Poincaré sections at x = 0.5 (a) and z= 0.5 (b) for 6 particles inserted at different initial positions into the flow. The motion of the tracers has been monitored for t = 0 .4 diffusive time-scales.

are shown in Fig.6. The streaklines of p2, p3, p4 and p5 are qualitatively similar to the ones described above, in the sense that they describe torii which essentially dif-

fer only in their small diameter. Tracer p6 has been inserted on the line x=y=0.5, which is a line of reflection symmetry for the velocity field (i.e. u(x,y,z) = -u(1-x,y,1-z) and w(x,y,z) = -w(1-x,y,1-z) within the reservoir). Along that streakline the x- and y -components of the velocity are zero, such that p6 moves to the outer boundary and stays there in a stagnation point. From the nested structure of the torii, it follows that there must be a torus with a small diameter being zero. Experimentally we have determined the position of this torus. The exact position of the degenerate torus depends sensitively on the structure of the flow field and may thus serve as a useful benchmark criterion for the comparison of the spatial structure of solutions obtained with different models. Table 1 shows the position of the intersections with the Poincaré surface in x and z direction for convection with a square pattern at three different Rayleigh numbers. For higher values of the Rayleigh number the degenerate torus is shifted closer to the boundaries and its effective radius (mean distance from torus to axis of symmetry) increases. This effect is presumably related to the thinning of the boundary layer structure with increasing Rayleigh number.

table 1 :
Position of the intersection points of the degenerated torus with the Poincaré sections at x = 0.5 and z = 0.5. The overturn time here refers to one overturn around the large diameter of the torus.

Ra	Δt for one overturn	Poincaré section at x = 0.5	Poincaré section at z = 0.5
10000	0.029	y = 0.226 +/- 0.005 z = 0.144 +/- 0.004	x = 0.241 +/- 0.004 y = 0.147 +/- 0.004
30000	0.0146	y = 0.236 +/- 0.005 z = 0.129 +/- 0.004	x = 0.220 +/- 0.006 y = 0.142 +/- 0.004
100000	0.00721	y = 0.252 +/- 0.005 z = 0.114 +/- 0.004	x = 0.197 +/- 0.004 y = 0.134 +/- 0.004

The time needed for the completion of one overturn around the large diameter of the torus (denoted by T_L) varies only slightly for different tracers which move on

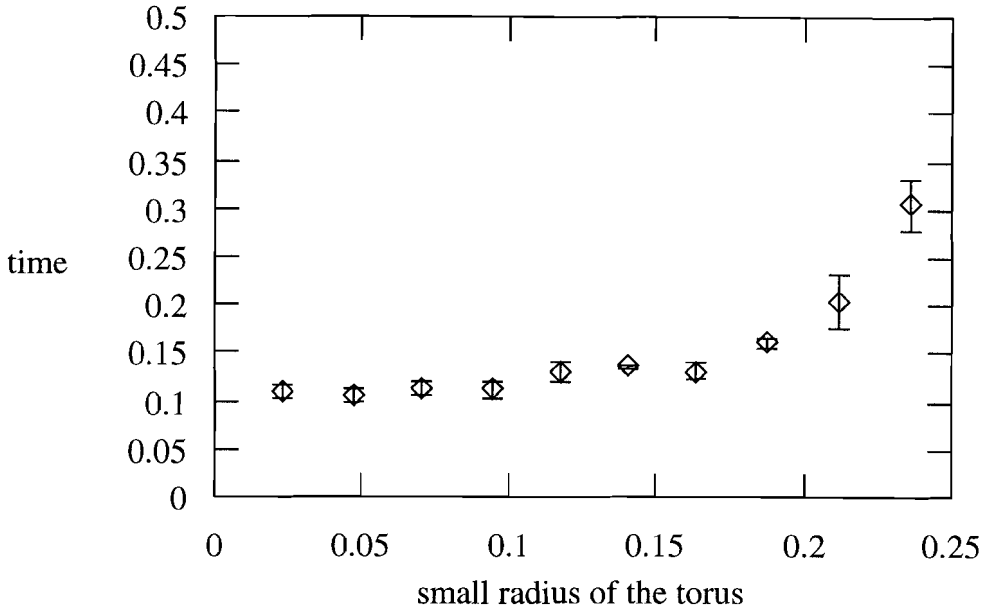

Figure 7:
Time needed for one orbit around the small diameter of the torus for Ra=30000 and increasing small diameter of the torus. Since the shape around the small diameter is far from being an ideal circle the radius is here defined from the intersection of the degenerate torus with the Poincaré section at x=0.5 which is at (y,z) = (0.236,0.129) (see tabl e 1.1) to one side of the wall at (y,z) = (0.,0.129). The error bars denote the mean variation of the measured overturn times for several overturns.

the surface of torii with different small diameter. The time for one orbit around the small-diameter of the torus (denoted by T_S) slowly increases with increasing small diameter, as shown in Fig. 7. The time is increasing by more than a factor of 3 from interior to exterior torii. The ratio $q := T_L/T_S$ indicates whether the streakline is closed or is surface filling. There are three possibilities:

- q is a natural number: the orbit is closed after one overturn around the small diameter
- q is a rational number: the streakline is closed after n overturn around the small diameters; where n is the smallest number with which one has to multiply q to get a natural number
- for q being a irrational real number the streakline is area-filling on the torus

This implies that the vast majority of streaklines will be surface filling, rather than being closed features. Further more those which are closed will typically become connected only after many overturns about the small diameter, while closure after one overturn will be the very exceptional behavior. The q values for the 6 tracer p1-p6 shown in Fig. 6 are : q1 = 0., q2 = 7.58, q3 = 10.69, q4 = 10.81, q5 = 15.94 and q6 is infinite.

7.4.2 Convection with a hexagonal pattern

As a second convective steady state pattern we investigated a hexagonal solution. The calculations have been carried out in a box with aspect-ratio $(x : y : z) = (2. : 2./\sqrt{3.} : 1.)$ which, due to the symmetries shown in Fig. 8, describes the full spatial structure of the flow. For the calculations a mesh size of $129 \cdot 65 \cdot 65$ was chosen. The maximum upwelling velocity is approximately twice the maximum downwelling velocity and the average temperature of the cell is reduced to 0.4283 (0.5 for square planform). The hexagons are unstable with respect to rolls, but are artificially stabilized for this calculation, by suppressing the 2 fundamental modes of the temperature field, which must be zero under hexagonal symmetry.
The Rayleigh number is 30000 and the boundary conditions are identical to the previous described calculations. In order to clarify the spatial structure of the flow we have plotted the isosurfaces for T=0.3 and T= 0.75 in Fig. 9.
The motion of the tracer is similar to those observed in convection with a square pattern: The tracer describes a regular orbit on the surface of a torus. Unlike the square-planform torii, the hexagonal torii have no symmetry axis and the torii are distorted due to the structural differences in the up and down wellings. In Fig. 10 the Poincaré section at z = 0.5 for the motion of 6 different tracers is plotted. The small radius of the torii is bigger near the sheet-like downwelling and smaller close to the plume-like upwelling. The flowfield in the rectangular box exhibits 6 different reservoirs which are strictly separated. The position of the nested torii becomes clear when looking at the geometry of the symmetries solution in Fig. 8. Therefore a complete hexagon would contain 12 distinct reservoirs each including a complete set of nested torii defined by helical paths of individual tracers.

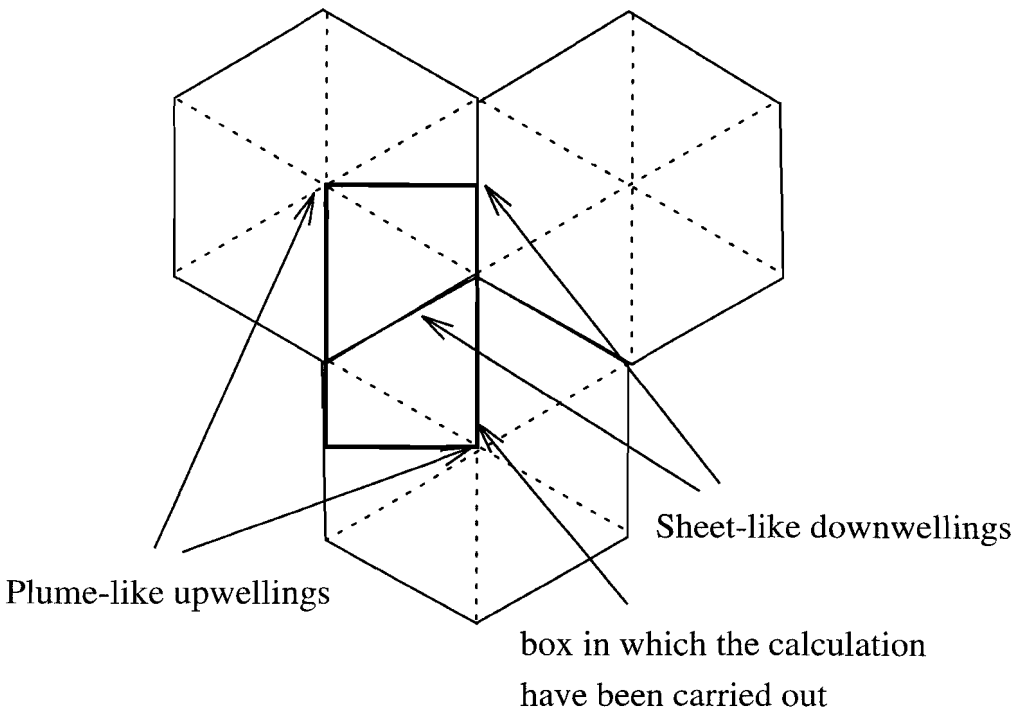

Figure 8:
Sketch of the symmetry for convection with a square pattern. The centers of the hexagons are, in our case, upwellings while the downwelling is concentrated on the vertices (solid lines) of the hexagon. The rectangular area is the unit cell of our calculations.

7.5 Conclusions

In this paper we investigated the motion of passive tracers in stationary flow-fields as obtained from numerical simulation of infinite Prandtl number convection.
For both convection with a square planform and convection with a hexagonal planform our calculation show that the dispersion of the tracers is limited by vertical surfaces which are also symmetry planes for the temperature and velocity field defining different distinct reservoirs. In each of these reservoirs the motion of the tracers is limited to the surface of a set of deformed torii. On each torus the tracers orbit around the large radius of the torus and, with about 1/10th of the frequency, around the small diameter of the torus. Each toroidal surface is defined by the helical orbit of any of the tracers initially embedded in it. The set of torii are nested

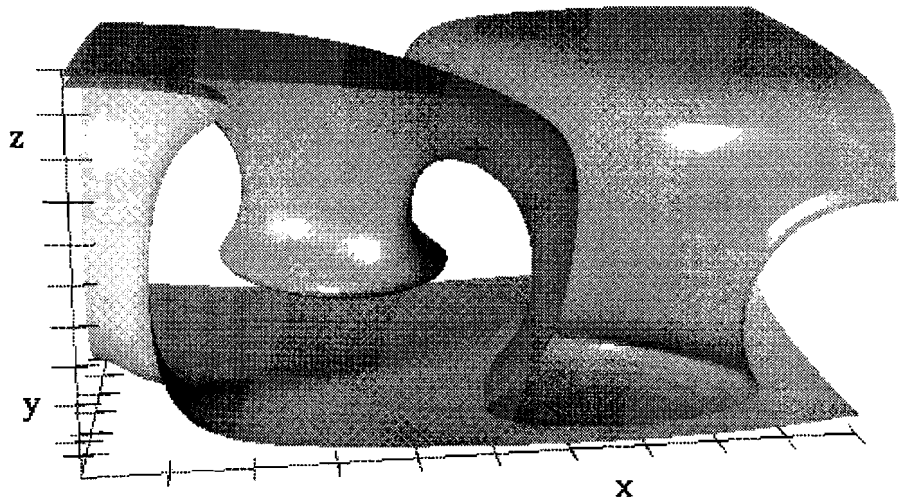

Figure 9:
Temperature isosurfaces for T = 0.3 and T = 0.75. The flow field has two plume-like upstreams in two opposing corners and one more sheet-like downwelling which cuts across the center of the cell.

one within another, and appear to form a complete set that fill the available cell volume. Mixing therefore only occurs on each 2D toroidal surface. In the center of these torii is a degenerate torus with a zero small diameter, thus being a closed streamline.

All the tracers perform a regular motion and we could not identify any chaotic regions as found in convection with finite Prandtl number (Arter, 1983; Arter, 1985) and investigations on the kinematic ABC flow (Dombre et al., 1986).

Concluding, we can state that 3-D steady state convective flows at infinite Prandtl number are only poorly mixing. Mixing in the 3-D steady-state case can be interpreted as a generalisation of mixing in the 2-D steady- state case; in 2-D any tracer remains always on the same streamline, with varying orbital period. In that case, mixing consists of the separation of tracers on adjacent streamlines, until the initial tracer cloud is stretched out around the set of streamlines on which it is originally injected (Hoffman and McKenzie, 1985). In 3-D, however, the initial tracer cloud is not only stretched out by virtue of tracers occupying adjacent toroidal surfaces,

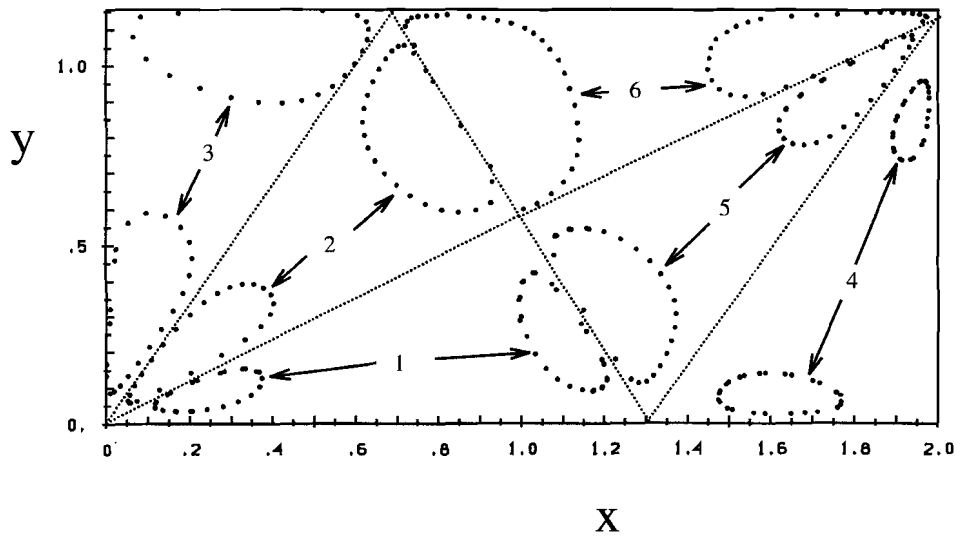

Figure 10:
Poincare section at z= 0.5 for 6 particles inserted at different positions into the flow. The motion of the tracers has been monitored for t = 0.4 diffusive time-scales.

but, the tracers are also efficiently mixed across each of the toroidal surfaces they occupy. In either 2-D or 3-D the mixing is restricted to part of the convection cell. Schmalzl and Hansen (1994) observed much more efficient mixing on all spacial length scales (2-D volume filling) in 2-D convection with an irregular time dependence, and we anticipate that an analogous increase in mixing efficiency will be observed in 3-D time-dependent convection.

7.6 References

Ottino, J. M., The kinematics of mixing: Streching, chaos and transport, Cambridge Univ. Press, Chapter 5, 1989

Arter, W., Ergodic stream-lines in steady convection, Phys. Lett., 97A, 171-174, 1983

Arter, W., Nonlinear Rayleigh-Bénard convection with square planform, J. Fluid Mech., 152, 391-418, 1985

Dombre, T., U. Frisch, J. M. Greene, M. Hénon, A. Mehr and A. M. Soward, Chaotic streamlines in ABC flows, J. Fluid Mech., 167, 353-391, 1986

Aref, H., Stirring by chaotic advection, J. Fluid Mech., 143, 1-21, 1984

Solomon, T. H. and J. P. Gollub, Passive transport in steady Rayleigh-Bénard convection, Phys. Fluids, 31, 1372-1379, 1988.

Christensen, U., Mixing by time-dependent convection, Earth and Planetary Scie. Let., 95, 382-394, 1989

Hoffman, N. R. A. and D. P. McKenzie, The destruction of geochemical heterogeneities by differential fluid motion during mantle convection, Geophys. J. R. Astron. Soc., 82, 163-206, 1985

Schmalzl J. and U. Hansen, Mixing the Earth's mantle by thermal convection: A scale dependent phenomenon, Geophys. Res. Lett., 21, 987-990, 1994.

Richter, F. M., Convection and the large scale circulation of the mantle, J. Geophys. Res., 78, 8735-8745, 1973.

McKenzie, D. P., Roberts, J. M. und N. O. Weiss, Convection in the Earth's mantle : towards a numerical simulation, J. Fluid Mech., 62, 465-538, 1974.

Houseman, G. A., Boundary conditions and efficient solution algorithms for the potential function formulation of the 3-D viscous flow equations, Geophys. J. Int.,

100, 33-38, 1990

Houseman, G. A., The thermal structure of mantle plumes: axisymetric or triple-junction ?, Geophys. J. Int., 102, 15-24, 1990

Busse, F. H., U. Chrstensen, R. Clever, L. Cserepes, C. Gable, E. Ginnandrea, L. Guillou, G. Houseman, H.-C. Nataf, M. Ogawa, M. Parmentier, C. Sotin and B. Travis, 3D convection at infinite Prandtl number in Cartesian geometry- A benchmark comparison, Geophys. Astrophys. Fluid Dyn., 75, 39-59, 1994

Golubitsky, M., Swift, J. W. and E. Knobloch, Symmetries and pattern selection in Rayleigh-Bérnard convection, Physica D, 10, 249-276, 1984

McKenzie, The symmetry of convective transitions in space and time, J. Fluid Mech., 191, 287-340, 1988.

8 Mixing in vigorous, time-dependent 3D convection and application to the Earth's mantle

J. Schmalzl †,

G. A. Houseman ‡

and

U. Hansen †

†(Department of Theoretical Geophysics, Utrecht University,
Budapestlaan 4, 3508 TA Utrecht, The Netherlands),

‡ (Deptartment of Mathematics and Australian Geodynamics Cooperative
Research Center, Clayton, VIC 3168, Australia)

This chapter has accepted for puplication in:
Journal of Geophysical Research, September, 1995.

8.1 Abstract

An understanding of the mechanism of mixing in highly viscous convecting fluids is of crucial importance in explaining the observed geochemically heterogeneous nature of the Earth's mantle. Using constant viscosity numerical experiments, we describe the mixing mechanism of time-dependent Rayleigh-Bénard convection in a three-dimensional rectangular container. Mixing is observed by following the positions of passive tracers advected by the flow. The major mixing mechanisms may be described in terms of the within-cell mixing and the cross-cell mixing. The toroidal flow structure previously observed in steady-state 3D convection systems is perturbed by boundary layer instabilities in the time-dependent experiments, but this toroidal flow structure allows a very efficient exchange of mass between the boundary layers and the core of the convection cell even in the absence of time-dependence. In similar 2D experiments, exchange of mass between boundary layers and core of the convection cell is entirely effected by the boundary layer instabilities. Mixing between neighbouring cells appears much slower in 3D than in similar 2D experiments, perhaps because the 3D cell structure is more stable relative to the boundary layer instabilities. The inferred mixing rates are observed to be relatively insensitive to initial tracer location, but the timescale for mixing, t_m, decreases with increasing Rayleigh number (t_m goes approximately as $Ra^{(-3/2)}$). The timescale of mixing is an important constraint on the large scale structure of the Earth, because large-scale geochemical heterogeneities persist to the present day, implying that the mantle is not well mixed.

8.2 Introduction

One of the most intriguing problems in understanding the evolution of the Earth's mantle is the investigation of the mixing behavior of the convective flow which ultimately drives the tectonic plates. Mixing is the process by which initially separate parts of a fluid are strained and folded so that subsequent sampling is only able to detect a volumetric average of the original discrete components. In the context of the Earth's mantle, the separate components are identified by characteristic isotopic ratios of particular elements and the sampling process is the extraction of partial melt to produce surface volcanic activity.

An understanding, derived from mathematical models, of the physical mixing pro-

cesses in the mantle flow field, would help the interpretation of isotopic and geochemical data from volcanic rocks formed at mid-ocean ridges and oceanic islands. As pointed out by Carlson (1994) in a recent review paper, at least four chemically and isotopically distinct components are observed in mantle derived rocks. These distinct regions may have survived since formation of the core and initial chemical differentiation of the Earth. This early differentiation may have caused the formation of chemically distinct upper and lower mantle, distinguished respectively by Mg/Si either higher or lower than chondritic.

Other prominent causes of differentiation in the Earth's mantle are the ongoing plate tectonic cycle and related crustal formation processes. Plate tectonics coupled with partial melting and volcanism provides a continuing mechanism for planetary differentiation. The plate tectonic cycle also constantly returns chemically distinct material into the mantle. Mixing processes within the mantle act, however, to negate the differentiation caused by the crustal formation processes. If the mixing caused by mantle convection were very efficient, it would have, by now, destroyed evidence of a possible early differentiation event, and produced a relatively homogeneous mantle with a composition identical to that of the original bulk Earth (minus the material now segregated into the core and crust). The survival of major mantle heterogeneities on the time scale of 4.5 Ga demonstrates, however, that some parts of the mantle at least are poorly mixed.

In understanding the chemical composition and evolution of the mantle, the underlying dynamics and physical mixing properties of the convective flow are critical factors.

A widely accepted view of convection in the Earth's mantle is that the mantle is a complex flow which is chaotic in both time and space (Solheim and Peltier, 1990, Hansen et al. 1990, Machetel and Yuen, 1986). As shown in 2D numerical investigations, such flows rapidly destroy chemical heterogeneities (Hoffmann and McKenzie, 1985, Christensen, 1989, Schmalzl and Hansen, 1994) thus being unable to explain geochemical observations which suggest that the mantle must be heterogeneous on scales from tens of meters up to thousands of kilometers (Zindler and Hart, 1986, Carlson 1994). Some authors have resolved this apparent contradiction by concluding that the mantle is layered, so that mixing, while efficient, mainly occurs within layers and not between (Hoffman and McKenzie, 1984). Such a conclusion is difficult to verify, and in some cases seems inconsistent with other evidence from seismic tomography of the mantle which appears to show subducted

slabs penetrating into the lower mantle (Creager at al., 1986).
Jeanloz (1989) suggested that an increase in the Fe/(Fe+Mg) ratio of 3 to 5% at the 670km level would stabilize the 670 km discontinuity as a barrier to convection, preventing mixing between upper and lower mantle.
Numerical investigations carried out so far lack, however, the third spatial dimension, which profoundly changes the mixing characteristics of the flow. One fundamental difference between 2D and 3D mixing is indicated by the observation that Lagrangian motion in 2D stationary flows is integrable, and therefore mixing is very poor. Three-dimensional flows can, however, exhibit a chaotic Lagrangian structure, even if the flow is stationary in time (Ottino, 1989).
In a previous paper (Schmalzl et al., 1995) we investigated the mixing properties of stationary 3D convective flows for highly viscous flow at high Prandtl number, as applicable to the Earth's mantle. Although we did not identify any examples where the Lagrangean particle paths are chaotic, the mixing process is very different to that of analogous 2D simulations. In summary, we found that an individual tracer orbits around a distorted toroidal surface embedded in the flow region (Fig. 1). Any tracer in the solution space lies on such a torus, and the entire solution space is filled with an infinite set of such torii, nested one within another (Fig. 1).

Each of these torii is characterised by the value of its small diameter, which increases continuously from zero. In these stationary solutions any tracer particle remains always on the toroidal surface with which it is first associated. Although tracers move on 2D surfaces, tracers which are initially close together may end up widely separated within the same convection cell. There is no mixing between adjacent cells in the stationary flow. In this paper we describe further mixing calculations in which we simulate fully developed 3D time-dependent flows, in a Rayleigh number range which is relevant to convection in the Earth's mantle.
We do not here include internal heating, non-Newtonian rheology, or any spatial variation of material properties like viscosity or thermal expansion coefficient. We limit these investigations to the more fundamental case of thermal convection in a rectangular box heated solely from below.
In section 2 we describe the numerical method used. In section 3 we summarise results from our 3D calculations and qualitatively compare them with mixing results from similar 2D calculations. Section 4 investigates the effect of varying the initial tracer distribution, and section 5 discusses the influence of the vigor of convection

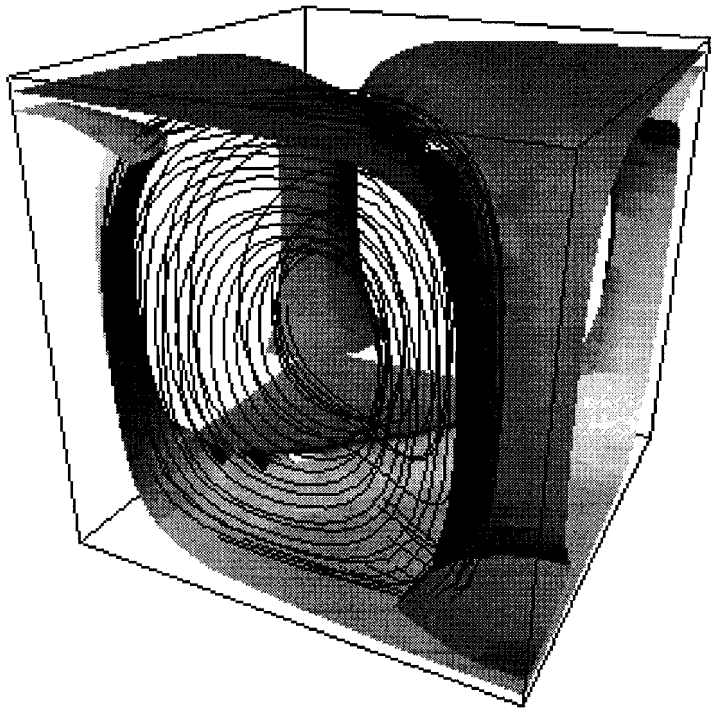

Figure 1:
Stationary thermal convection at a Rayleigh number of 100000. As indicated by the two temperature isosurfaces for T=0.3 and T=0.7 this flow exhibits a square pattern with two warm upstreams in two opposing corners and two cold downwellings in the two other corners. The black line shows the trajectory of a passive tracer. The tracer motion is restricted to the surface of a deformed torus.

on the mixing process.
In conclusion, section 7 discusses possible implications for our understanding of how mixing in the mantle proceeds.

8.3 Model and Methods

Convection in a very viscous incompressible flow is defined by three conservation

equations for mass, momentum and energy (Richter, 1973; McKenzie et al., 1974):

$$\nabla \cdot \underline{u} = 0, \tag{8.1}$$

$$\eta \nabla^2 \underline{u} + \rho \underline{g} = \nabla p \tag{8.2}$$

$$\frac{\partial T}{\partial t} + \underline{u} \cdot \nabla T = \kappa \nabla^2 T. \tag{8.3}$$

Where $\underline{u}$ is the velocity field, ρ is density, p is pressure, $\underline{g}$ is acceleration due to gravity in $-z$ direction, η is dynamic viscosity, T is temperature and κ is thermal diffusivity. We assume a Boussinesq fluid with constant physical properties, except that density is linearly dependent on temperature:

$$\rho = \rho_0(1 - \alpha(T - T_0)) \tag{8.4}$$

where ρ_o is the density at $T = T_0 = 0$ and α is the coefficient of thermal expansion. The equations are non-dimensionalised by the depth scale d, temperature scale ΔT and timescale d^2/κ. The dimensionless equations are then completely specified by the Rayleigh number

$$Ra = \frac{\rho g \alpha \Delta T d^3}{\kappa \eta} \tag{8.5}$$

with ΔT being the temperature difference between upper and lower surfaces. Internal heating is assumed negligible.

For the 2D calculations this set of equations has been solved with a finite-element method. Details of the solution procedure are given in (Hansen and Ebel, 1988). The code has been benchmarked for accuracy, as documented in the study of (Blankenbach et al., 1988).

For the 3D calculations the momentum equation (2.2) is formulated as a biharmonic equation and solved by expressing the velocity field in terms of a solenoidal vector potential function $\underline{A}$ (Houseman, 1987; 1990a)

$$\underline{u} = \nabla \times \underline{A} \tag{8.6}$$

where the vertical component of A is zero in the constant viscosity problem with homogeneous boundaries. The solutions are obtained by using mixed spectral and finite difference techniques with an anisotropic mesh of gridpoints. The code has been tested for accuracy as described in the benchmark study of Busse et al. (1994). On horizontal and vertical bounding surfaces, the normal component of velocity and the tangential components of traction are set to zero. The side

walls are insulating and the top and bottom surfaces are set to the constant non-dimensional temperatures 0 and 1, respectively.
Velocity components are obtained on the regular mesh at discrete time levels $t_i, i = 1,2,...$ (where $\Delta t_i = t_{i+1} - t_i$), by inversion of Equation (2.2). The Lagrangean particle paths are calculated by using a 4th order correct Runge-Kutta method to integrate particle locations from time level t_i to time level t_{i+1}, using the average of the velocity fields at those two levels, and

$$\partial_t x = u(x,y,z), \partial_t y = v(x,y,z), \partial_t z = w(x,y,z) \tag{8.7}$$

The accuracy of calculated tracer paths is discussed by Schmalzl et al. (1995).

8.4 Results

As a qualitative example of how mixing proceeds we first describe the mixing of a patch of passive tracers in a 4x4x1 tank. The Rayleigh number for this experiment is $8 \cdot 10e5$ and the solution is computed on an isotropic mesh of 129x129x33 grid points. Before the tracer experiment begins, the temperature and velocity field has first been allowed to evolve over a time interval of 0.5 thermal diffusion times, in order to diminish any transient effects due to the arbitrary initial temperature field.
Fig. 2 displays the temperature isosurface for T=0.3 (dark isosurface) and T=0.7 (light-grey isosurface). Parts of the T=0.3 isosurface in the upper thermal boundary have been removed from the plot in order to reveal structures that would otherwise be obscured. The Figure shows four major upwelling plumes which are connected by hot sheet-like structures along the basal surface. The sheets form a triple junction near the middle of the cell. For a detailed description of the thermal structure of plumes we refer to Houseman (1990). The cold downwellings are concentrated at irregular locations near the sidewalls of the box.
Observing the time evolution of the flow we note that, although the flow has an apparently chaotic time signal, the spatial cell structure is persistent. As observed in 2D flows, the major up and down wellings typically undergo irregular oscillations of relatively small amplitude about almost fixed locations. Occasionally (and unpredictably) there is a significant reorganisation of cell structure, if one cell splits into two, or two cells merge. Superimposed on the large scale cell pattern are boundary layer instabilities which circulate with the large scale flow. They account for the

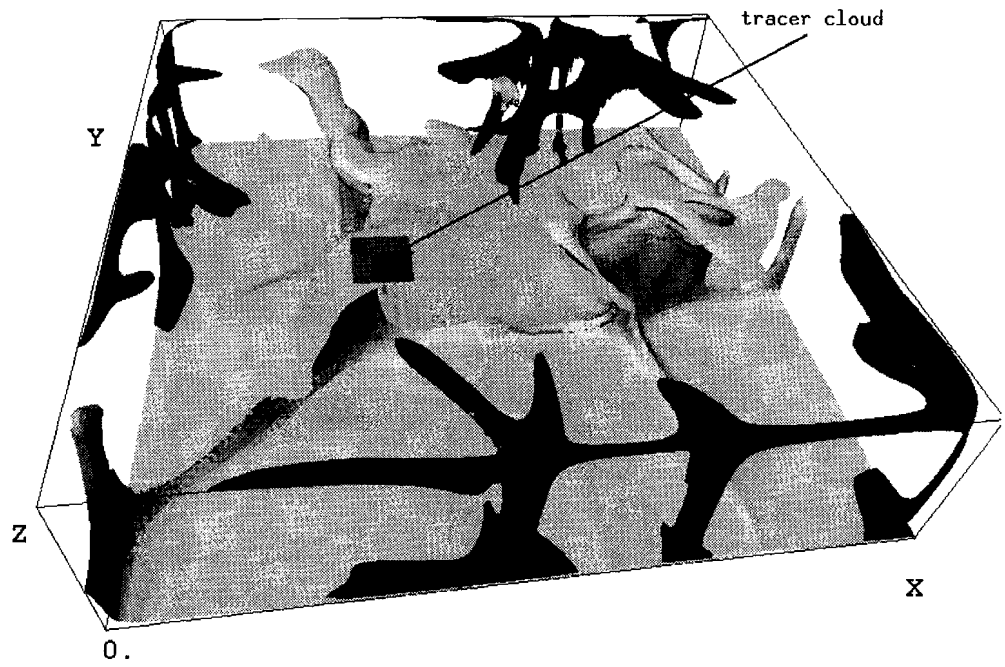

Figure 2:
Temperature isosurface for T=0.7 (light grey) indicating the position of the hot upstreams and T=0.3 (dark grey) indicating the cold down wellings. The part of the T=0.3 isosurface positioned in the upper boundary layer was removed in order to see see inside the box. The grey square marks the position and size of the initial tracer patch.

short period fluctuations in quantities such as surface heat-flow.
In order to investigate the mass transport we have inserted a patch of $60 \cdot 60 \cdot 10 = 36000$ passive tracers, distributed evenly in a tabular volume of dimensions (0.3, 0.3, 0.05), centered at the arbitrarily chosen location (x, y, z) = (1.35, 1.35, 0.975) in the upper boundary layer. This tracer cloud, visualized as the grey square in Fig. 2, is in the upper boundary layer, initially close to one of the major upwellings. The motivation for investigating a heterogeneity initially placed in the upper boundary layer is the geophysical problem of how lithospheric material gets entrained into the main mantle circulation.
In Fig. 3 we display snapshots at different times of the dispersion of the tracer cloud

projected onto the x-y plane. To provide a reference frame temperature isolines at a height of z=0.5 are also plotted. The solid lines (T=0.3) indicate downwellings whereas the dashed lines (T=0.7) show the positions of upwellings.
Fig. 3a shows the initial tracer configuration in the temperature field shown in detail in Fig. 2. In Fig. 3b the evolution of the tracer cloud after t=0.0103 is displayed. This time corresponds to approximately three overturn times of $t \approx 0.003$. We here define the overturn time as the time needed for a tracer to be transported from the upper part of the cell down to the lower part of the cell and back again. This time depends on the initial z-position and, of course, may fluctuate with the time dependence of the flow. In order to determine a statistical mean for the overturn time we used a spectral analysis of the time series of the z-position of representative tracers. We then take the overtun time to be the reciprocal of the dominant frequency, averaged over the tracers.
In Fig. 3b the initial cloud has already been stretched out and folded on the scale of the circulation in one cell. A few tracers are already transported to adjoining cells. After 12 overturns (Fig. 3c), the tracers are apparently well mixed within the original cell, and leakage to the neighbouring cells is significant at several locations. Fig. 3d shows the tracer positions after 31 overturn times. Although the tracers are now widely distributed over the entire solution domain, the original cell still has a significantly higher concentration than the surrounding cells, and some small parts of the box still contain very few tracers.
Concluding these observations we can state that there are two main processes involved in the mixing process: intra-cell mixing which works on a time scale comparable to 10 overturns, and inter-cell mixing which operates on a much larger time scale. The idea of dividing the mixing process into these two subprocesses is not new, and has been proposed by several authors dealing with numerical experiments on mixing in 2D convective flows (Hoffman and McKenzie, 1984; Christensen, 1989, Hansen and Yuen 1992, Schmalzl and Hansen, 1994). However, we will demonstrate in the following two sections that the mixing in 3D has characteristics which differ significantly from those observed in 2D simulations.

8.4.1 Mixing within a cell

In this chapter we will first discuss the intra-cell mixing as observed in the 2D experiments because these are more intuitive to understand and are a base for un-

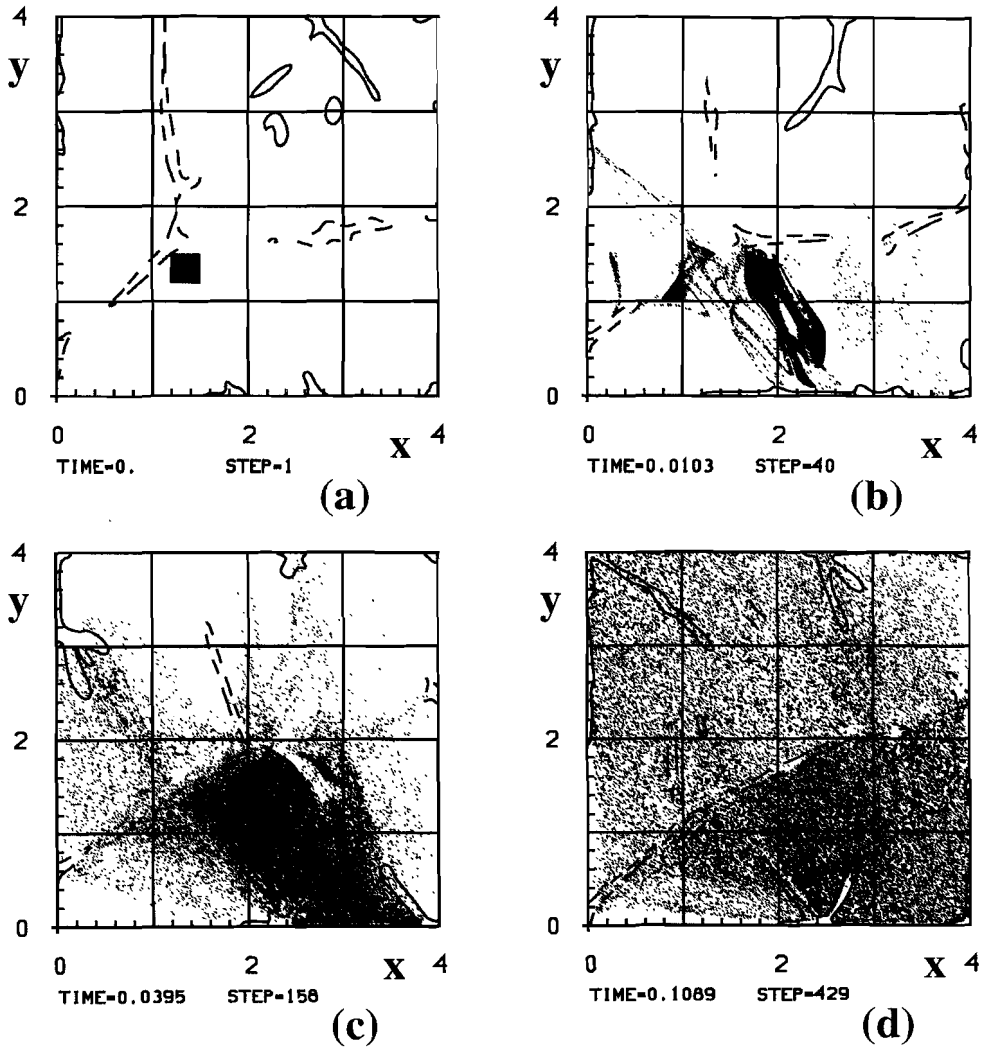

Figure 3:
Snapshots of the tracer distribution at (a) time zero and after approximately (b) 3, (c) 12 and (d) 31 overturn times, in the 3D experiment with $Ra = 8 \cdot 10^5$. The tracers are projected onto the x-y plane. The solid lines denote temperature isolines at z=0.5 and T=0.3 whereas the dashed lines account for T=0.7.

derstanding the 3D experiments. Furthermore most of the knowledge about mixing in very viscous convecting flow has been derived from such 2D experiments and

thus it is important to describe the effects of the third spatial dimension.
In 2D stationary convective flows (equivalent to a 3D roll pattern) the tracer trajectories are identical with the streamlines (e.g. Ottino, 1988). A tracer patch which is initially positioned in the upper boundary layer will be transported down to the lower boundary layer and up again. During this process the patch will be stretched, due to the velocity gradient, as it circulates between upper and lower boundary layers, but it is excluded from mixing with the core of the convection cell (e.g. Schmalzl and Hansen, 1994). A 2D time-dependent flow at a moderate Rayleigh number ($< 10^6$) consists of a large scale circulation, similar to the stationary case, with superimposed boundary layer instabilities (BLI's), which are drifting with the large scale circulation (Hansen and Ebel, 1988). These BLI's can exchange material between the boundary layers and the central region of the cell. Fig. 4 shows an example of this type of 2D flow calculation, also with $R = 8 \cdot 10e5$. Using the same definition of overturn time, we find that the 2D overturn time is significantly greater (approx. 0.005) than the 3D overturn time. The initial tracer patch in this experiment (Fig. 4a) gets stretched out and folded around a plume head (Fig. 4b) after 3/4 of an overturn. After 3 overturns (Fig. 4c) the tracer patch is already folded several times but most of the tracers are still in the vicinity of the boundary layers. Fig 4d shows a snapshot after 7 overturns where the material within the cell is already relatively well mixed.
For 3D stationary convection patterns, like square pattern or hexagonal pattern, the situation is very different. As shown in a previous paper (Schmalzl et al., 1995) the paths of passive tracers are confined to a 2D surface with a distorted toroidal topology. These torii are nested one within another, filling the solution space, and each torus may be characterised by a small radius parameter which increases continuously from zero. Fig. 1 shows the trajectory of a tracer originating close to one of the thermal boundaries. The tracer is transported towards the center of the cell in the course of its orbit around the toroidal surface on a time scale of 6-10 overturns. The number of overturn times needed to transport the tracer to the inner part of the cell depends, however, on the initial position of the tracer. In this way tracers move between the boundary layers and the centre of the cell without time-dependence of the flow.
We find that this topological structure of the flow field is also present in time-dependent simulations, although it is disturbed by the BLI's. In Fig.5 we show the time evolution of the z-component of position of a single tracer from the experiment

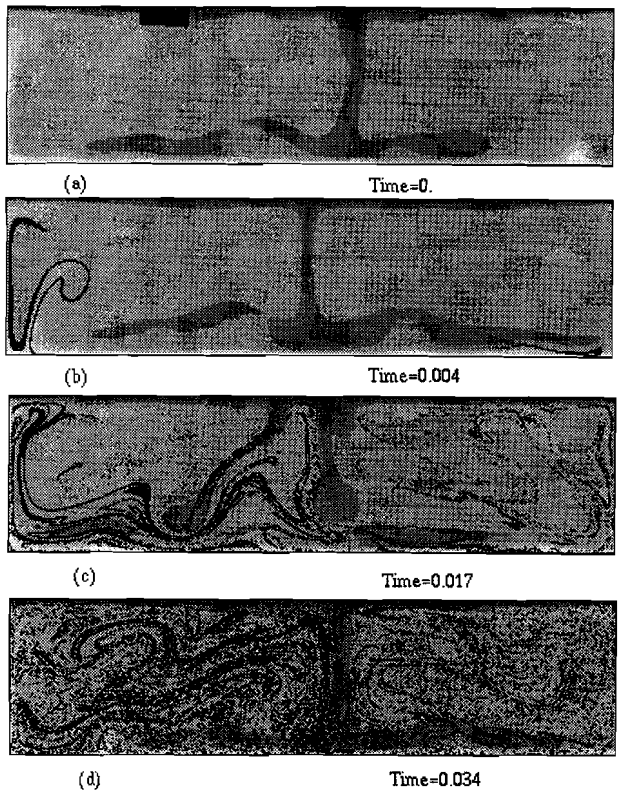

Figure 4:
Time evolution of a tracer patch in the 2D experiment with $Ra = 8 \cdot 10^5$. The tracer patch includes 6000 tracers initially in a 0.3 x 0.1 rectangle, cent redat (1.0, 0.95) in the upper boundary layer. The dark grey indicates cold material the light grey indicates warm material.

of Fig. 2.

Starting in the upper boundary layer, the tracer orbits with a z-amplitude comparable to the box depth d. The amplitude of the orbit continuously decreases, and, after 10 overturns, the particle is orbiting close to the center at z=0.5. Thereafter amplitude increases again and the amplitude modulation is repeated. In a stationary 3D flow the amplitude modulation of this signal appears harmonic; the high frequency carrier signal is due to the orbit of the tracer around the large diameter of the torus, while the low frequency amplitude modulation is due to the orbit

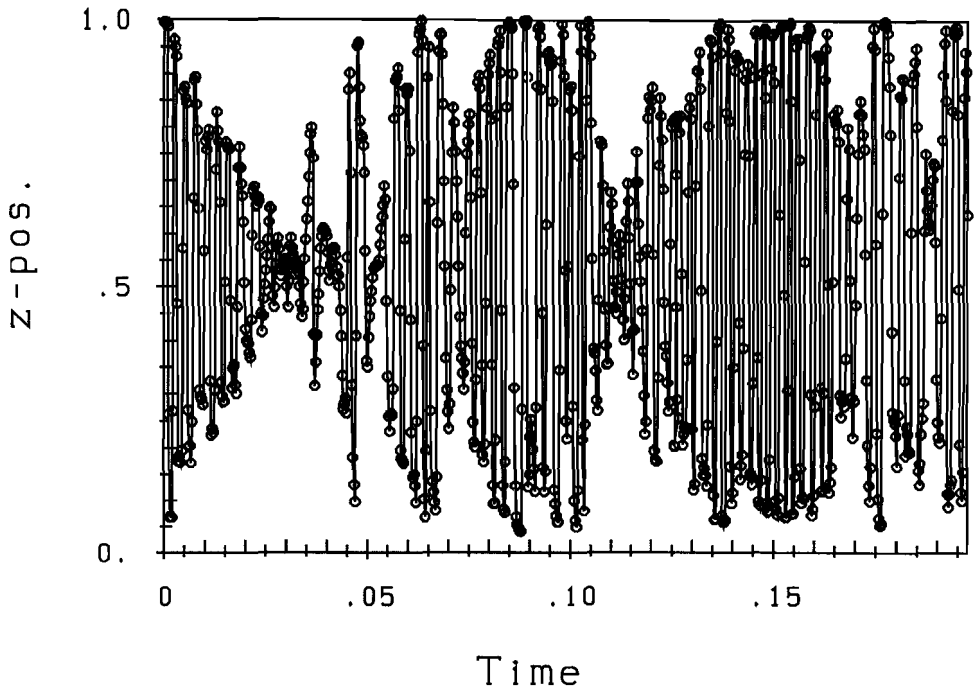

Figure 5:
Z-position of a single tracer in the 3D calculation versus time. The circles ind icate the data which have been saved (every 80th timestep).

of the tracer around the small radius of the torus. In this experiment, however, the regular variation of amplitude is disturbed by irregular excursions (e.g., at t = 0.035 and t = 0.045 approximately) which we attribute to the time-dependence of the flow induced by the BLIs.

In order to show that this description is relevant to all the tracers in the 3D experiment, we divide the solution space into 50 different height levels and count the number of tracers in each level. Fig. 6a shows that all of the tracers are initially located in the upper boundary layer.

Fig. 6b (after 7 overturns) shows that, although the tracer cloud has been strongly streaked out, maximum tracer concentration is found in two regions above and below the mid-level of the cell. After another 4 four overturns (Fig. 6c) these maxima have disappeared as many tracers have migrated back to the outer part of the torus. In terms of the vertical distribution of tracers, the cell now appears well

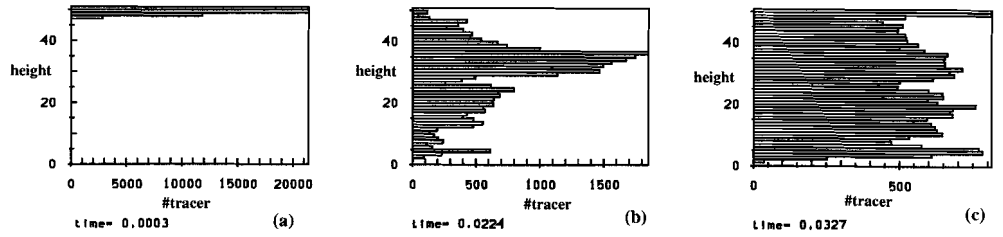

Figure 6:

Histogram of the tracer distribution on 50 horizontal levels. (a) Initially there is a very high concentration in the upper boundary layer. (b) After 7 over turn times the tracers are concentrated on two maxima centered around z=0.5. (c) After another 5 overturns this maximum has vanished again.

mixed. By comparison with Fig. 3c, however, we see that distribution of the tracers is still largely confined to the original cell. To show that the vertical movement of tracers, as described by Figs. 5 and 6, occurs throughout the mixing process, we have monitored the z-component of position of 200 tracers for the complete duration of the experiment ($\Delta t = 0.2$). In order to extract the the amplitude modulation signal from the time series $Z(t_i), i = 1, N$ we have calculated the envelope function for the set of the 200 tracers. Figure 7 shows the power spectrum obtained from a spectral analysis of the envelope function $e(t)$.

We identify a maximum at frequencies around 12 cycles per dimensionless time unit, correspondng to an overturn time around the small diameter of the torus of $t \approx 0.08$ time units. This time interval is the time required for material originating in one of the boundary layers to be transported, with decreasing overturn radius, towards the center of the cell and, with increasing overturn radius, back to the boundary layer again. The effects of time dependence are of course averaged out by this measure.

To summarise the differences between intra-cell mixing in 2D and 3D experiments at this Rayleigh number, we may say that 2D mixing is dominated by the effects of BLIs, while 3D mixing is dominated by the basic toroidal cell-structure of the flow. Because the major vertical flow structures in 3D are more nearly cylindrical than sheet-like, vertical velocity components are greater and the blob-like BLI's are advected into the plumes and sinkers before growing to large amplitude. Although the boundary layer instabilities rarely penetrate to the center of the cell in the 3D case, they undoubtedly cause some enhancement of the rate of intra-cell mixing.

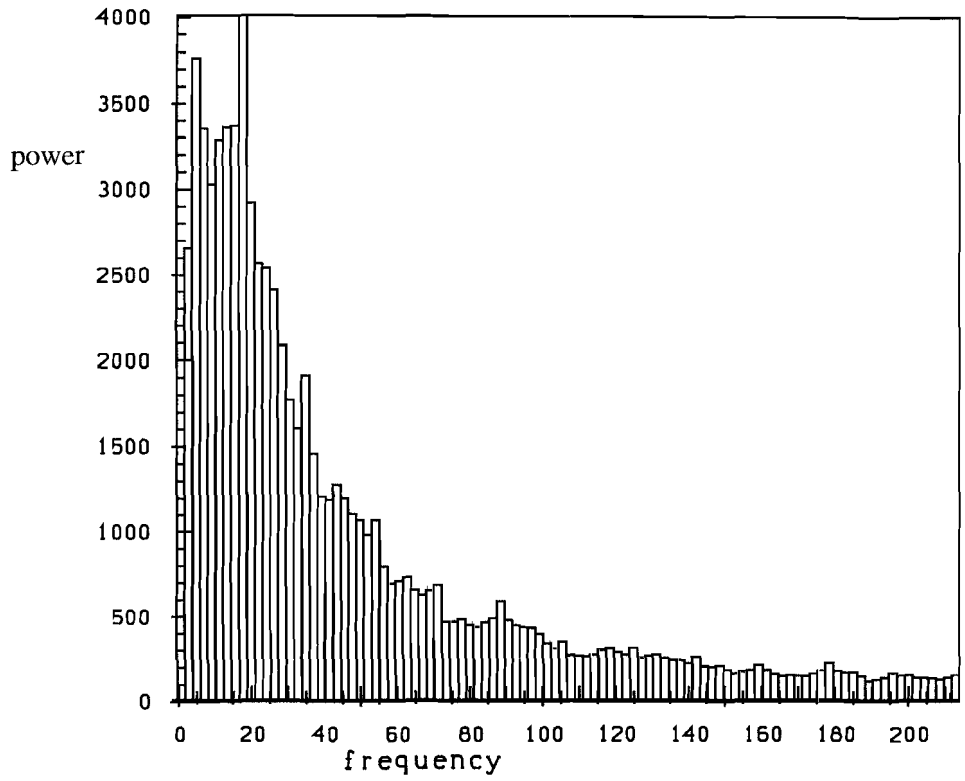

Figure 7:
Histogram of the spectral analysis of the envelope function of the z-component of the position for 200 tracer. Note that the frequency of the envelope is twice the frequency of the amplitude modulation. Although the signal is noisy the maximum of this distribution center s around $f \approx 12$ which corresponds to an overturn time around the small diameter of $t \approx 0.08$.

8.4.2 Mixing between cells

The efficiency of inter-cell or cross cell mixing is crucial in any understanding of the existence of different chemical reservoirs in the Earth's mantle. As in the previous section, we will first discuss results obtained from 2D experiments and than compare the observations with 3D experiments.
In 2D time-dependent flow the major up and down welling flow structures hinder the mass transport between adjoining cells. Since they do not completely block the mass transport, we refer to this type of boundary as a quasi-seperatrix. The mass

transport across a quasi-seperatrix illustrated by the major downwelling in Fig. 4 is primarily due to BLI's which distort the downwelling and cause it to move laterally. Horizontal movement of the downwelling transfers material from one cell to the other simply by translating the separation point at the base of the layer where the downwelling flow diverges to left or right. The sequence shown in Fig. (4a-c) shows the impact of BLIs running into the major downwelling and pulling it to left or right. In Fig. 4b a small sample of the tracers has already been moved into the right hand cell by the left moving down-welling, and the continuing movement of tracers into the right cell can be seen clearly in Fig. (4c).

This mechanism of separatrix migration leads to efficient cross cell mixing, particularly when most of the tracers are transported within the cell close to the boundary layers.

The cross-cell mixing mechanism described for the 2D flows also partly partly explains the cross-cell mixing in the 3D case. We observed earlier that the distortion of the dominant cell structure caused by BLI's is relatively smaller in 3D due to the cylindrical structure and greater vertical velocity of the major up and downwelling structures. In addition, because of the toroidal orbits of the tracers within the cell, the tracer concentration near the outer part of the cell is generally lower than in the 2D case. These two effects contribute to a significantly reduced rate of tracer transport across the cell boundaries. The experiment in Fig 3d shows that even after 30 overturn times the initial cell still has a much higher concentration of tracers than the surrounding cells.

Another effect which contributes to cross cell mixing in these experiments is reorganisation of the cell structure. An example of this can be seen in Fig. 3: A strong down welling in the lower right corner of Fig. 3c is indicated by the T = 0.3 isoline enclosing an area between (x, y) = (4., 0.) and (x, y) = (3.3 , 0.6), but this down welling has disappeared in Fig. 3d, resulting in a greater rate of tracer transport to the right of the original cell.

The effect of cell re-organisation is not unique to the 3D experiments but is also known from 2D calculations in large aspect ratios (≈ 10). Another measure of how the mixing process evolves in the 3D experiment is obtained by dividing the solution region into a set of a 40x40x10 boxes, and determining how many of the boxes contain at least one tracer. This statistic is plotted versus time in Fig. 8(a), with the expected value of 89.5 % of the boxes being populated by at least one tracer (for a random distribution) shown also as a dashed line.

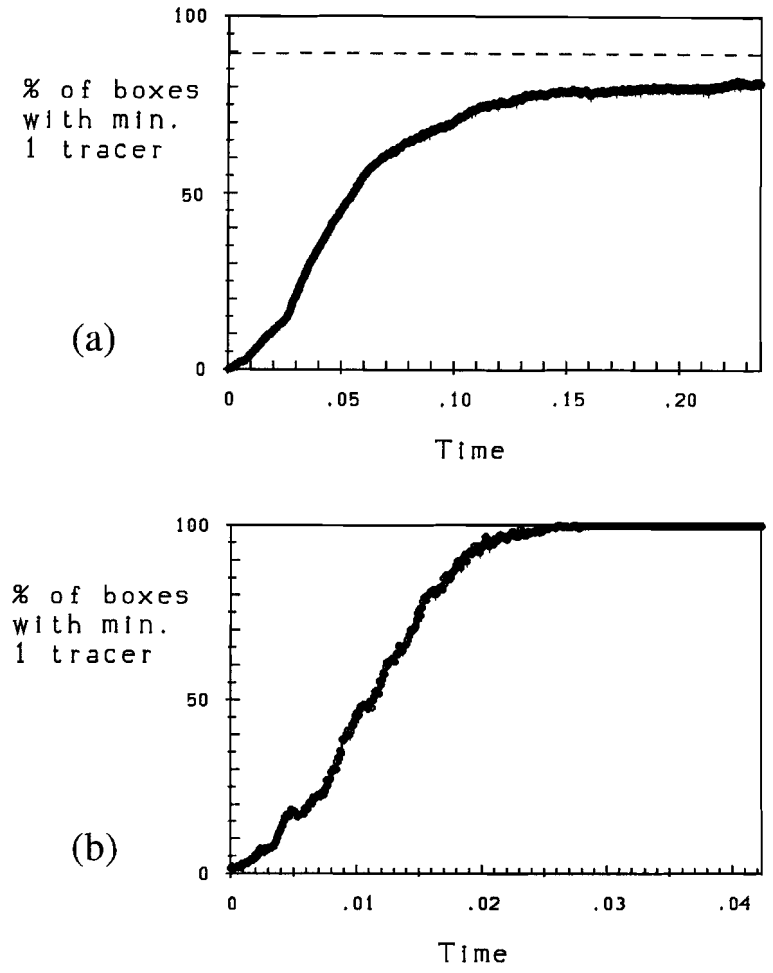

Figure 8:
(a) For the 3D experiment, the percentage of boxes of a 40x40x10 sampling grid which contain at least one tracer. The dashed line indicates the expected value of 89% of boxes being populated if mixing is random. After 30 overturns ($t \approx 0.1$) 30% of the boxes still contain no tracer. (b) For the 2D experiment, the anaologous statistic for a 40 x 10 sampling grid. After 7 overturns ($t \approx 0.03$) 100% of the boxes are populated by at least one tracer.

The time-axis with its maximum of t=0.24 represents approximately 75 overturn times in the experiment. After 30 overturns (t=0.1), 30 % of the boxes still contain

no tracers, even though the horizontal projection of tracer locations at this time (Fig. 3d) shows a relatively high degree of mixing in the horizontal directions. At the end of the calculation (t=0.24) still only 81 % of the boxes are populated and there clearly remain significant regions of the solution space which are unaffected by the introduction of the tracers.
As a qualitative comparison, Fig. 8(b) shows the analogous statistic for the 2D case. After only 7 overturns ($t \approx 0.01$) all bins in a 40x10 grid contain already at least one tracer. It is important to point out that these 2D and 3D mixing statistics measure quantities of different dimensionality. Any quantitative comparison of the mixing rate of line elements (2D) and point elements (3D) includes an arbitrary geometrical factor.
This box-counting algorithm does not provide information about the position and the geometry of regions still containing few or no tracers. Nor does it tell us about regions which still contain a greater than average number of tracers. The question of whether the limited size of the computational domain has influenced our mixing statistics is also difficult to address here. The important point, however, is that the time-scale required for the homogenization of heterogeneities between cells is considerably longer than that required in comparable 2D experiments (Hoffman and McKenzie, 1985; Christensen, 1989; Schmalzl and Hansen, 1994).

8.4.3 Dependence of the mixing process on the initial position of the tracer cloud

In order to investigate the importance of the initial position of the tracer patch on the mixing behaviour we have repeated the 3D experiment for a Rayleigh number of $8 \cdot 10^5$ with 5 distinct tracer clouds. The evolution of the temperature field was repeated exactly. The size and shape of each tracer cloud (0.3, 0.3, 0.05), and the central Z-coordinate (0.975) were, in each case, the same as used in the previous 3D experiment, but the number of tracers (30x30x5) was reduced by a factor of 8. The initial X and Y coordinates of each block were chosen randomly.
For each of these 5 tracer clouds, we analysed tracer distribution as a function of time, by again dividing the solution region into 40x40x10 boxes and counting how many boxes contain at least one tracer. In the long time limit of a randomly mixed tracer block, 25% of the boxes would be populated by at least one tracer.

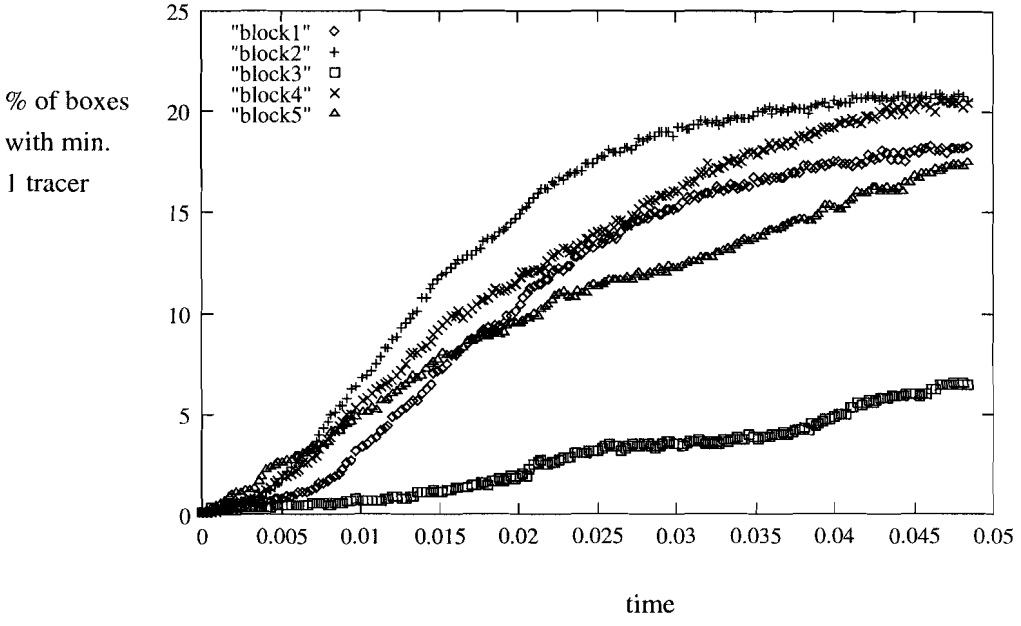

Figure 9:
Mixing statistics of 5 distinct tracer blocks with different initial position, s howing, versus time, the number of boxes of a 40x40x10 sampling grid which contain at least one tracer. Tracer block 3 has an exceptionally low rate of increase in o ccupied bins due to its initial position close to a corner of the computational domain.

The results of these 5 experiments are plotted in Fig. 9.
One can see that the mixing histories of 4 of the 5 tracer blocks are similar, whereas the rate of increase of occupied boxes for tracer block 3 is significantly slower. The initial position of block 3 was, however, very close to one of the corners of the solution region. where the convective flow was relatively stable. The other tracer patches were placed closer to the center of the cell, so we attribute the very poor mixing rate of tracer block 3 to the artificial stabilization of the cell by the adjacent side walls. The mixing statistics from the other four patches (Fig. 9) indicate that the mixing rate of such a flow may typically vary within about a factor of 2.

8.4.4 The influence of the vigor of convection on the mixing process

For convection in the Earth's mantle the Rayleigh number, specifying the vigor of

convection, is probably greater than the value of $8 \cdot 10^5$ used in the experiments described above. To investigate how the above results change as Rayleigh number is increased, we also completed an experiment with $R = 3 \cdot 10^6$. Due to the thinner thermal boundary layer at high Rayleigh number, this calculation requires increased numerical resolution. This experiment was therefore carried out on a mesh of 257x257x65 points, requiring an eight-fold increase in computational effort per timestep and a reduction in timestep size by more than a factor of two, to comply with the Courant- Lewy-Friedrichs criterion. Limited computing resources therefore required that this mixing experiment is significantly shorter duration than the one described above. The initial temperature field for this experiment was obtained by starting with a temperature field from the $R = 8 \cdot 10^5$ experiment and advancing the calculation through 0.01 dimensionless time units in order to pass the initial transient caused by the sudden increase in Rayleigh number. Boundary conditions and initial tracer location are identical to those described in section 2. Fig. 10 shows some snapshots of the tracer distribution, projected onto the horizontal plane after approximately 0.7, 2. and 5. overturn times.

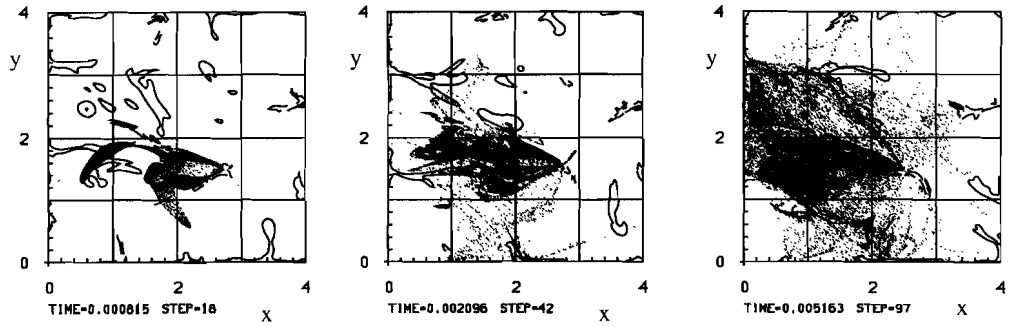

Figure 10:
Snapshot of the mixing evolution in a convective flow at a Rayleigh number of $Ra = 3 \cdot 10^6$ after approximately (a) 0.7, (b) 2, and (c) 5 overturn tim es. Other graphical conventions are as in Figure 3.

Visual inspection of the 3D time-dependent solutions shows that, as in similar 2D calculations (Christensen, 1989, Schmalzl and Hansen 1994), an increase of the Rayleigh number causes the separating influence of the cell boundaries to be diminished. In Figure 10a one can still identify the folded structure of the initial

tracer patch although the patch is already streaked out on a scale comparable to the box length.

In order to estimate how the mixing timescale depends on the Rayleigh number, we again measured the population statistics of the 40x40x10 boxes which cover the solution region. We compare the mixing statistic versus time for the two experiments with Rayleigh number $8 \cdot 10^5$ and $3 \cdot 10^6$ in Figure 11.

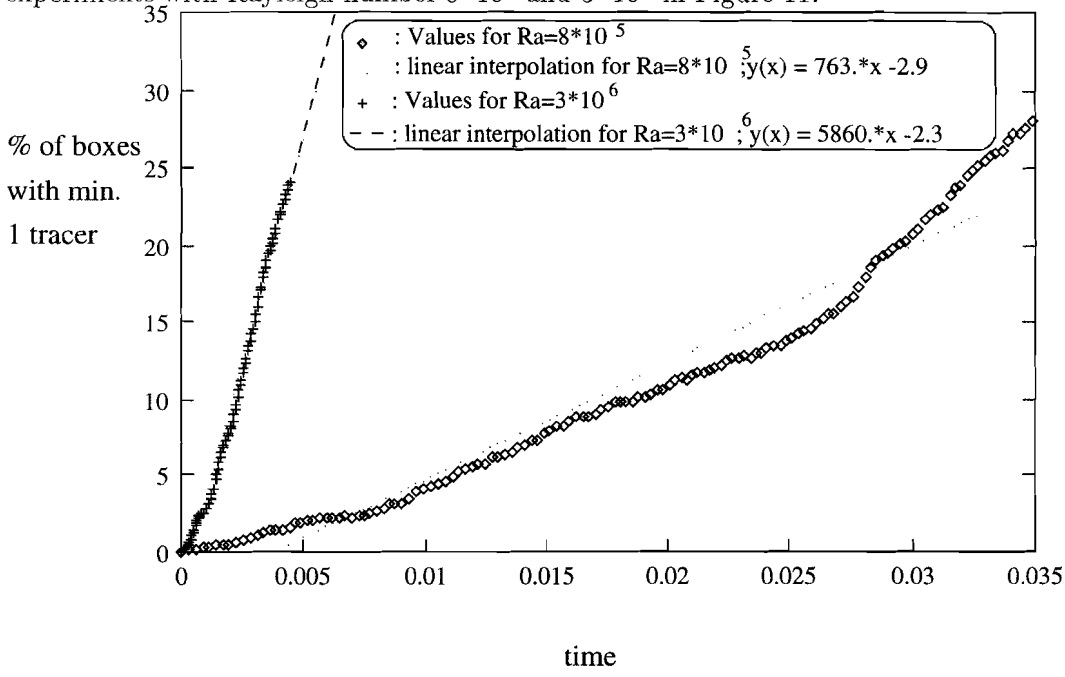

Figure 11:
Box-counting applied on the mixing evolution in a flow with $Ra = 8 \cdot 10^5$ and $Ra = 3 \cdot 10^6$. The increase in occupied boxes is a factor of eight higher for the highr Ra. calculation.

By measuring the slope of the best-fit straight line through each of the two curves, we see that the rate of increase in occupied boxes is about a factor of 8 larger for $Ra = 3 \cdot 10^6$ than for the mixing calculation we carried out at $Ra = 8 \cdot 10^5$.

In the previous section we showed that there may be a factor of two or more difference in the observed rate of mixing, due to variation in the initial location of the tracer cloud. There may therefore be a similar uncertainty in the factor of 8 increase in mixing rate shown in Figure 11. Bearing this uncertainty in mind we may examine reasons for the observed increase in mixing efficiency. We attribute

the increase to two separate effects:
First there is the increase in mean flow velocity at higher Rayleigh number. Boundary layer theory predicts that the root mean square velocity (v_{rms}) scales like $v_{rms} \sim Ra^{\beta}$ with β around 2/3 (Chandrasekkar, 1961). Scaling the rate of mixing by the increase in root mean square velocity, we appear to observe an additional factor of 3 increase in mixing rate.
The second effect which influences the mixing efficiency is the stability of the flow structure. As discussed by several authors in the context of 2D convection experiments (e.g. Hansen et al., 1990), the coherent cell structure of the flow is diminished with increasing Rayleigh number and the heat transport by the BLI's increases. In the context of our earlier discussion on the mechanisms of mixing in 3D flows, the cross-cell mixing will be enhanced by the relative decrease in strength of the major up and down welling flow structures. We therefore attribute part of the observed increase in mixing rate to this structural change in the flow pattern.
To obtain an accurate estimate of the dependence of mixing rate on Rayleigh number will, however, require more extensive experimentation, in which we take account of the statistical fluctuations in mixing rate caused by varying the initial tracer location and the initial temperature field.

8.5 Discussion and Conclusion

We have described numerical simulations of the mixing of passive tracers in very viscous convecting flows (in both 2D and 3D). The motivation for this study is to further our understanding of the processes by which isotopic and geochemical anomalies are mixed within the Earth's mantle. While these calculations are greatly simplified relative to the actual process of convection in the mantle, they advance our understanding of the differences between mixing in 2D and mixing in 3D. The present study indicates that extrapolating the results of 2D experiments to the 3D problem presents many difficulties. The influence of factors such as internal heating, temperature-dependent viscosity, or non-Newtonian rheology are properly left to future studies.
The mixing process on the scale of one convection cell has proven to be fundamentally different in the 2D and 3D simulations. In the 2D simulations, material inserted at the upper boundary of the convection cell tends to remain in the boundary layers for several overturns. Time dependence, in the form of boundary layer

instabilities, exchanges material between the boundary layers and the core of the 2D cell. In 3D convective flows, the topological structure of the velocity fields causes the tracers to spiral towards the center of the cell and then back to the boundary again. This process operates on a time-scale on the order of 10 large scale overturns. This toroidal structure of the 3D velocity field is defined by the steady state solutions, but it also dominates the circulation pattern of the time-dependent 3D solutions. Boundary layer instabilities in the 3D solutions may increase the rate of mixing between boundary layers and core of the cell, but the increase appears relatively minor.

A second important conclusion of this paper is that the exchange of material between cells (the cross-cell mixing) in the 3D calculations works on a longer time-scale than expected from earlier 2D calculations. The main mechanism for cross-cell mixing is the relatively small scale fluctuation in the horizontal position of the cell separatrices. These fluctuations are caused by the boundary layer instabilities, in both 2D and 3D calculations. Tracers moving vertically near the cell separatrices are transferred to the adjoining cell as the separatrix migrates horizontally. The longer time-scale for cross-cell mixing in 3D appears to be explained primarily by the more stable cell structure of the 3D calculations. The 3D planform with its column- like up- and down-wellings is more like square-cell convection than roll convection. Frick et al. (1983) showed that heat transport in convection with square planform exceeds the heat transport of rolls. This observation may explain the apparently greater stability of the 3D cell pattern and the fewer boundary layer instabilities observed in the 3D case than in the 2D case. The blob-like boundary layer instabilities in 3D are volumetrically less significant than the roll-like boundary layer instabilities in 2D and therefore appear to have less impact in disturbing the stable cell structure.

Major re-organisation of the background cell structure can occur occasionally, but it is not a significant factor in the 3D experiments we report. The additional spatial dimension seems to allow the flow to choose a pattern of convection which is more stable against large- scale rearrangement of the cell structure. We note however that greatly increased Rayleigh number, or factors such as internal heating or non-linear rheology, could cause major cell re-organisation to occur more frequently by increasing the chaotic properties of the flow. Since the cross-cell mass transport is very sensitive to structural changes in the flow pattern, it is possible that 3D mixing timescales could be significantly reduced by these factors.

The apparent difference we observe between the timescales for cross-cell mixing in 3D and 2D is contrary to earlier expectations. It has previously been argued that: a) Mixing in flows which exhibit a chaotic Lagrangian structure proceeds more rapidly than in regular flows (e.g., Ottino, 1989; Kellogg, 1993). b) Unlike 2D flows, time dependence of the flow is not a necessary prerequisite for 3D flows to exhibit a chaotic Lagrangian structure (Aref, 1984; Dombre et al., 1986). c) Therefore mixing in 3D flows is expected to be more rapid than in 2D flows (e.g., Davies, 1990). This is a complex argument which may apply in some circumstances to mixing within a single cell, but certainly does not appear to apply to the cross-cell mixing in our experiments. In attempting to compare mixing timescales of 2D and 3D problems, it becomes clear that we compare 2 distinct physical phenomena and there is an arbitrary geometrical factor present when we compare the mixing timescales for the two problems. While we might conclude from Figure 8 that mixing appears to be perhaps 5 times faster in 2D than in 3D, it is important to add the caveat that the measure of mixing in the two cases is only superficially comparable. In the 2D calculation the cells are actually rolls, and the tracers are actually line elements, both extending indefinitely in the 3rd dimension. By comparing 2D and 3D mixing calculations we compare the mixing of line elements (2D) with point tracers (3D). We cannot make an unambiguous comparison of the magnitude of two quantities whose dimensionality differs.

Nevertheless, we can state that, when comparing the time needed to homogenize a heterogeneity in a 3D convective flow (constant viscosity, basal heating) with a comparable quantity for a 2D convective flow, (e.g., Hoffman and McKenzie, 1985; Christensen, 1989; Schmalzl and Hansen, 1994) the implied mixing timescale appears much greater in the 3D problem.

To link the geochemical observations with the geophysical view of the Earth much work is still required. The toroidal structure of the 3D cells may have interesting implications for the interpretation of the observed geochemical heterogeneities. If, for example, subducted lithospheric material from oceanic plates is rapidly incorporated in the core of the convection cell, it is unlikely that this material will remain, after more than one or two overturn times, as a coherent potential source for the observed geochemical heterogeneities (McKenzie and O'Nions, 1995).

If the mixing rate in 3D is so much slower than was implied by earlier 2D calculations, we may be able to avoid the conclusion that the mantle may be layered in order to preserve the observed geochemical and isotopic heterogeneities. From our

mixing experiment with $Ra = 0.8 \cdot 10^6$ we take, from Figure 8, the time at which 75% of the boxes contain at least one tracer as defining a mixing timescale of 0.1 dimensionless time units. In using this definition, we recognise however that, while the initial mass of tracers is widely dispersed (Figure 3d), there remain large parts of the box which do not contain any tracers. The inferred mixing timescale is then 1.5 Gyr for an upper mantle layer (d = 700 km), and 25 Ga for a whole mantle layer (d = 2900 km), and it is easy to preserve heterogeneities on a timescale of the age of the Earth. Increasing Ra to $3.0 \cdot 10^6$, however, reduces the mixing timescales to 0.2 and 3 Ga respectively. If Ra is an order of magnitude greater at $3.0 \cdot 10^7$, we would infer that distinct geochemical reservoirs in even a whole mantle layer can only be preserved for a small fraction of the age of the Earth, unless they are continuously renewed by injection of new source material. The unknown effects of internal heating and temperature-dependent or non-Newtonian rheology may change this analysis, so it remains difficult to conclude that layering of the mantle is either required or not required by the observed geochemical anomalies.

8.6 References

Aref, H., Stirring by chaotic advection, J. Fluid Mech., 143, 1-21, 1984

Blankenbach, B., F. Busse, U. Christensen, L. Cserepes, D. Gunkel, U. Hansen, H. Harder, G. Jarvis, M. Koch, G. Marquart, D. Moore, P. Olson, H. Schmeling and T. Schnaubelt, A benchmark comparison for mantle convection codes, Geophys. J. Int, 98, 23-38, 1989.

Busse, F. H., U. Chrstensen, R. Clever, L. Cserepes, C. Gable, E. Ginnandrea, L. Guillou, G. Houseman, H.-C. Nataf, M. Ogawa, M. Parmentier, C. Sotin and B. Travis, 3D convection at infinite Prandtl number in Cartesian geometry- A benchmark comparison, Geophys. Astrophys. Fluid Dyn., 75, 39-59, 1994

Carlson R. W., Mechanisms of Earth differentiation: Consequences for the chemical structure of the mantle, Rev. of Geophys., 32, 337-361, 1994

Christensen, U., Mixing by time-dependent convection, Earth and Planetary Scie. Let., 95, 382-394, 1989

Creager, K.C., and Jordan, T.H., Slab penetration into the lower mantle beneath the Mariana and other island arcs of the Northwest Pacific, J.Geophys. Res., 91, 3573-3589, 1986

Davies, G. F., Comment on 'Mixing by time-dependent convection' by U. Christensen, Earth Planet. Sci. Lett., 98, 405-407, 1990

Dombre, T., U. Frisch, J. M. Greene, M. Hénon, A. Mehr and A. M. Soward, Chaotic streamlines in ABC flows, J. Fluid Mech., 167, 353-391, 1986

Frick, H., F. H. Busse and R. M. Clever, Steady three-dimensional convection at high Prandtl numbers, J. Fluid Mech., 127, 141-153, 1983.

Hansen, U. and A. Ebel, Time-dependent thermal convection - a possible explanation for a multiscale flow in the Earth's mantle, Geophys. J., **94**, 181-191,

1988

Hansen, U., Yuen, D. A. und S. Kroening, Transition to hard turbulence in thermal convection at infinite Prantdl number, Physics of Fluids, A2(12), 2157-2163, 1990.

Hansen, U., D. A. Yuen and S. E. Kroening, Heat and Mass Transport in strongly time dependent convection at infinite Prandtl number, Geophys. Astrophys. Fluid Dynamics, 63, 67-89, 1992

Hoffman, N. R. A. and D. P. McKenzie, The destruction of geochemical heterogeneities by differential fluid motion during mantle convection, Geophys. J. R. Astron. Soc., 82, 163-206, 1985

Houseman, G. A., TDPOIS, a vector-processor routine for the solution of the three-dimensional Poisson and biharmonic equation in a rectangular prism, Comp. Phys. Comm, 43, 257-267, 1987

Houseman, G. A., Boundary conditions and efficient solution algorithms for the potential function formulation of the 3-D viscous flow equations, Geophys. J. Int., 100, 33-38, 1990

Houseman, G. A., The thermal structure of mantle plumes: axisymetric or triple-junction ?, Geophys. J. Int., 102, 15-24, 1990

Jeanloz, R., High pressure chemistry of the Earth's mantle and core, in in Peltier, W.R. (Ed.), Mantle Convection plate tectonics and global dynamics, Gordon and Breach, pp 203-260, 1989

Kellogg, L. H., Chaotic mixing in the Earth's mantle, Advances in Geophysics, 34, 1-33, 1993.

Machetel, P. and D. A. Yuen, The onset of time-dependent convection in spherical shells as a clue to chaotic convection in the Earth, Geophys. Res. Lett., 16, 1470-1473, 1986

McKenzie, D. P., Roberts, J. M. und N. O. Weiss, Convection in the Earth's mantle : towards a numerical simulation, J. Fluid Mech., 62, 465-538, 1974.

McKenzie, D. and R. K. O'Nions, The Source Regions of Ocean Island Basalts,

J. of Petrol., 36, 133-159, 1995.

Ottino, J. M., The kinematics of mixing: Streching, chaos and transport, Cambridge Univ. Press, Chapter 5, 1989

Richter, F. M., Convection and the large scale circulation of the mantle, J. Geophys. Res., 78, 8735-8745, 1973.

Schmalzl J. and U. Hansen, Mixing the Earth's mantle by thermal convection: A scale dependent phenomenon, Geophys. Res. Lett., 21, 987-990, 1994.

Schmalzl J., G. A. Houseman and U. Hansen, Mixing properties of three-dimensional stationary convection, Phys. Fluids, 7, 1027-1033, 1995.

Solheim, L.P. and W.R. Peltier, Heat transfer and the onset of chaos in a spherical, axisymmetric, anelastic model of whole mantle convection, Geophys. Astrophys. Fluid Dyn., 53, 205-255, 1990.

Zindler, A. and S. Hart, Chemical geodynamics, Ann. Rev. Earth Sci., 14, 493-571, 1986.

9 Samenvatting (summary in Dutch)

Het is in de afgelopen twintig jaar algemeen aanvaard dat convectieve stroming in de mantel van de Aarde het mechanisme vormt waarmee de warmte uit het inwendige van de Aarde wordt omgezet in mechanische arbeid, en dat convectie aldus het mechanisme vormt achter tektonische processen. Daarnaast geldt dat het proces van mantelconvectie grotendeels bepalend is voor de thermische structuur en de chemische samenstelling van het inwendige van de Aarde. Als gevolg van het feit dat het inwendige van de Aarde niet toegankelijk is voor directe observatie, is onze kennis omtrent het karakter van convectieve stroming onvolledig. De beschikbare informatie over de structuur en evolutie van de Aarde is voor het grootste deel gebaseerd op 'remote sensing' technieken, in het bijzonder de seismologie. Ondanks de toenemende kracht van de seismologie en andere 'remote sensing' technieken blijft het probleem bestaan dat al deze technieken uitsluitend een momentopname van het inwendige van de Aarde kunnen bieden. Hoewel dergelijke momentopnamen een belangrijke rol spelen als randvoorwaarde in studies van de dynamische evolutie stellen zij ons niet in staat reconstructies te maken (of voorspellingen te doen) ten aanzien van de evolutie van het inwendige van de Aarde.

Geochemisch onderzoek daarentegen, biedt waarnemingen gemiddeld over een zekere periode en is daardoor in staat inzicht te verschaffen in de ontwikkeling van de Aarde door de tijd. De isotoopverhoudingen van basaltisch gesteente, bemonsterd bij mid-oceanische ruggen en op oceanische eilanden, geven aan dat de mantel van de Aarde heterogeen is op een schaal die varieert van minder dan een meter tot enkele duizenden kilometers. Men heeft wel geconcludeerd dat deze observatie alleen te verklaren is wanneer er in de mantel meerdere reservoirs bestaan die, in de loop van de geschiedenis van de Aarde, niet zijn gemengd ten gevolge van convectie. Het zwakke punt van de geochemische waarnemingen betreft het feit dat zij uitsluitend informatie verschaffen op bepaalde locaties en slechts beperkt inzicht leveren in de ruimtelijke verdeling van de potentiële bronreservoirs van het basaltisch gesteente.

Het in dit proefschrift beschreven onderzoek heeft als doel, door middel van de studie van de meng-eigenschappen van convectieve stroming, de kloof te over-

bruggen tussen, enerzijds, geochemische observaties en, anderzijds, de daaruit voortvloeiende implicaties voor een dynamisch model van de Aarde.

In hoofdstuk 2 worden enkele van de resultaten van het onderzoek aan isotoopverhoudingen van basalten van spreidingsgruggen en oceanische eilanden besproken. Deze resultaten geven duidelijk aan dat de mantel van de Aarde chemisch gezien heterogeen is en ten minste vier verschillende chemische reservoirs omvat. De geobserveerde lengteschaal varieert van minder dan een meter tot enkele duizenden kilometers. Een deel van de reservoirs lijkt te hebben bestaan sinds 150 miljoen jaar na de vorming van de Aarde. Het bestaan van deze reservoirs geeft enige houvast ten aanzien van het mogelijke karakter van mantelconvectie en tevens ten aanzien van het proces van subductie van lithosfeerplaten dat een rol speelt als bron van geochemisch afwijkend materiaal in de mantel.

In hoofdstuk 3 behandelen wij enkele algemene aspecten van de kinematica van het proces van menging van twee vloeistoffen. Gezien de veelomvattendheid van dit onderwerp concentreer ik me op het recentelijk ontdekte verschijnsel van Lagrangische chaos. Op plaatsen binnen de stroming waar een chaotische Lagrangische structuur bestaat is de menging sterk verhevigd. Dergelijke structuren zijn zowel in twee-dimensionale tijdsperiodische stroming, als in drie-dimensionale stroming waargenomen.

De wiskundige vergelijkingen waarmee ons fysische model wordt beschreven zijn te vinden in hoofdstuk 4. Ook worden in dit hoofdstuk de benaderingen die zijn toegepast en de geschikte schaling behandeld.

De in dit proefschrift gebruikte numerieke methoden zijn beschreven in hoofdstuk 5. Voor de twee-dimensionale experimenten is een eindige- elementen-model gebruikt. De drie-dimensionale experimenten zijn gedaan met behulp van een zogenaamde 'mixed spectral finite-difference' benadering. Het 'passive tracer' algoritme dat in zowel de twee- als de drie-dimensionale simulaties is gebruikt ten einde het massatransport te volgen, wordt beschreven aan het eind van dit hoofdstuk.

In hoofdstuk 6 introduceren wij een deeltjes-correlatie functie en de bijbehorende correlatie-dimensie waarmee de meng-efficiëntie van een twee-dimensionale convectiestroming kan worden gekenmerkt als functie van zijn sterkte en structuur. Er zal worden aangetoond dat deze methode het mengproces op gedetailleerde wijze

beschrijft. De studie in dit hoofdstuk geeft aan dat de meng-eigenschappen van de stroming afhankelijk zijn van de ruimtelijke schaal. Bij convectie van matige sterkte worden heterogeniteiten binnen een circulatiecel snel uitgewist terwijl twee naast elkaar gelegen cellen aanzienlijk langer ongemengd kunnen blijven.

De meng-eigenschappen van drie-dimensionale stationaire convectie vormen het onderwerp van het volgende hoofdstuk 7. Afzonderlijke stroomlijnen, zoals aangetoond door middel van Poincaré doorsneden van de 'tracer'-paden, liggen op twee-dimensionale oppervlakken met een verwrongen toroïdale topologie. De door de convecterende vloeistof ingenomen ruimte is gevuld met series van deze, in elkaar genestelde, toroïdale oppervlakken. In tegenstelling tot hetgeen gevonden bij experimenten met minder viskeuze vloeistoffen, zijn door ons geen gebieden geobserveerd waarin de Lagrangische 'tracer'-beweging chaotisch was.

In het laatste hoofdstuk 8 presenteren wij numeriek onderzoek naar menging in sterke drie-dimensionale convectie. In vergelijking met de twee-dimensionale experimenten bleek dit type stroming zeer efficiënt te zijn in het homogeniseren van heterogeniteiten binnen iedere convectiecel. Dit is in de eerste plaats het gevolg van de toroïdale structuur van het snelheidsveld. De toroïdale beweging komt overeen met de beweging geobserveerd in de stationaire drie-dimensionale stromingen. Menging door de grenzen van de convectiecellen werd daarentegen veel langzamer bevonden dan verwacht op basis van de twee-dimensionale simulaties. Laatstgenoemde bevinding vormt een mogelijke verklaring voor de heterogeniteiten die in de mantel van de Aarde zijn geobserveerd.

10 Acknowledgements

First of all, I want to thank Ulrich Hansen for his guidance and for giving me plenty of freedom to do research. His advise, especially during the final phase of this thesis, was very helpful. I am also very grateful to Greg Houseman for the excellent cooperation we had during the last years. Further, I would like to express my gratitude to Prof. Dr. N. J. Vlaar for his willingness to be my promotor. I would like to thank Paul Meijer and Andrew Curtis for their help on some parts of this thesis. My largest vote of thanks goes to Dagmar Olbertz for her help and patience during the writing of this thesis.

11 Curriculum Vitae

15.4.1964	Born in Wesseling, Germany
June 1984	Abitur at the Gymnasium in Wesseling
1984-1991	Study of Geophysics at the University Köln, Germany
1991-1996	Research assistant (OIO) at the department of Theoretical Geophysics, Utrecht University, The Netherlands